

2

AD-A231 734

**NAVAL POSTGRADUATE SCHOOL
Monterey, California**



THESIS

DTIC
S ELECTE **D**
FEB 06 1991
E

**SOME ASPECTS OF FILM CONDENSATION
OF STEAM ON FINNED TUBES**

by

James M. Coumes

December 1989

Thesis Advisor

P. J. Marto

Approved for public release; distribution is unlimited

91 2 04 138

Unclassified

security classification of this page

REPORT DOCUMENTATION PAGE

1a Report Security Classification Unclassified		1b Restrictive Markings	
2a Security Classification Authority		3 Distribution Availability of Report Approved for public release; distribution is unlimited.	
2b Declassification/Downgrading Schedule		5 Monitoring Organization Report Number(s)	
4 Performing Organization Report Number(s)		7a Name of Monitoring Organization Naval Postgraduate School	
6a Name of Performing Organization Naval Postgraduate School	6b Office Symbol (if applicable) 34	7b Address (city, state, and ZIP code) Monterey, CA 93943-5000	
6c Address (city, state, and ZIP code) Monterey, CA 93943-5000		9 Procurement Instrument Identification Number	
8a Name of Funding Sponsoring Organization National Science Foundation	8b Office Symbol (if applicable) CBI-S603-582	10 Source of Funding Numbers	
8c Address (city, state, and ZIP code) Washington, D.C. 20550		Program Element No	Project No
		Task No	Work Unit Accession No
11 Title (include security classification) SOME ASPECTS OF FILM CONDENSATION OF STEAM ON FINNED TUBES			
12 Personal Author(s) James M. Coumes			
13a Type of Report Master's Thesis	13b Time Covered From 70	14 Date of Report (year, month, day) December 1989	15 Page Count 161
16 Supplementary Notation The views expressed in this thesis are those of the author and do not reflect the official policy or position of the Department of Defense or the U.S. Government.			
17 Cross Codes		18 Subject Terms (continue on reverse if necessary and identify by block number)	
Field	Group	Subgroup	Filmwise Condensation, Low Integral-Fin Tubes, Outside Heat-Transfer Coefficient, Condensate Inundation.
19 Abstract (continue on reverse if necessary and identify by block number)			
<p>Heat-transfer measurements were made for filmwise condensation of steam on smooth tubes and finned tubes with rectangular-shaped fins. The influence of fin root diameter on a single horizontal finned tube was examined by taking data for two families of tubes whose fin root diameters were 12.7 and 19.05 mm. Each family of tubes had fins that were 1 mm thick and 1 mm high, but with fin spacings of 0.25, 0.50, 1.0, 1.5, 2.0, and 4.0 mm. To compare results being obtained in a concurrent research project with Queen Mary College (University of London), data were collected on two tubes whose fin root diameters were 12.7 mm, and which had fin thicknesses of 0.5 mm, fin heights of 1.59 mm, and fin spacings of 1.0 mm. A comparison of the enhancement ratios (based on constant vapor-side temperature drop) with past Naval Postgraduate School (nps) studies showed good agreement. The apparatus was then modified in order to study the effects of condensate inundation. Preliminary flow visualization studies of the condensate motion were made. On finned tubes, the condensate falling on the tubes has a tendency to be channeled between fins and does not spread out axially as occurs on smooth tubes.</p>			
20 Distribution Availability of Abstract <input checked="" type="checkbox"/> unclassified unlimited <input type="checkbox"/> same as report <input type="checkbox"/> DTIC users		21 Abstract Security Classification Unclassified	
22a Name of Responsible Individual Paul J. Martin		22b Telephone (include Area Code) (408) 646-2898	22c Office Symbol 69X1

Approved for public release; distribution is unlimited

**Some Aspects of Film Condensation
of Steam on Finned Tubes**

by

James M. Coumes
Lieutenant, United States Navy
B.S., Oregon State University, 1982

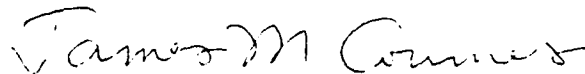
Submitted in partial fulfillment of the
requirements for the degree of

MASTER OF SCIENCE IN MECHANICAL ENGINEERING

from the

NAVAL POSTGRADUATE SCHOOL
December 1982

Author:

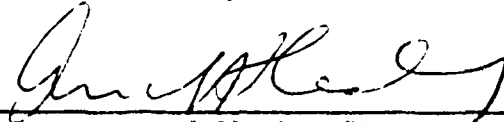


James M. Coumes

Approved by:



P. J. Marfo, Thesis Advisor



A. J. Healey, Chairman
Department of Mechanical Engineering

ABSTRACT

Heat-transfer measurements were made for filmwise condensation of steam on smooth tubes and finned tubes with rectangular-shaped fins. The influence of fin root diameter on a single horizontal finned tube was examined by taking data for two families of tubes whose fin root diameters were 12.7 and 19.05 mm. Each family of tubes had fins that were 1 mm thick and 1 mm high, but with fin spacings of 0.25, 0.50, 1.0, 1.5, 2.0, and 4.0 mm.

To compare results being obtained in a concurrent research project with Queen Mary College (University of London), data was collected on two tubes whose fin root diameters were 12.7 mm, and which had fin thicknesses of 0.5 mm, fin heights of 1.59 mm, and fin spacings of 1.0 mm. A comparison of the enhancement ratios (based on constant vapor-side temperature drop) with past Naval Postgraduate School (NPS) data showed good agreement.

The apparatus was then modified in order to study the effects of condensate inundation. Preliminary flow visualization studies of the condensate motion were made. On finned tubes, the condensate falling on the tubes has a tendency to be channeled between fins and does not spread out axially as occurs on smooth tubes.



UNCLASSIFIED	
Justification <input checked="" type="checkbox"/>	
By _____	
Distribution/	
Availability Codes	
Dist	Avail and/or Special
A-1	

TABLE OF CONTENTS

I. INTRODUCTION	1
A. BACKGROUND	1
B. CONDENSATION	1
C. HEAT-TRANSFER ANALYSIS	2
D. CURRENT TRENDS	4
E. OBJECTIVES	6
II. LITERATURE SURVEY	7
A. INTRODUCTION	7
B. CONDENSATE RETENTION ANGLE	8
C. HEAT-TRANSFER PERFORMANCE OF A SINGLE TUBE	13
1. Smooth Tube	13
2. Finned Tube	17
D. HEAT-TRANSFER PERFORMANCE INCLUDING CONDENSATE INUNDATION	19
1. Smooth Tubes	20
2. Finned Tubes	22
III. APPARATUS AND TUBES TESTED	27
A. DESCRIPTION OF APPARATUS	27
B. MODIFICATIONS TO APPARATUS FOR INUNDATION TESTS	30
C. TUBES TESTED	35

D. INSERTS	43
E. SYSTEM INTEGRITY	48
IV. SYSTEM OPERATION AND DATA REDUCTION	50
A. SYSTEM PROCEDURES	50
B. DATA REDUCTION	51
C. PROGRAM MODIFICATIONS	60
V. RESULTS AND DISCUSSION	61
A. SINGLE TUBE	61
1. Repeatability	61
2. Inside Heat-Transfer Coefficient	77
3. Outside Heat-Transfer Coefficient	79
4. Enhancement Ratios	88
5. QMC and QMCNPS Tubes	106
B. INUNDATION EFFECT	113
VI. CONCLUSIONS AND RECOMMENDATIONS	132
A. CONCLUSIONS	132
B. RECOMMENDATIONS	132
APPENDIX A SYSTEM START-UP	
AND SHUTDOWN PROCEDURES	134
APPENDIX B UNCERTAINTIES AND ASSUMPTIONS	137
APPENDIX C RAW DATA	141
LIST OF REFERENCES	143
INITIAL DISTRIBUTION LIST	148

TABLE OF SYMBOLS

a	coefficient, as defined in Equation (4.17)
a_f	coefficient for finned tube
a_s	coefficient for smooth tube
A	surface area for heat transfer (m^2)
A_c	cross-sectional flow area of test tube (m^2)
A_f	surface area of fin, including flanks and tips (m^2)
A_i	effective inside surface area of tube (m^2)
A_o	effective outside surface area of tube (m^2)
A_p	profile area of fin (m^2)
A_r	tube surface area between fins (m^2)
b	as defined in Equation (4.15)
C_1	Sieder-Tate type coefficient, as defined in Equation (4.8)
c_p	specific heat at constant pressure ($J/kg \cdot K$)
D_f	fin diameter (m)
D_i	inside diameter of tube (m)
D_o	outside diameter of tube (m)

D_1	fin root diameter (m)
e	fin height (m)
F	as defined in Equation (2.13)
F	as defined in Equation (2.16)
F^*	as defined in Equation (4.9)
F_f^*	F^* for finned tube
F_s^*	F^* for smooth tube
G	as defined in Equation (2.11)
g	gravitational acceleration (9.799 m/s ²)
h	heat-transfer coefficient (W/m ² ·K)
h_{EK}	Beatty-Katz heat-transfer coefficient (W/m ² ·K)
h_{EK}^*	modified Beatty-Katz heat-transfer coefficient (W/m ² ·K)
h_{fg}	specific enthalpy of vaporization (J/kg)
h_i	inside heat-transfer coefficient (W/m ² ·K)
h_N	heat-transfer coefficient of Nth tube (W/m ² ·K)
\bar{h}_N	average heat-transfer coefficient for a column of N tubes (W/m ² ·K)
h_{Nu}	Nusselt heat-transfer coefficient (W/m ² ·K)

h_o	outside heat-transfer coefficient (W/m^2K)
h_{of}	outside heat-transfer coefficient for finned tube (W/m^2K)
h_{os}	outside heat-transfer coefficient for smooth tube (W/m^2K)
h_1	heat-transfer coefficient of top tube in vertical column (W/m^2K)
K	dimensionless quantity, equal to $\Gamma(g/\rho_l)^{1/4}/\sigma^{3/4}$
k_c	thermal conductivity of cooling water ($W/m\cdot K$)
k_f	thermal conductivity of condensate film ($W/m\cdot K$)
k_w	thermal conductivity of tube wall material ($W/m\cdot K$)
L	length of exposed (condensing) tube (m)
L_e	effective length, defined in Equation (2.17) (m)
L_1	length of inlet portion of tube (m)
L_2	length of outlet portion of tube (m)
LMTD	log mean temperature difference (K)
m	as defined in Equation (4.14)
\dot{m}	mass flow rate (kg/s)
\dot{m}_c	mass flow rate of condensed liquid (kg/s)
\dot{m}_i	mass flow rate of inundation (kg/s)
n	as defined in Equation (4.17)

N	number of tubes in a vertical column
Nu	Nusselt number, given by $h_c D_o / k_f$
p	fin pitch (m)
p _t	tube pitch (m)
Pr	Prandtl number
Q	heat-transfer rate (W)
q	heat flux (W/m ²)
Re	Reynolds number
Re _{2φ}	two phase Reynolds number, defined in Equation (2.9)
R _i	inside resistance (m ² ·K/W)
R _o	outside resistance (m ² ·K/W)
R _v	vapor-side resistance (m ² ·K/W)
R _w	wall resistance (m ² ·K/W)
s	interfin spacing for rectangular fin (m)
s _b	interfin spacing at fin base (m)
S	as defined in Equation (2.25)
t	fin thickness for rectangular fin (m)
t _b	fin thickness at base (m)
t _t	fin thickness at tip (m)

T_c	average coolant temperature (K)
T_{con}	condensate temperature (K)
T_{film}	film temperature (K)
T_{sat}	vapor saturation temperature (K)
T_w	average wall temperature (K)
T_1	cooling water inlet temperature (K)
T_2	cooling water outlet temperature (K)
U	overall heat-transfer coefficient (W/m ² K)
U_o	overall heat-transfer coefficient, based on outside area (W/m ² K)
U_∞	free stream velocity (m/s)
V	average cooling water velocity through tube (m/s)
X	as defined in Equation (2.10)
X_f	as defined in Equation (4.13)
X_s	as defined in Equation (4.12)
α	dimensionless coefficient, defined in Equation (4.9)
α_f	dimensionless coefficient for finned tube
α_s	dimensionless coefficient for smooth tube
β	fin tip half angle (degrees)

I. INTRODUCTION

A. BACKGROUND

As technological advancements continue to enter naval vessels in the form of more powerful and capable weapon systems, the allocation of space in ship design is critical. Modern marine propulsion plants must be designed to provide maximum power with the smallest, lightest, as well as the most cost effective equipment. Heat exchangers constitute a significant portion of that equipment.

The Naval Postgraduate School (NPS), in association with David Taylor Research Center and with support from the National Science Foundation, is currently conducting research to reduce the size and weight of condensers. Present condensers are larger than actually required because of the use of smooth tubes and conservative design margins. The heat-transfer performance of all condenser tubes is limited by the thermal resistances present on the steam-side, in the tube wall, and on the water-side. By reducing any of these resistances, performance is increased and weight and size are decreased.

B. CONDENSATION

Condensation occurs in two different modes: filmwise and dropwise. Dropwise condensation, where thousands of microscopic size discrete droplets form randomly on the condensing surface. Filmwise condensation occurs when the entire condensing surface is

covered with a thin, continuous film of condensate material. Dropwise is the preferred mode because heat-transfer takes place through a much thinner effective thickness of condensate and is therefore more efficient. However, the necessary conditions for predictable, continuous dropwise condensation have not been practically obtained. Condenser design assumes that filmwise condensation will usually occur, so that a conservative margin exists in present equipment.

C. HEAT-TRANSFER ANALYSIS

The well-known relationship between temperature difference and heat-transfer rate in a heat exchanger is:

$$Q = UA(LMTD) \quad (1.1)$$

where

Q = heat-transfer rate (W),

U = overall heat transfer coefficient ($W/m^2 \cdot K$),

A = surface area for heat-transfer consistent with U (m^2), and

LMTD = log mean temperature difference (K).

The overall heat-transfer coefficient (U) is a function of the thermal resistances of the water side, the vapor side and the resistance of the tube wall. After tube material is selected, the tube wall resistance is a constant. Generally, the thermal resistance on the water side dominates. Water-side enhancement techniques include turbulence

promoters and twisted-tape inserts, however these may come with an undesirable increase in required pumping power caused by the increased internal pressure drop. In addition, these tube-side enhancement techniques may be susceptible to additional fouling. Although the vapor-side resistance is smaller than the water-side resistance, a measurable size and weight benefit may still result by using vapor-side enhancement. Vapor-side enhancement techniques include the use of low integral fins, roped tubes, fluted tubes, attached drainage strips, and dropwise promoting coatings. These methods have been reviewed by Marto [Ref. 1].

The overall heat-transfer coefficient is commonly based on outside surface area (A_o) and is denoted as U_o . Therefore, upon neglecting fouling and noncondensable gas resistances, the overall thermal resistance may be written :

$$1/(U_o A_o) = 1/(h_i A_i) + R_w + 1/(h_o A_o) \quad (1.2)$$

where

h_i = inside heat-transfer coefficient (W/m^2K),

h_o = outside heat transfer coefficient (W/m^2K),

A_o = outside surface area (m^2),

$$A_o = \pi D_r L \quad (1.3)$$

D_r = fin root diameter (m).

L = active condensing length of tube (m), and

R_w = wall thermal resistance based on outside surface area (K/W),

where

$$R_w = \ln [D_o / D_i] / (2\pi k_w L) \quad (1.4)$$

D_i = inside diameter (m), and

k_w = thermal conductivity of tube wall material (W/m·K).

The value of the LMTD in a condenser depends on the characteristics of the vapor/condensate and the cooling water flow through the tube. The saturation temperature of the vapor and the temperature of the cooling water source effectively limit the value:

$$LMTD = (T_2 - T_1) / \ln [(T_{sat} - T_1)/(T_{sat} - T_2)] \quad (1.5)$$

where

T_1 = cooling water inlet temperature (°C),

T_2 = cooling water outlet temperature (°C), and

T_{sat} = vapor saturation temperature (°C).

D. CURRENT TRENDS

Modern steam condensers are equipped with smooth tubes. To increase their heat-transfer rate, the addition of integral fins has been investigated. Wanniarachchi et al. [Ref. 2] reported that externally finned tubes have been widely used in the refrigeration industry for

many years, but that such tubes were thought to be unsuitable for use in steam condensers. This belief was based, in part, on the observation that the high surface tension of water causes liquid retention (flooding) of the bottom portion of these tubes. However, after recent research was conducted, their data and the data of other investigations have shown that extended surfaces can provide significant improvements in steam-side heat-transfer. Yau et al. [Ref. 3] and Wanniarachchi et al. [Refs. 2,4] report that for condensation of steam, under most conditions, the heat-transfer performance of finned tubes exceeds the performance expected on the basis of area increase alone.

Marto [Ref. 5] provides a comprehensive review of both experimental and theoretical developments in the study of condensation on horizontal integral-fin tubes. He states that no generalized design method exists to accurately predict the thermal performance of surface condensers operating with a bundle of horizontal finned tubes. A systematic study to determine the effects of varying fin geometry and vapor/liquid environment began at NPS in June 1982. Van Petten [Ref. 6] provides a synopsis of that research. The majority of this previous work has concentrated its focus on the performance and characteristics of single horizontal tubes. It is well known that condensation in an actual multi-tube condenser is much different than that which occurs on a single tube. Condensate

inundation is one reason for the difference. The amount of published material on the effect of condensate inundation upon finned tube performance is very small compared to that of single tubes, and most of it pertains to low surface tension fluids used in refrigerant cycles.

E. OBJECTIVES

The main objectives of this thesis were:

1. Collect steam condensation data on single horizontal tubes of differing diameters for comparison with previously obtained NPS results.
2. Modify a tube being used in a concurrent research project at Queen Mary College (University of London) and collect steam condensation data in an attempt to resolve an inconsistent trend previously observed when comparing enhancement ratios with this tube for condensation of R-113 and steam.
3. Design and construct modifications to existing apparatus to support a study of condensate inundation effects.

II. LITERATURE SURVEY

A. INTRODUCTION

During filmwise condensation, the condensate wets the solid surface and spreads out in all directions to form a continuous film. This layer forms a relatively high conduction resistance to heat transfer, as heat must be conducted through a liquid with a relatively low thermal conductivity. Additionally, this resistance increases as the film thickness increases; on smooth horizontal tubes, film thickness increases circumferentially from the top to the bottom of the tube. In order to enhance heat-transfer, this condensate film must be reduced. Thinning of the condensate film may be accomplished by the use of finned surfaces, wire-wrapped or roped tubes, and porous drainage strips. The focus of this, and recent NPS, research has been the systematic study of enhancement by the use of finned surfaces.

During film condensation on finned tubes, there are a large number of variables which can affect the heat-transfer process. The three-dimensional condensate flow pattern around the fins and off the tube, vapor shear forces, surface tension forces, wall conduction effects, and condensate retention between fins can all be important parameters. The surface of a finned tube during condensation has two distinct regions: flooded and unflooded. The presence of fins increases the condensing surface area and in the unflooded region,

surface tension forces thin the condensate film over the fin tips as well as on the fin flanks. The combined effects of surface tension and gravitational forces then cause condensate to drain down into the fin root channel, thereby exposing the maximum amount of tube surface for heat-transfer. However, in the lower, flooded portion of the tube, surface tension forces cause the condensate to be retained between the fins, decreasing the effective heat-transfer area.

The use of low integral-fin tubes for enhanced heat transfer with high surface tension fluids like water was previously considered impractical. Thick films of retained condensate on the lower portion of tubes were thought to effectively eliminate heat-transfer, but Wanniarachchi, et. al. [Ref. 7] and Yau, et. al. [Ref. 8] have reported significant enhancements for even fully flooded tubes. Apparently, in the flooded region, heat-transfer at the tips of the fins is still effective. Therefore, a more complete understanding of the processes which control heat-transfer in the flooded region must be obtained.

B. CONDENSATE RETENTION ANGLE

The condensate retention angle (Ψ) has been defined as the angle measured from the bottom of a horizontal finned tube to the place around the tube circumference where the condensate film just fills the interfin space. The term, flooding angle (Φ_f) often appears in the literature, and is the angle measured from the top of a horizontal

finned tube to the place around the tube circumference where the condensate film just fills the interfin space. Thus,

$$\Phi_f = 180 - \Psi \quad (2.1)$$

A schematic representation of retention angle is presented in Figure 2.1.

Van Petten [Ref. 6] provides a detailed account of retention angle theory, so only a short review is presented here. The first investigation of retention angle was conducted by Katz, et. al. [Ref. 9]. They developed an equation based on observations and measurements taken on various fluids under static conditions (no condensation), and found that fin geometry and fluid properties were controlling factors. Equation 2.2 shows the relationship they derived.

$$\Psi / \sin \Psi = [\sigma / (\rho_f g)] [(4D_f + 2D_r - 2s)] / [(\pi/4)(D_f^2 - D_r^2)s] \quad (180/980) \quad (2.2)$$

where:

Ψ = condensate retention angle (degrees),

σ = surface tension (N/m),

g = gravitational constant (9.799 m/s²),

ρ_f = density of condensate film (kg/m³),

D_f = fin tip diameter (m), and

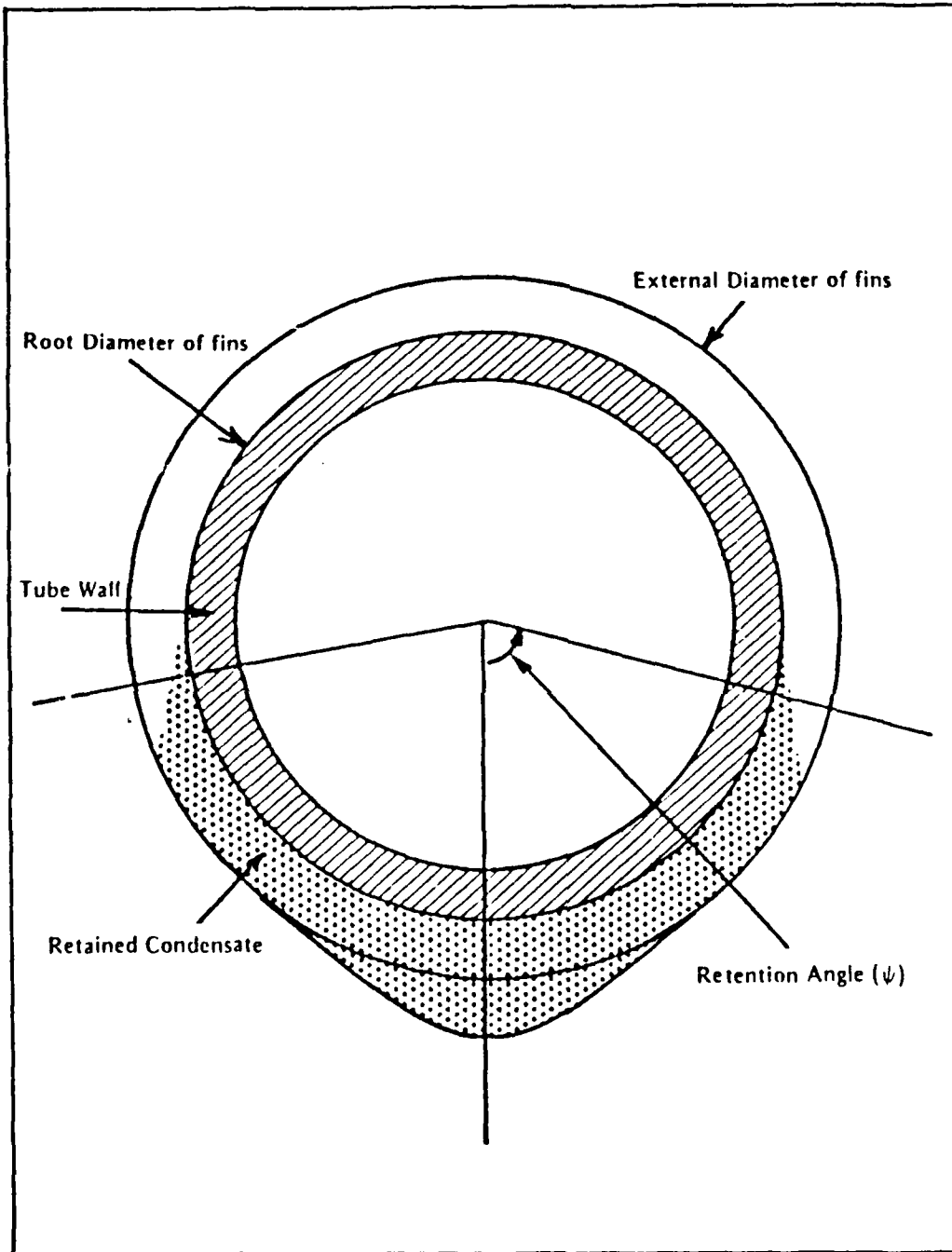


Figure 2.1 Schematic of Condensate Retention Angle on Finned Tube

s = interfin spacing for rectangular fin (m).

In the above expression, as the ratio of surface tension to condensate density is increased and as fin spacing is decreased, retention angle increases, and as fin height and spacing are kept constant, a decrease in root diameter will produce an increased condensate retention angle.

In 1981, Rudy and Webb [Ref. 10] made measurements for several fluids under both static and dynamic conditions. They confirmed the Katz, et. al. relationship and also concluded that the condensate retention angle was not altered significantly under dynamic conditions (i.e. with condensation). To account for variations in fin geometry, Rudy and Webb [Ref. 11] developed the following relationship:

$$\Psi = \cos^{-1} \left\{ 1 - \left[\frac{2 \sigma (2e-t)}{D \rho g s} \right] \right\} \quad (2.3)$$

where

e = fin height (m) and

t = fin thickness for rectangular fin (m).

This expression, shows similar effects of surface tension, to condensate density and root diameter as Equation (2.2).

A photographic study was undertaken by Honda, et. al. [Ref. 12], which confirmed the conclusion of Rudy and Webb that static and dynamic retention angles were approximately the same. They developed the following relationship:

$$\Psi = \cos^{-1}[1 - 4\sigma \cos\beta / D_f \rho_f g_s] \quad (2.4)$$

where

β = fin tip half angle (degrees).

Rudy and Webb [Ref.13] modified their previous relationship to account for the general geometry of a trapezoidal fin:

$$\Psi = \cos^{-1}\{1 - [(2\sigma(t_t + 2e - t_b)) / (D_f \rho_f g_s (t_t - s_b e - e t_b))]\} \quad (2.5)$$

where

t_t = fin thickness at tip (m),

t_b = fin thickness at base (m), and

s_b = interfin spacing at base (m).

For a rectangular fin, Equation (2.5) reduces to:

$$\Psi = \cos^{-1}[1 - 4\sigma / D_f \rho_f g_s] \quad (2.6)$$

which reduces to Equation (2.3) when $(2e - t) \sim 2e$ (i.e., fin thickness is small compared to fin height), and identical to the Honda relationship, Equation (2.4), when $\beta = 0$ degrees. As before, both Equations (2.5) and (2.6) yield a decreasing retention angle as root diameter is increased.

Masuda and Rose [Ref. 14] conducted a careful photographic study of the condensate flooding process which revealed that condensate was also retained at the base of the fin in the upper portion of the

tube, in what was previously termed, the unflooded region. They defined several separate conditions based on the meniscus profile in the interfin spacing. As a result, Masuda and Rose [Ref. 14] gave four different definitions of flooding, and stated that Equation (2.6) is valid for the most common definition. Figure 2.2 is a schematic of the four conditions which they identified. Marto et. al. [Ref. 15] observed similar condensate profiles during condensation of steam on wire-wrapped tubes.

C. HEAT-TRANSFER PERFORMANCE OF A SINGLE TUBE

1. Smooth Tube

The basis for analysis of laminar film condensation on a horizontal tube was formulated by Nusselt [Ref. 16] in 1916. His analysis yielded the well-known relationship for the heat-transfer coefficient:

$$h_{Nu} = 0.728 \left[\frac{k_f \rho_f g h_{fg}}{\mu_f D_o (T_{sat} - T_w)} \right]^{0.25} \quad (2.7)$$

where

k_f = thermal conductivity of the condensate film (W/m-K),

h_{fg} = latent heat of vaporization (J/kg),

μ_f = dynamic viscosity of the condensate film (N-s/m²), and

T_w = wall temperature (°C) (assumed constant around the tube).

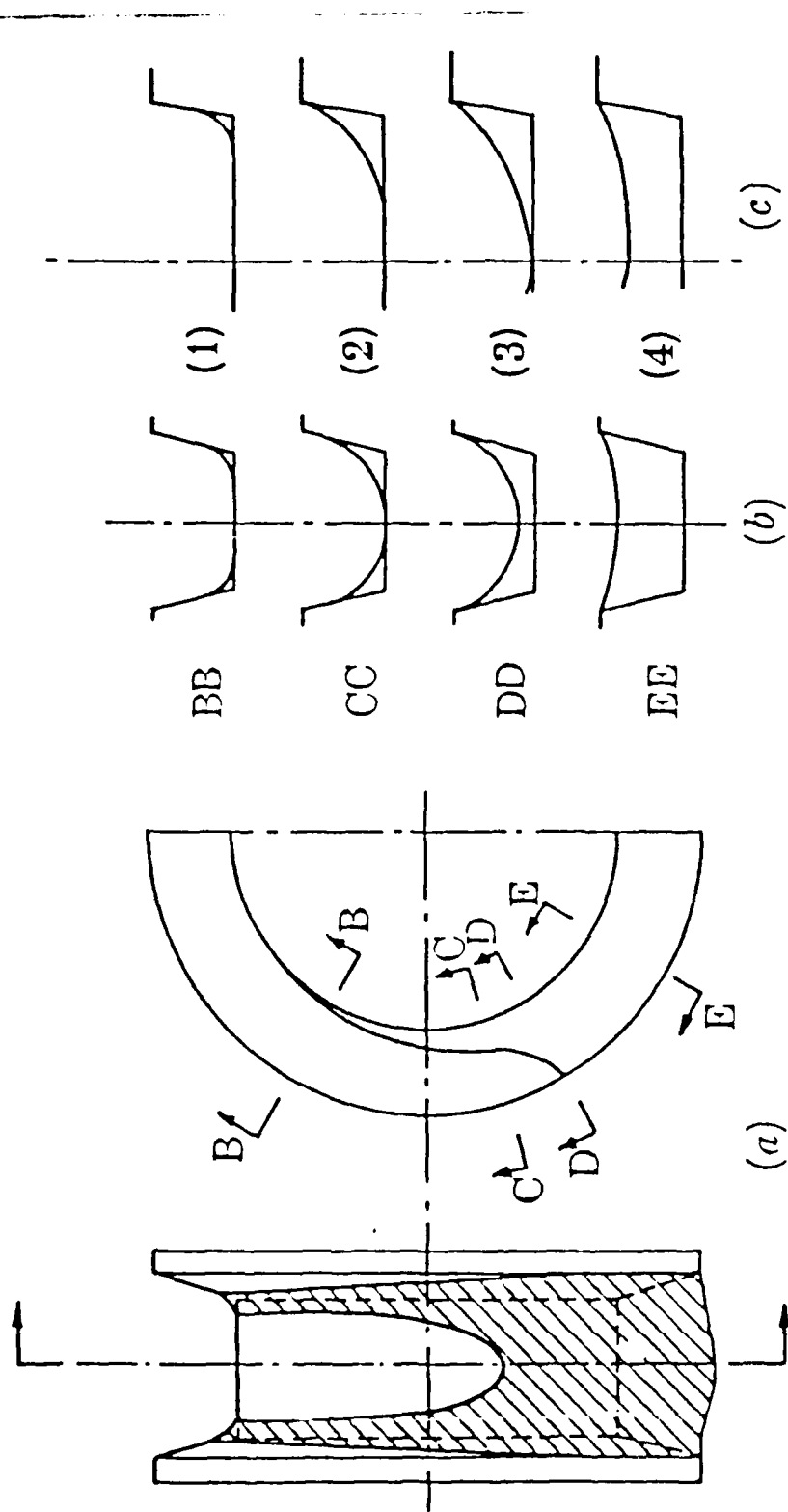


Figure 2.2 Flooding Conditions Proposed by Masuda and Rose
[Ref. 14]

As Nobbs [Ref. 17] states, the Nusselt relationship is subject to the following restrictions:

1. the wall temperature is constant
2. the flow is laminar in the condensate film
3. the film thickness is small compared to normal tube diameters
4. the fluid properties are constant within the condensate film
5. the heat-transfer in the film is by conduction
6. the forces due to hydrostatic pressure, surface tension, inertia, and vapor/liquid interfacial shear are negligible when compared to viscous and gravitational forces
7. the vapor/liquid interface and the surrounding condensate are at the saturation temperature

Hopkins [Ref. 18], who conducted research at NPS on the effect of vapor velocity, details the developments of Shekriladze and Gomelauro [Ref. 19] and Fujii et. al. [Refs. 20 and 21] in modifying the Nusselt relationship to account for vapor shear effects. Fujii et. al. [Ref. 20] theoretically investigated laminar filmwise condensation of downward-flowing vapor on a single horizontal cylinder and they developed the following expression for the average heat-transfer coefficient:

$$\text{NuRe}_{2\frac{1}{2}} = X(1+0.276FX^{-4})^{0.25} \quad (2.8)$$

where

Nu = Nusselt number given by $h_o D_o / k_f$

$Re_{2\phi}$ = two-phase Reynolds number given by,

$$Re_{2\phi} = \rho_f U_{\infty} D_o / \mu_f \quad (2.9)$$

U_{∞} = free stream vapor velocity (m/s),

$$X = 0.9(1 + 1/G)^{1/3} \quad (2.10)$$

and

$$G = ((\Delta T_f k_f) / (\mu_f h_{fg})) ((\rho_f \mu_f) / (\rho_v \mu_v))^{0.5}, \quad (2.11)$$

where

$$\Delta T_f = T_{sat} - T_w, \quad (2.12)$$

ρ_v = density of vapor (kg/m^3),

μ_v = dynamic viscosity of the vapor ($N \cdot s/m^2$), and

$$F = g D_o \rho_f h_{fg} / (U_{\infty}^2 k_f \Delta T_f) \quad (2.13)$$

After considering the more general case of approach velocities in a tube bundle, Fujii et. al. [Ref. 21] arrived at the following empirical correlation:

$$Nu Re_{2\phi} = 0.96 F^{1/5} \quad (\text{for } 0.03 < F < 600) \quad (2.14)$$

2. Finned Tube

Marto [Ref. 5] and Van Petten [Ref. 6] both provide an extensive review of the development of horizontal finned tube heat-transfer, so just a brief description is provided here.

Beatty and Katz [Ref. 22] were the first to develop a simple analytical model to predict the condensing heat-transfer coefficient on a horizontal finned tube. They combined the Nusselt models for vertical plates and smooth horizontal tubes and derived the following:

$$h_{EF} = 0.689 F^{0.25} [(A_r/A_c)(1/D_r)^{0.25}] + 1.3 \eta_f (A_f/A_c)(1/L_e)^{0.25} \quad (2.15)$$

where

$$F = ((k_f \rho_f g h_f) / (\mu_f \Delta T_{vs})) \quad (2.16)$$

and

$$L_e = \pi [(D_o^2 - D_i^2) / (4D_o)] \quad (2.17)$$

and

η_f = fin efficiency,

ΔT_{vs} = temperature drop across condensate film (K),

A_r = tube surface area between fins (m^2),

A_f = surface area of fin (m^2) (including flanks and tips),

and

A_c = total effective external surface area (m^2),

$$A_c = A_r + \eta_f A_f \quad (2.18)$$

Note that Equation (2.15) yields a heat-transfer coefficient which decreases as tube diameter is increased.

Rudy and Webb [Ref. 10] found that the Beatty-Katz model overpredicted results for high surface tension fluids. They tried to use the Beatty-Katz expression for the unflooded region only and neglected all heat-transfer in the flooded region:

$$h_{EF}^* = ((180-\Psi)/\Psi)h_{EF} \quad (2.19)$$

where

h_{EF}^* = modified Beatty-Katz heat-transfer coefficient ($W/m^2 \cdot K$)

Owen et al [Ref. 23] concluded that the Rudy-Webb model underpredicted experimental results because of the assumption that no heat-transfer took place in the flooded region. His model attempted to include heat transfer in the flooded region but provided only slightly improved results. These analyses neglected completely the effect that surface tension forces play in thinning the condensate film.

Marto [Ref. 6] points out that the first analysis to recognize the contribution of surface tension forces was Karkhu and Borovkov [Ref.

24). Webb et. al. [Ref. 25] re-examined the Beatty-Katz model and concluded that in the unflooded portion of the tube, surface tension, not gravity, was the controlling factor in the movement of condensate. They proposed a simplified surface-tension-driven model on the fin flanks, but this theoretical result did not agree well with experimental results. Therefore, Webb et. al. [Ref. 25] made further modifications using the mathematical development of Adamek [Ref. 26] and obtained results which were slightly better than in their previous model.

Honda et. al. [Ref. 27] have also recently produced a prediction model which shows considerable promise. However, it entails an intensive computer-solved iteration procedure that is rather cumbersome to use. In addition, the probability that actual processes occurring on a flooded tube are more complex than can be explained in a one- or two-dimensional conduction model is apparent. A more practical, simplified model, that is adaptable to universal design use, is required.

D. HEAT-TRANSFER PERFORMANCE INCLUDING CONDENSATE INUNDATION

Morrison [Ref. 28] and Brower [Ref. 29] were involved in previous NPS research on the effects of condensate inundation on enhanced condenser tubing. They provide a comprehensive review of the pertinent literature up through 1985.

1. Smooth Tube

Jakob [Ref. 30] extended the Nusselt analysis to film condensation on a vertical in-line column of horizontal tubes by assuming that all the condensate from a tube drains as a laminar sheet onto the tube beneath. For this ideal condition, the average coefficient for a vertical column of N tubes was predicted as:

$$\bar{h}_N = 0.728[(k_f^3 \rho_f^2 h_{fg}) / (D_o N \mu_f (\Delta T_f))]^{0.25} \quad (2.20)$$

When Equations (2.7) and (2.20) are combined, the Nusselt theory for the average coefficient for a column of N tubes compared to the coefficient of the top tube (h_1) gives:

$$\bar{h}_N / h_1 = N^{-1/4} \quad (2.21)$$

Kern [Ref. 31] realized that condensate does not flow in a laminar sheet, but by discrete droplets or columns. He proposed a less conservative expression to account for the disturbances in the condensate film. The Kern relationship is:

$$\bar{h}_N / h_1 = N^{-1/6} \quad (2.22)$$

Eissenberg [Ref. 32] conducted experimentation with a staggered tube bundle which included the effects of steam velocity, condensate inundation, and noncondensable gases on the condensation heat-transfer coefficient. As a result of his investigations, he developed a side-drainage model. In this model,

condensate may drain to tubes that are not directly below one another.

This side drainage could be influenced by:

1. bundle orientation - triangular spaced arrays are more susceptible to side drainage than are inline tube arrays
2. tube pitch - as it becomes smaller, side drainage should occur more frequently
3. momentum - the greater the horizontal momentum of a drop leaving the tube, the greater is its tendency to undergo side drainage
4. vapor velocity and direction - the more horizontal it is, the more lateral momentum it will impart
5. tube alignment - a tube misaligned in a bundle may receive and then release a greater or lesser amount of condensate

If the condensate drains purely by side drainage, Eissenberg's model predicted:

$$\overline{hN}/h_{Nu} = 0.60 + 0.42N^{-1/4} \quad (2.24)$$

Figures 2.2 a,b,c depict the three models theorized by Nusselt, Kern, and Eissenberg, respectively. Figure 2.3 is a graphical representation of the three theories with a superimposed spread of experimental data.

Nobbs [Ref. 17], although unable to find a general correlation for his experimentation on the combined effects of vapor velocity and

condensate inundation in a tube bundle, did supply the following conclusions:

- vapor velocity increases the condensate heat-transfer coefficient on both inundated and uninundated tubes
- the effect of inundation generally reduces the heat-transfer coefficient
- the condensate drainage path is often not vertically downwards, but is in a diagonal direction, particularly in triangular-shaped arrays

Because experimental results vary considerably, results have been fitted to an equation using the following form:

$$\overline{h_N}/h_1 = N^{-S} \quad (2.25)$$

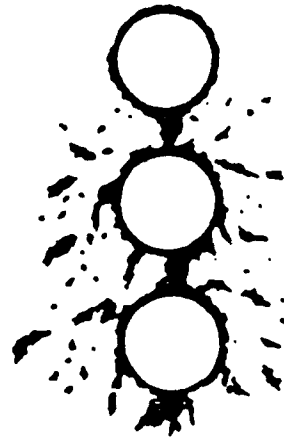
where S is determined empirically. Reported values of S vary in the range of 0.07 to 0.20.

2. Finned Tubes

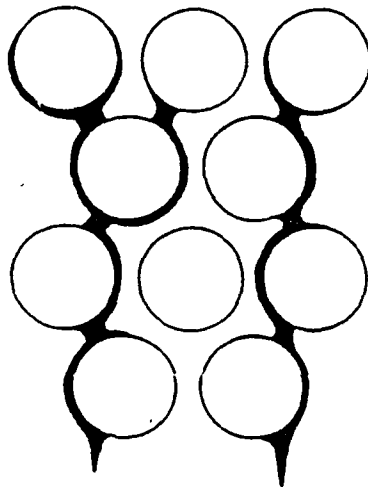
Very little data has been published for finned tubes, most of which details refrigerants and small tube bundles. Marto [Ref. 5] provides an accounting of published works which indicate that inundation effects are less for finned tubes. Most recently, Honda et. al. [Ref. 33] performed experiments using R-113, methanol, and normal propanol to study the characteristics of falling condensate on a vertical column of horizontal low finned tubes. They reported the observation of four major flow modes: droplet, column, column and



(a)



(b)



(c)

Figure 2.3 Schematic Representations of Condensate Flow

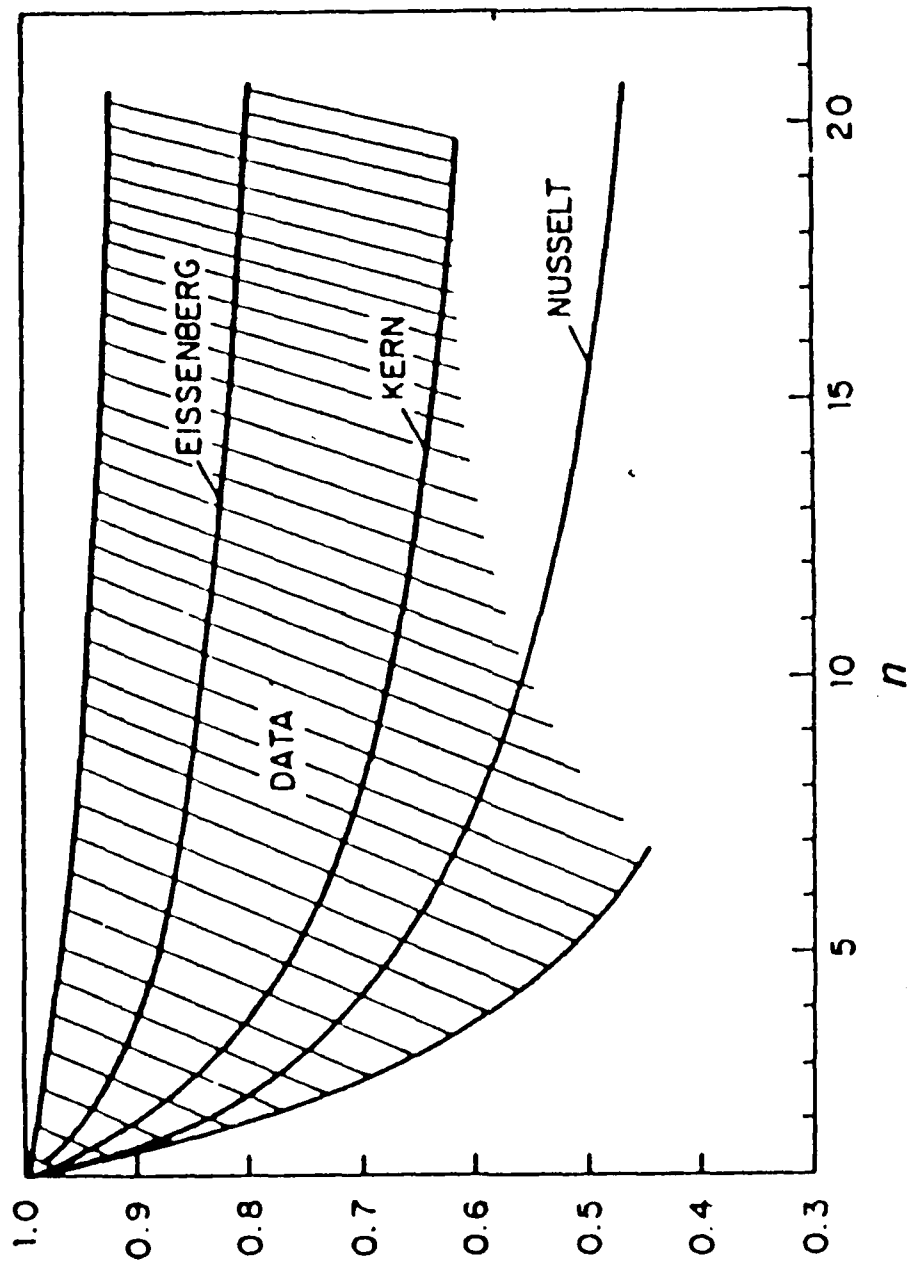


Figure 2.3 The Effect of Condensate Inundation on Smooth Tube Performance

sheet, and sheet as inundation flow rate was increased. Flow mode transition was associated with the value of a dimensionless group, K:

$$K = \Gamma(g/\rho_1)^{0.25}/\sigma^{0.75} \quad (2.26)$$

where

Γ = liquid film flow rate per unit length from one side of the tube (kg/m·s).

Photographs, as well as visual observations, showed that at relatively low rates of inundation, liquid droplets or columns fell from an upper tube onto a lower one and flowed around the tube circumference through a number of grooves between adjacent fins. Thus, the rest of the tube surface was not affected by the falling liquid. Therefore, at these low inundation rates, heat-transfer performance of finned tubes would be expected to be less affected than the performance of smooth tubes.

Honda et. al. [Ref. 34] then made heat-transfer measurements for the film condensation of R-113 on in-line bundles of both flat-side-finned (rectangular-finned) tubes and three-dimensional finned tubes (i.e. spines). The effect of vapor shear and condensate inundation were both examined. They found that the flooding level of condensate for the unaffected region of the flat-sided-finned tubes was independent of vapor velocity. Their data demonstrated that heat-transfer enhancement due to vapor shear was considerably smaller for

finned tubes than for smooth tubes, and that condensate inundation was more significant for the three-dimensional-fin tube than for the flat-sided-finned tube.

III. APPARATUS AND TUBES TESTED

A. DESCRIPTION OF APPARATUS

The test apparatus used to conduct the single tube studies was identical to that utilized by Van Petten [Ref. 5], and is shown in Figure 3.1. It consisted of a boiler, glass piping, auxiliary condenser, purging system, and test section. The boiler was made from a 0.3048 m diameter Pyrex glass section circumferentially fitted from below with ten 4kW, 440V, Watlow immersion heaters. Vapor produced there flowed upward through a 2.44 m long section of 0.152 m Pyrex glass piping; it negotiated a 180 degree turn and then travelled downward through a 1.52 m long section of Pyrex glass piping before arriving at the test section. The test section, Figure 3.2, was fabricated from stainless steel with nylon and Teflon fittings to support the test tube and provide cooling water connections. Cooling water to the test tube was pumped from a sump tank and its flow rate was controlled by a throttle valve at the flowmeter inlet. A continuous flow of filtered tapwater was supplied to the water sump. A manometer and thermocouple placed just above the test tube provided vapor pressure and temperature readings. A circular viewing port allowed visual observation of the condensing process. The auxiliary condenser, located directly below the test section, consisted of two concentrically wound copper coils inside Pyrex glass piping. Auxiliary cooling water

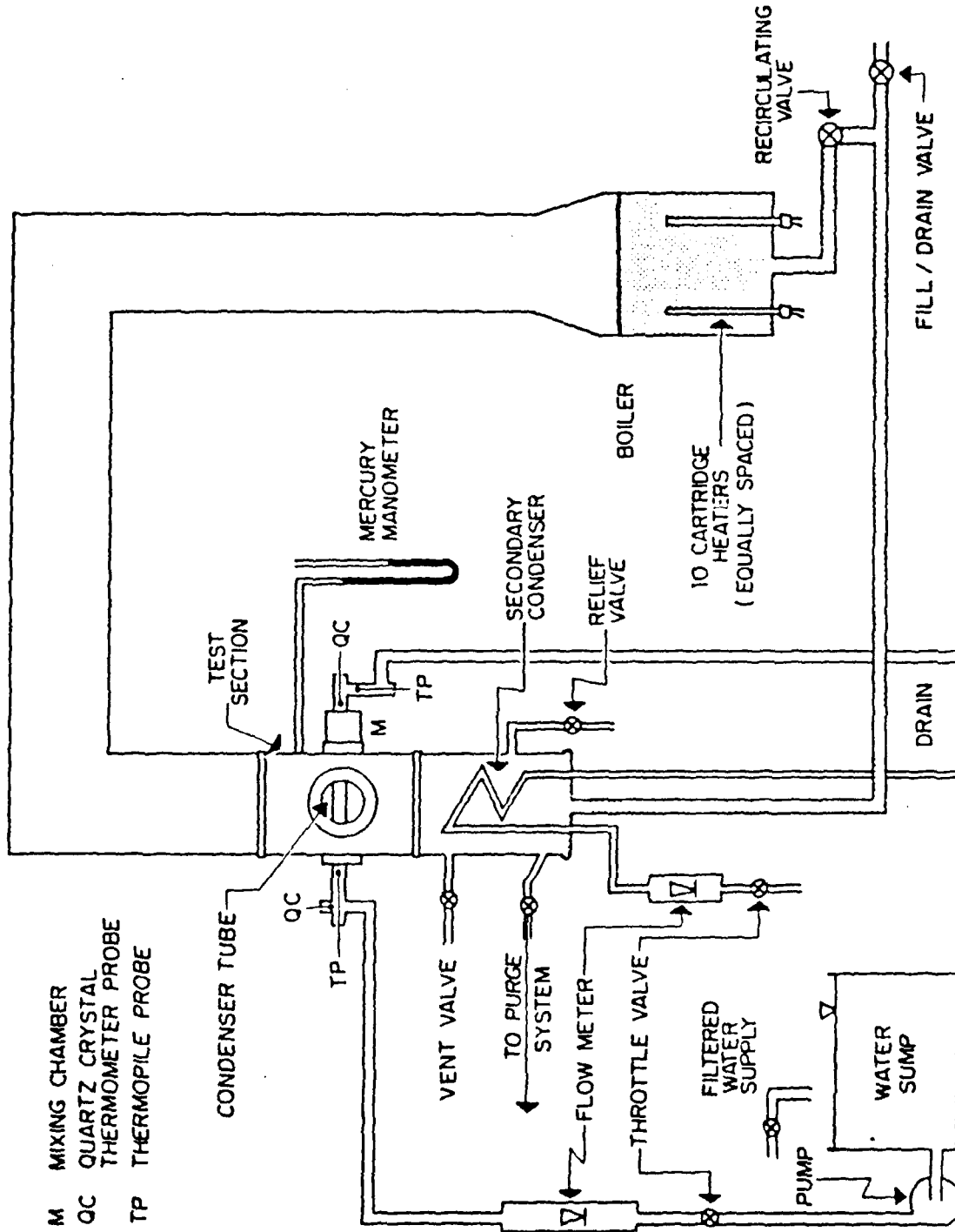


Figure 3.1 Schematic of Single Tube Apparatus

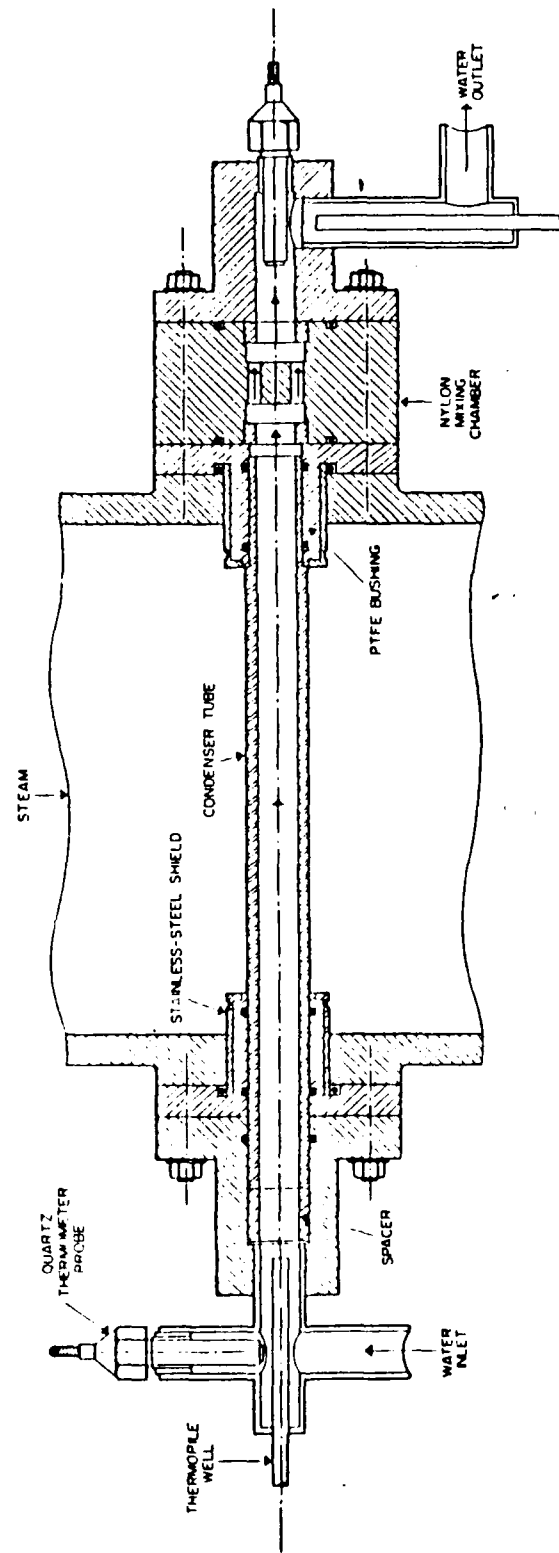


Figure 3.2 Schematic of Test Section (Insert Removed)

was supplied by tapwater throttled at the inlet of a flowmeter. The purging system consisted of copper tubing, a copper coil, Plexiglass cylinder, and a vacuum pump. Gases drawn by the pump left the auxiliary condenser through the copper tubing and flowed into the copper coil which was situated inside the cooling water sump. It was hoped that heat exchange here would condense any residual working vapor before it reached the operating vacuum pump. The noncondensable gases and residual working fluid were collected in the Plexiglass cylinder and the fluid was emptied using a drain valve at the conclusion of each data set. The gases were sucked to the top of the container and drawn into the vacuum pump. Figure 3.3 is a schematic of the purging system. Other system details can be found in [Refs. 6, 18, 35, 36, 37, 38, and 39].

B. MODIFICATIONS TO APPARATUS FOR INUNDATION TESTS

Modifications were made to the apparatus to allow for the study of condensate inundation. The test section used by Hopkins [Ref. 18] was used after several modifications were installed. This test section was designed to support the installation and visual observation of several in-line tubes. Removable tube sheets manufactured from Teflon (with aluminum backing plates for rigid fastening support and sealing) allowed for the possible installation of up to five tubes. Hopkins conducted his investigation using a single tube. He installed a

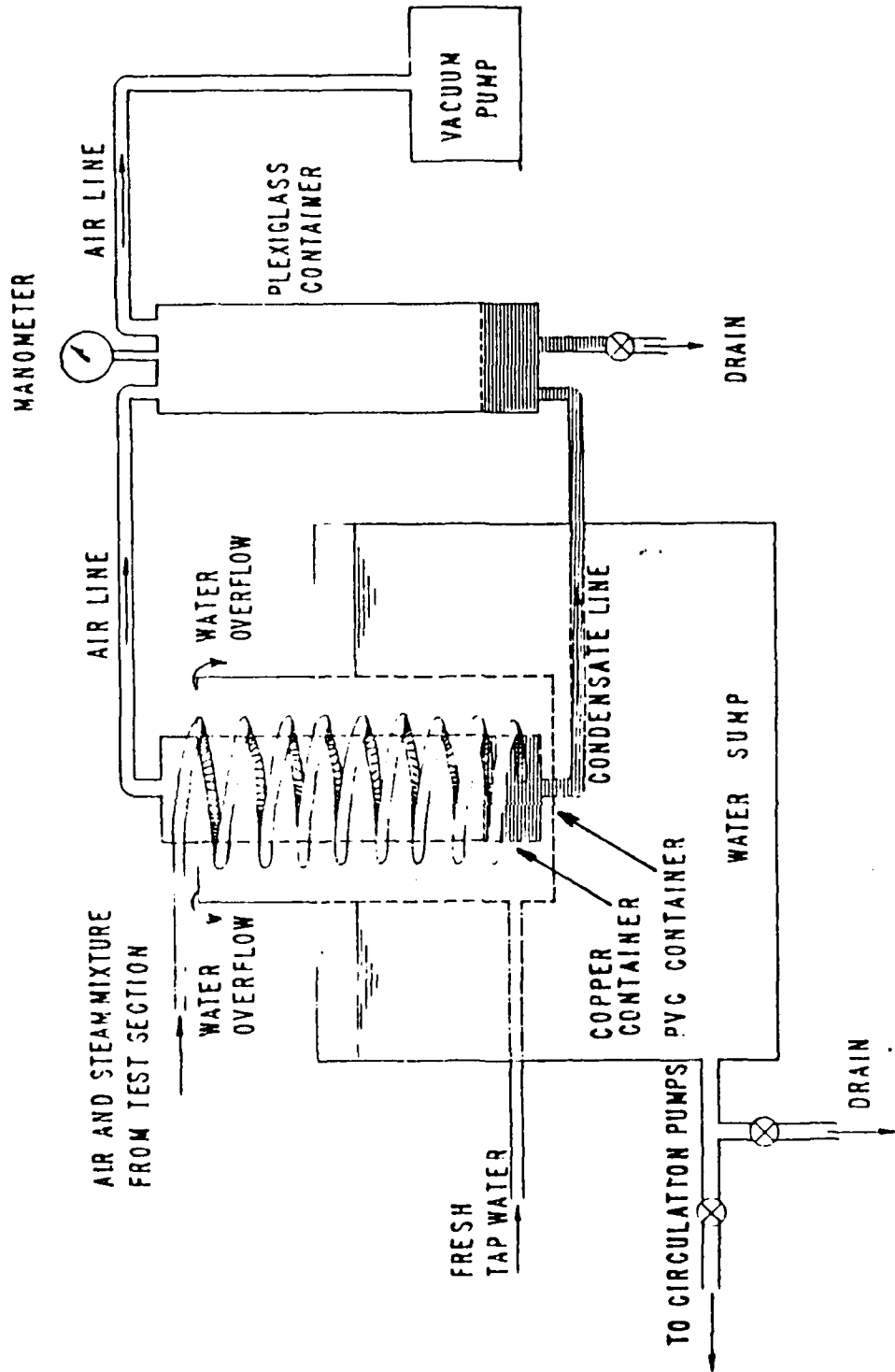


Figure 3.3 Schematic of Purging System

removable converging nozzle arrangement in order to increase the vapor velocity through the test section. This section was removed, leaving a test section almost identical to the single-tube apparatus. New inlet and outlet tube blanks were manufactured to support a pitch to diameter ratio of 1.25 for the four tubes that would be installed. A laser sighting procedure was utilized to ensure proper vertical and horizontal alignment of the four tubes within the test section. Figure 3.4 is a schematic of the test section (which looks at the tube blank side). Figure 3.5 is a cross-sectional view of the test section showing the installed tubes. The bottom tube was the active tube upon which condensation took place and for which cooling water temperature increase measurements were taken. The tube above it matched the geometric parameters exactly to ensure that the flow mode of the falling condensate would not be altered because of geometric configurational differences. The top two tubes were inundation tubes connected to a condensate return system. The original design consisted of a larger, constant speed pump throttled through two flowmeters, but operation of that configuration was plagued by cavitation of the pump. The second system, designed only for flow visualization, was capable of supporting a single inundation tube. The pump, throttling valves and flowmeters were replaced with copper and tygon tubing, and a condensate pump with a controller that accurately varied its output through a calibrated range. Condensate

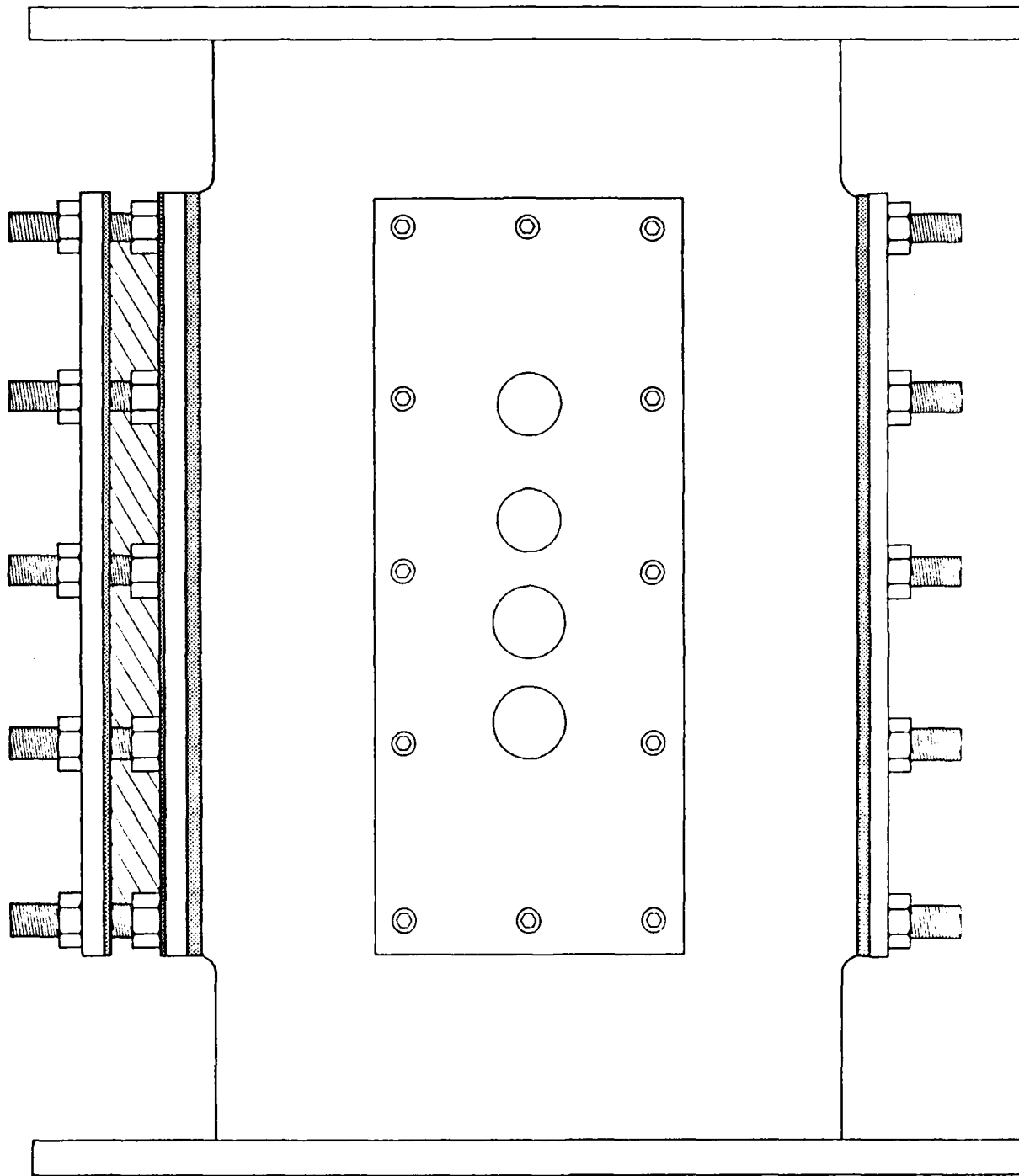


Figure 3.4 Schematic of Test Section Showing Tube Sheet

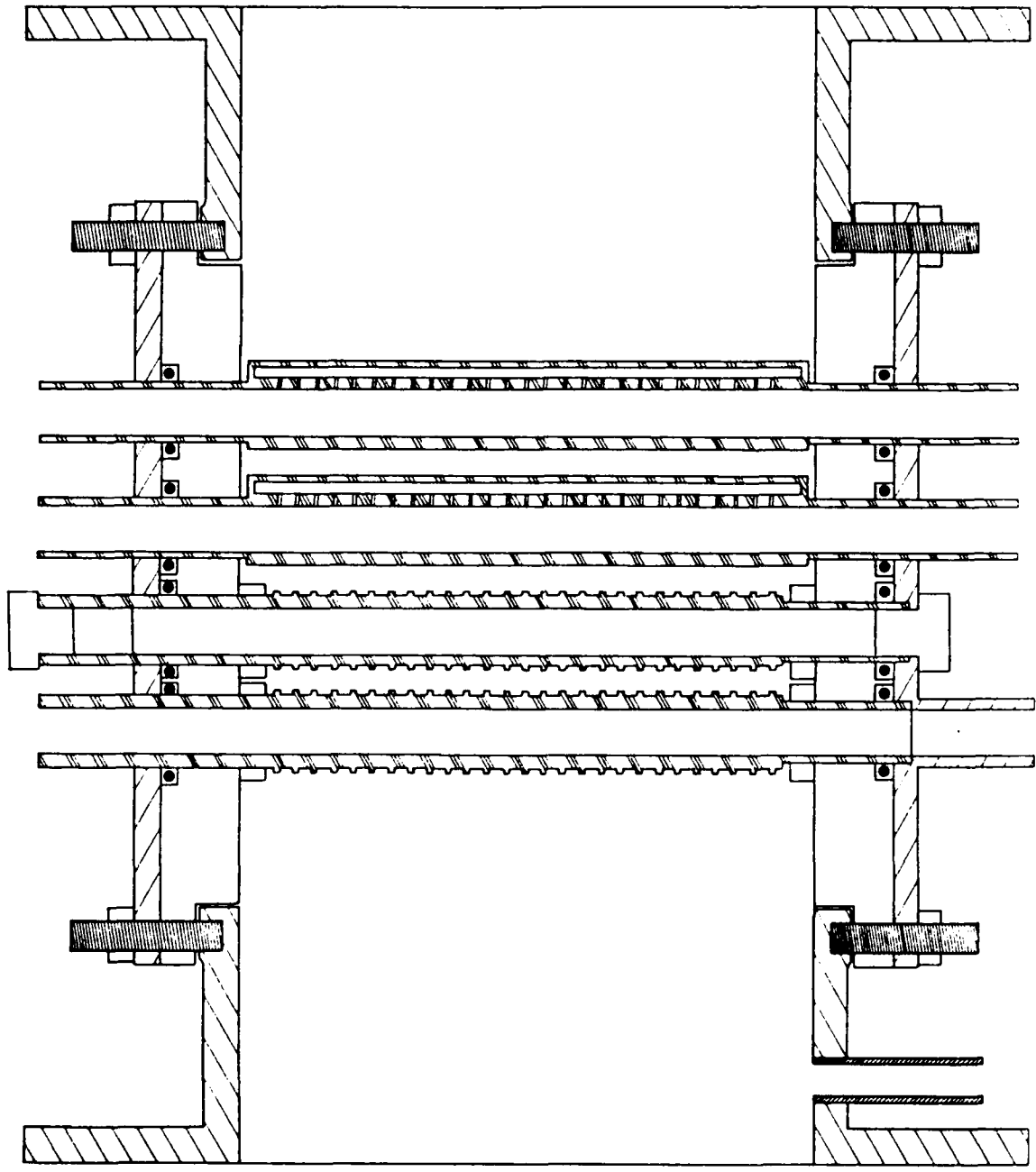


Figure 3.5 Cross - Sectional View of Test Section

was suctioned from the condensate drain line by the condensate pump and sent upward toward the test section. There it was split and approached the bottom inundation tube from both ends (on an equal pressure drop basis). The inundation tubes, pictured schematically in Figure 3.6, were manufactured so that their internal and external diameters matched the finned tubes' internal and root diameters, respectively. Condensate was forced outward through a series of 27 1.0 mm diameter holes, drilled on 5 mm centers, in the top of the tube. An umbrella/cap mounted longitudinally atop of the tube deflected all the condensate downward along the entire tube's surface where it could then freely flow down to the tubes below. This was needed to prevent geysering of the liquid at high inundation flow rates. Figure 3.7 is a photograph of both inundation tubes. The top tube is viewed from the side, clearly showing the umbrella in place. The lower tube is viewed from the top. A schematic diagram of the modified apparatus, with the original condensate return system, appears as Figure 3.8.

C. TUBES TESTED

Two smooth tubes and 14 finned tubes were to be tested with steam as the working fluid. All tubes were manufactured from copper. Of the finned tubes, 12 of them consisted of two families of six tubes each whose root diameters differed. Those with a root diameter of 12.7 mm were termed small tubes, and those with a root diameter of

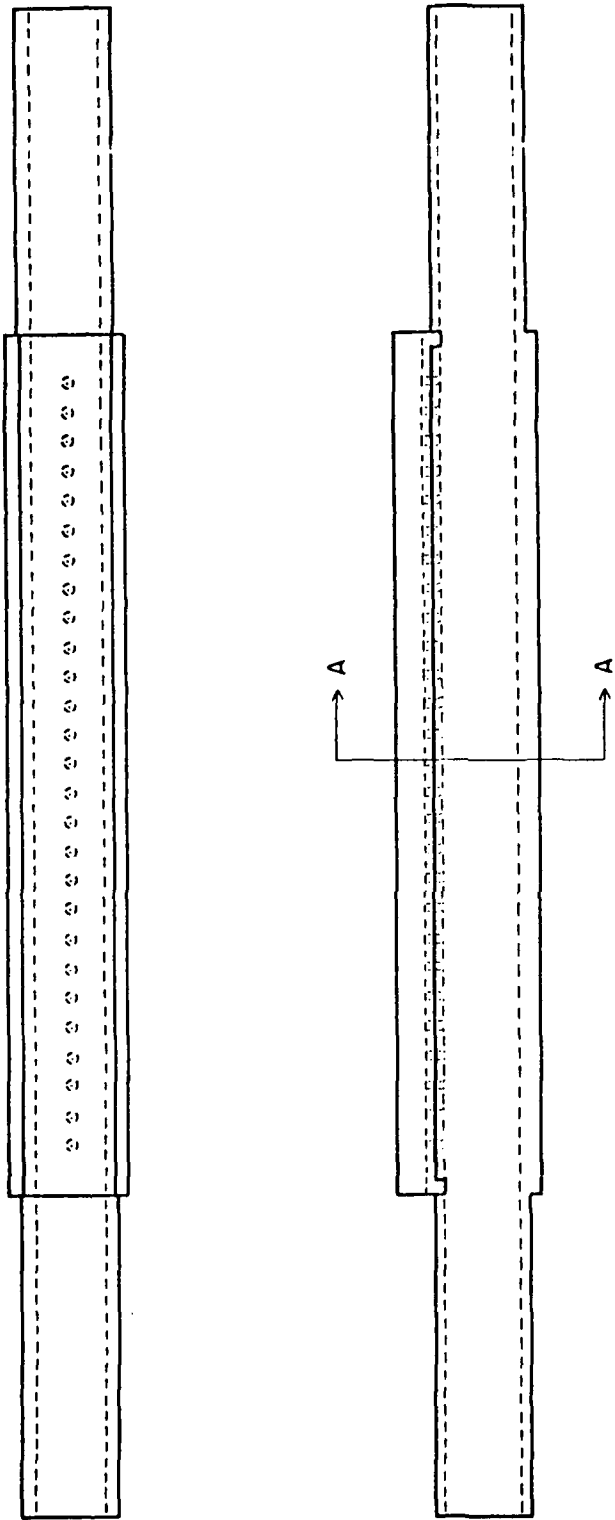


Figure 3.6 Schematic Of Inundation Tube

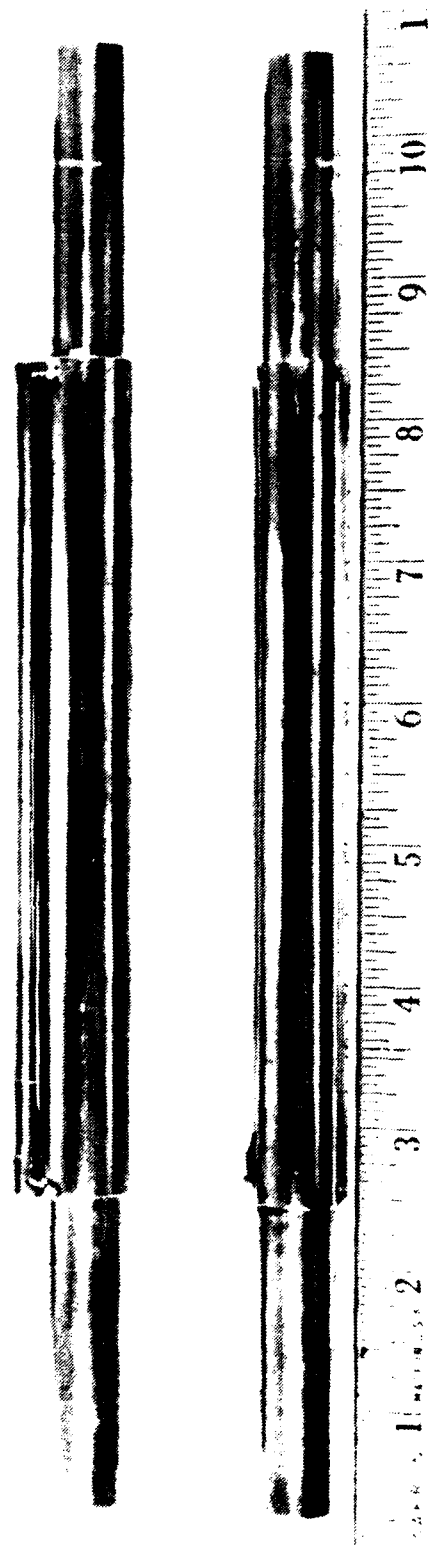


Figure 27 Photograph of Inundation Tubes

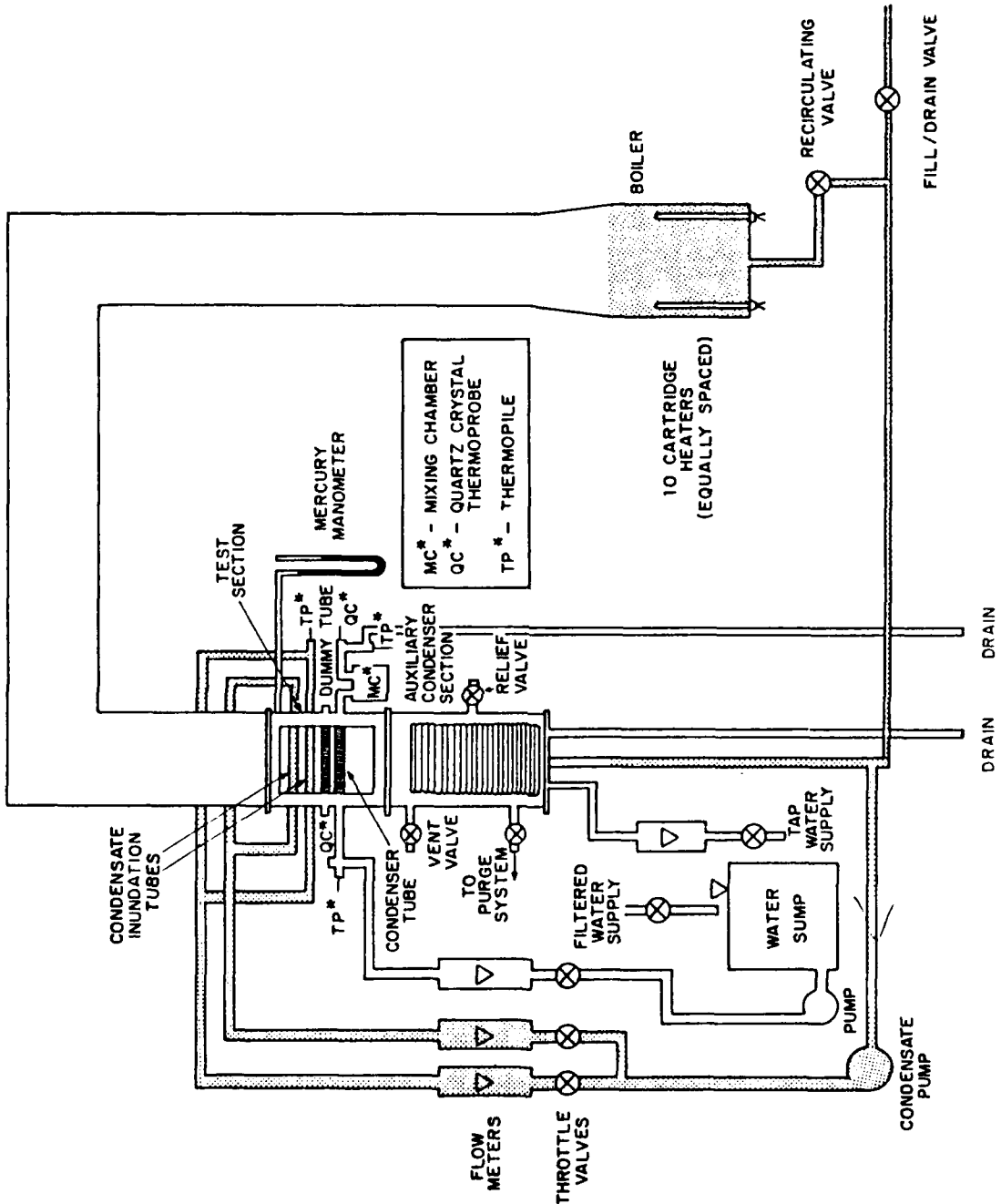


Figure 3.8 Schematic of Modified Test Apparatus

19.05 mm were termed medium tubes. Van Petten [Ref. 5] tested an additional family of tubes whose root diameter was 25.0 mm. These were known as the large tubes. Each tube in a family matched its corresponding member in the other family; fin height, thickness, and spacing were identical. These finned tubes had a fin height of 1 mm and a fin thickness of 1 mm, with fin spacings of 0.25, 0.50, 1.0, 1.5, 2.0 and 4.0 mm. Each smooth tube's outside diameter matched the root diameter of its corresponding family. Figure 3.9 is a photograph of the medium-diameter tube family and Figure 3.10 is a photograph of small- and medium-diameter tubes with a 1.50 mm fin spacing.

The remaining two finned tubes were the basis for a comparison of results being obtained in a collaborative experimental program with Queen Mary College (QMC) of the University of London. Van Petten [Ref. 6] conducted preliminary research using a tube which had been manufactured to meet the geometric specifications of the a tube being used in the QMC study (termed the QMCNPS tube). However, as he reported, data taken for R-113 and steam appeared to show unexplainable inconsistencies. Therefore, a tube that was used in the QMC study of Masuda and Rose [Ref. 40] was obtained from QMC and was then modified for use in the NPS apparatus (termed the QMC tube). Tube parameters are listed in Table 3.1. As denoted in Table 3.1, and elaborated upon in Table 3.2 there were some small differences between the QMC and QMCNPS tubes. Because of its



Figure 3.9 Medium Diameter Tube Family

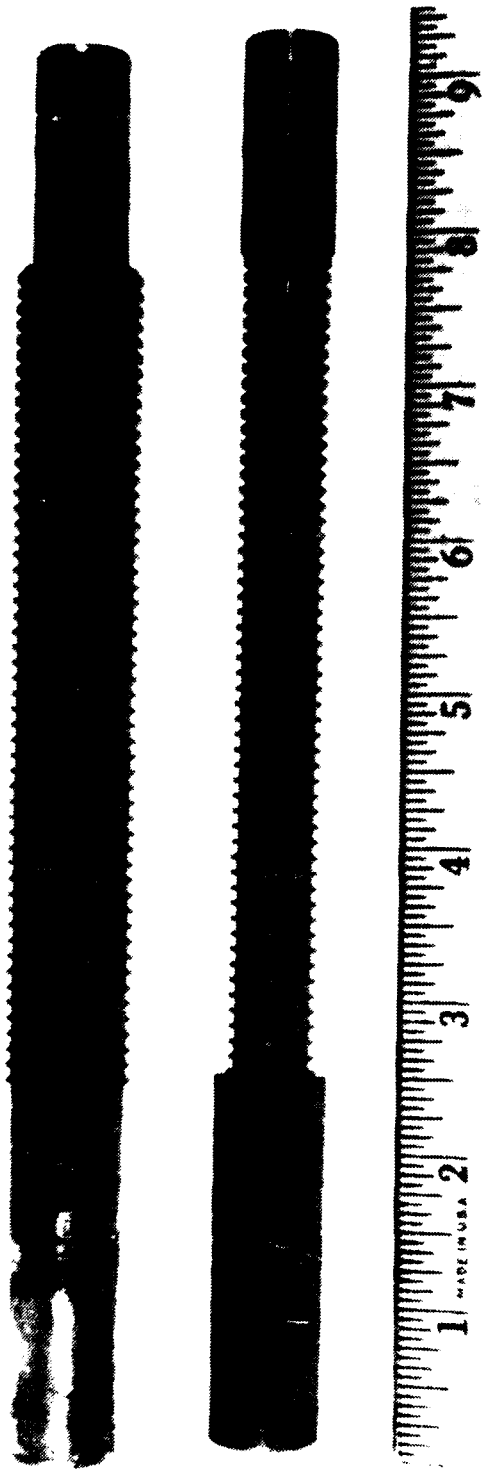


Figure 3.10 Photograph of Tubes With 1.5 mm Spacing

TABLE 3.1
DIMENSIONS OF TUBES TESTED

Tube	D_o (mm)	D_i (mm)	s (mm)	t (mm)	e (mm)
Small Smooth	12.70	9.53	-	-	-
Small Finned					
2	12.70	9.53	0.25	1.0	1.0
3	12.70	9.53	0.50	1.0	1.0
4	12.70	9.53	1.0	1.0	1.0
5	12.70	9.53	1.5	1.0	1.0
6	12.70	9.53	2.0	1.0	1.0
7	12.70	9.53	4.0	1.0	1.0
QMC*	12.60	9.84	1.0	0.5	1.59
QMCNPS*	12.70	9.53	1.0	0.5	1.59
Medium Smooth	19.05	12.70	-	-	-
Medium Finned					
8	19.05	12.70	0.25	1.0	1.0
9	19.05	12.70	0.50	1.0	1.0
10	19.05	12.70	1.0	1.0	1.0
11	19.05	12.70	1.5	1.0	1.0
12	19.05	12.70	2.0	1.0	1.0
K	19.05	12.70	4.0	1.0	1.0

* Average values, see Table 3.2 for details

TABLE 3.2
COMPARISON OF QMC AND QMCNPS TUBES

	QMC	QMCNPS
Inside diameter (mm)	9.84	9.53
Outside diameter (mm)	12.60	12.70
Overall length (mm)	167.5	228.0
Condensing Length (mm)	100.0	133.4
Fin Thickness (mm)	0.38 - 0.71	0.48-0.51
Fin Spacing (mm)	0.94 - 1.02	0.94-1.01
Fin Height (mm)	1.59	1.59

shorter overall length, the QMC tube had to be modified in order to be tested in the NPS apparatus. Adaptors were designed for each end to match the lengths of the inlet and outlet sections of the standard NPS tube and then soft-soldered in place. The QMC tube also has a shorter condensing length so insulating Teflon sleeves were placed at either side of the active condensing finned area to prevent condensation on the remaining exposed area. Finally it also had a small (~ 1 mm wide) longitudinal slot machined in the fins to accept a porous drainage plate. When tested, the tube was oriented so that this slot was at the bottom. Figures 3.11 and 3.12 are photographs of the two tubes, before and after modifications to the QMC tube, respectively. An enlarged photograph of the tube surfaces, Figure 3.13, along with the measurements presented in Table 3.2 clearly show differences in the machined quality of the two tubes.

D. INSERTS

As mentioned previously, the water-side thermal resistance can contribute substantially to the overall thermal resistance. Search [Ref. 41] reported that as much as 56% of the overall resistance could be attributed to the water-side in a Naval condenser. Therefore, in order to improve the accuracy in calculating that outside coefficient, Georgiadis [Ref. 35] designed and analyzed the use of spiral inserts for the water-side, shown in Figure 3.14.

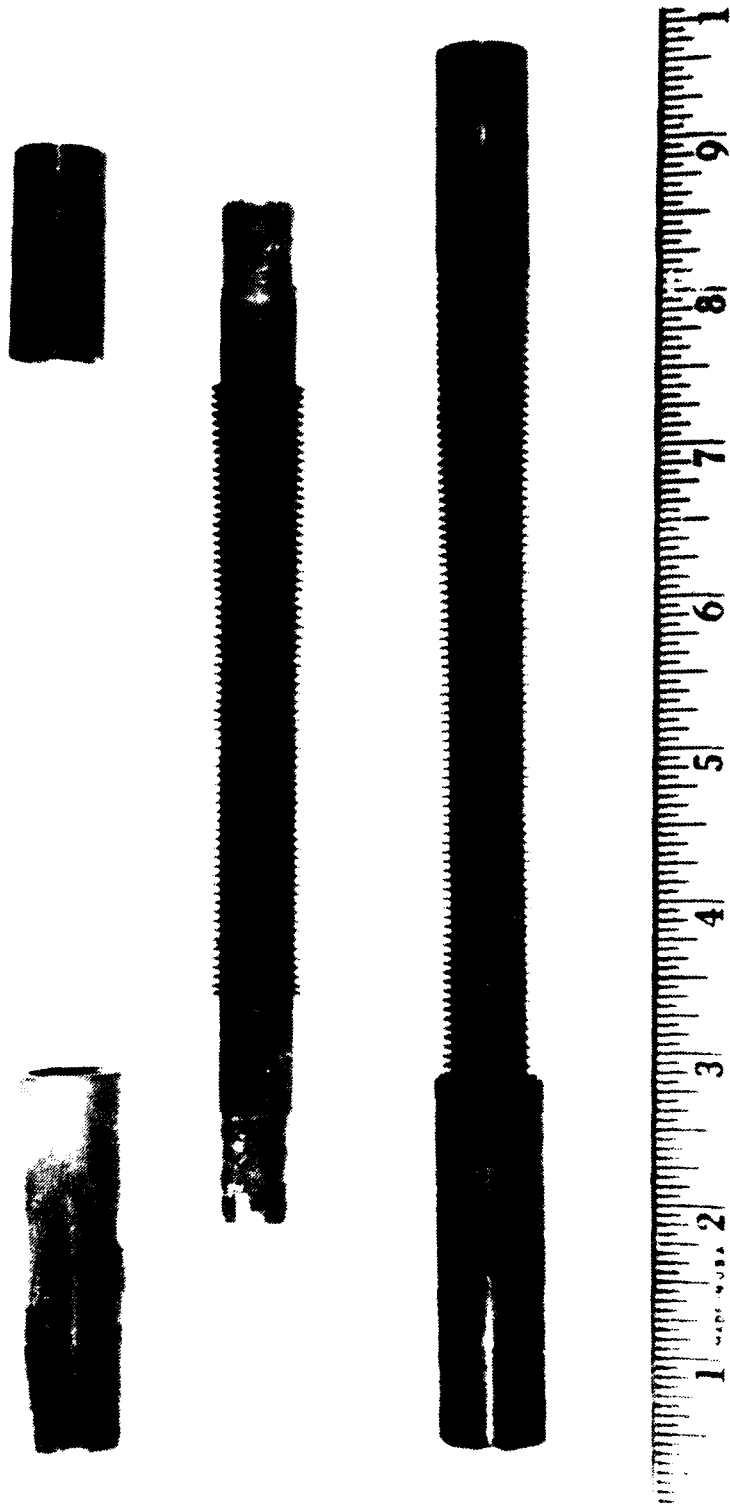


Fig. 1 QMC, Before Modification, and QMC/PS Tube

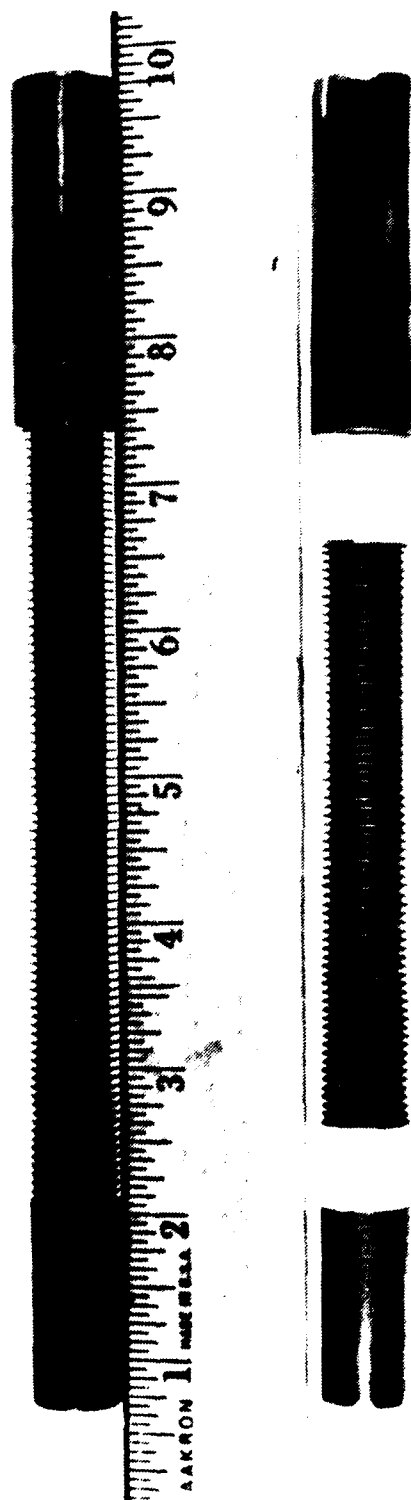


Figure 3.12. QMC After Modification, and QMCNPS Tubes.

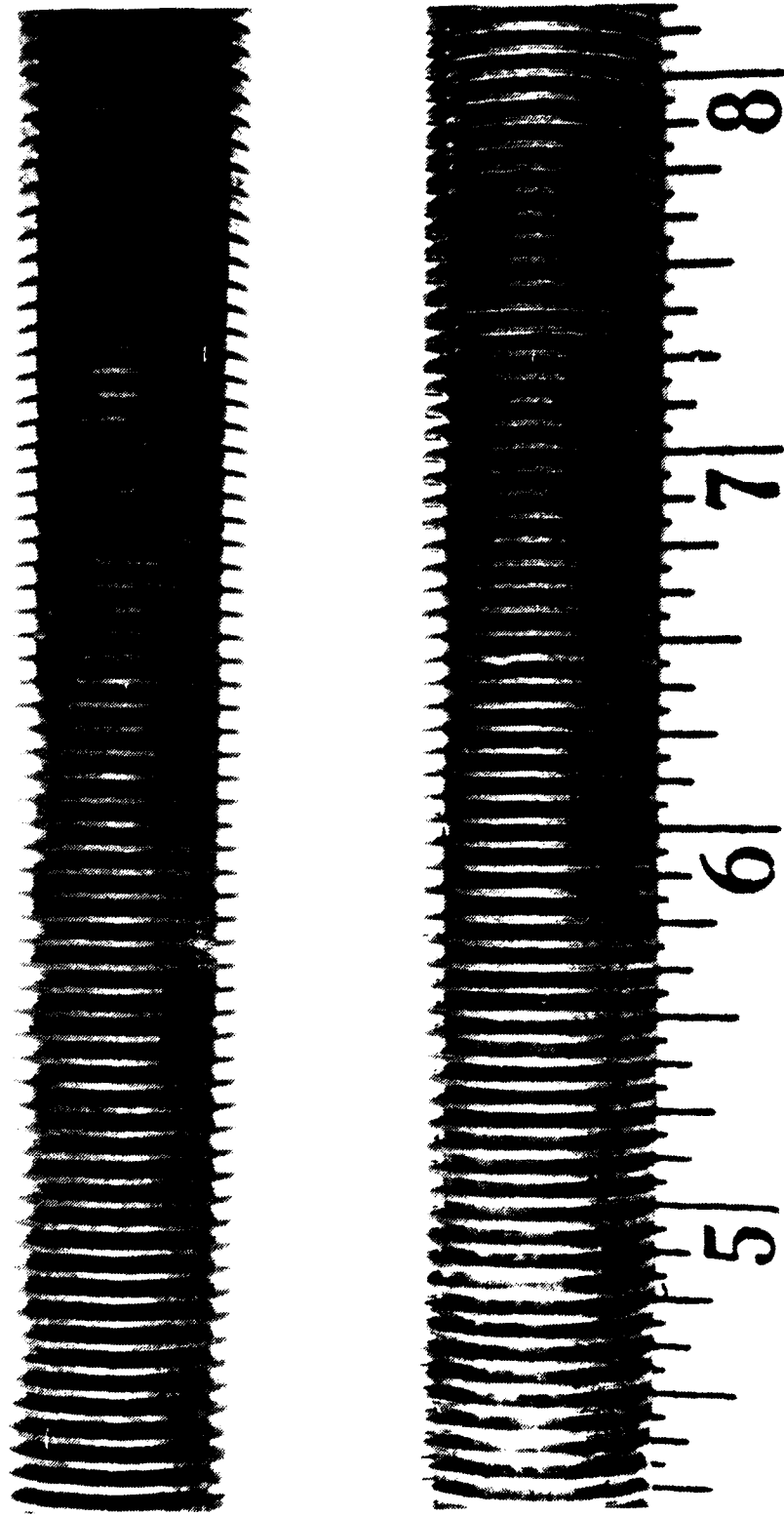


Figure 3.13 Enlargement of Machined Surfaces, QMC (Top) and QMCNPS (Bottom).

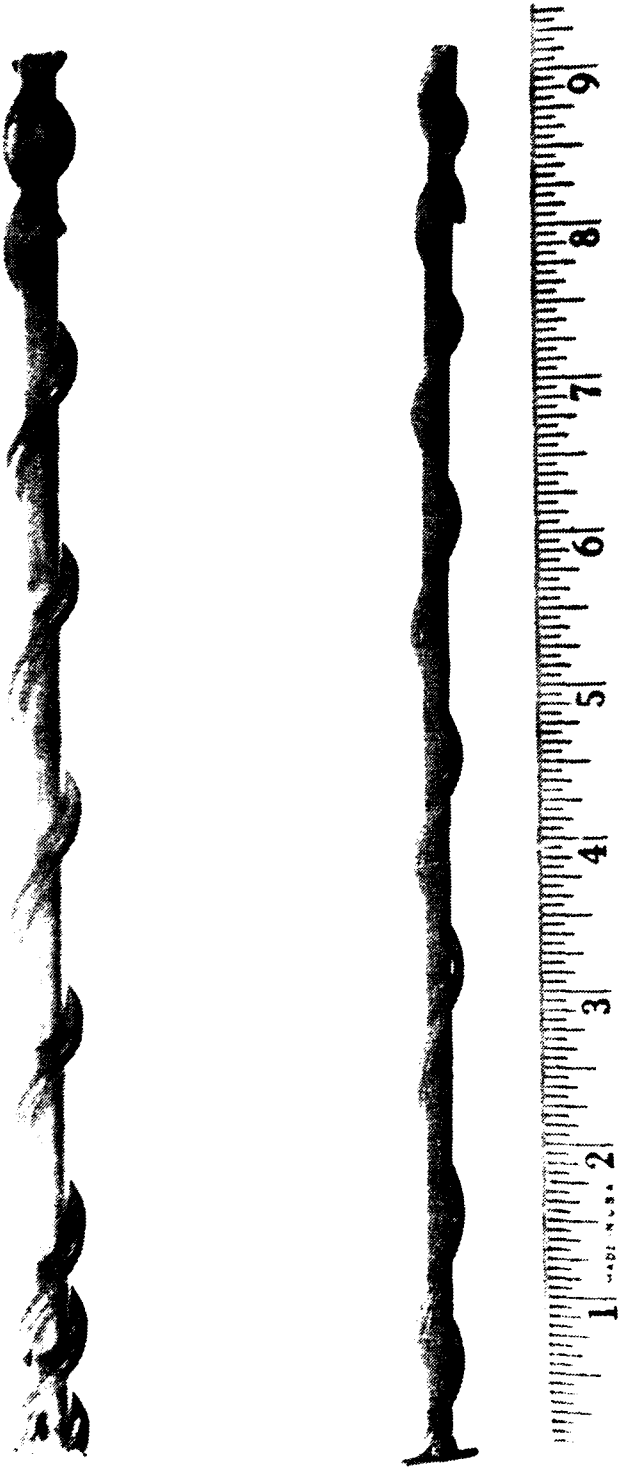


Figure 3.14 Spiral Inserts

In the absence of inside enhancement, the tube-side resistance is substantially greater than that of that vapor-side. Therefore, an error in the inside resistance results in a significantly larger error on the outside resistance. Internal enhancement also acts to reduce circumferential wall temperature variation and increases the heat transfer rate for a given cooling water velocity, which thereby reduces the relative error in total heat-transfer. The spiral insert greatly reduces thermal entrance effects and their associated uncertainties.

E. SYSTEM INTEGRITY

System integrity describes the vacuum-tightness of the test apparatus. The system had been inoperative for a period of approximately six months before this investigation, so all of the system's rubber gaskets were replaced before operations commenced. A vacuum test was periodically conducted by using the vacuum-purge system to bring the system pressure down to about 20 mm of mercury. The system was secured and the vacuum system was turned off. The manometer was closely monitored over a 24 hour period to ensure that any increase in system pressure was within prescribed limits. A leak rate from 12 - 20 mm of mercury over a 24 hour period was typical (in earlier investigations, a leak rate as low as 2 mm of mercury was sometimes obtained).

The modification of the apparatus to the inundation scheme

introduced a whole new series of potential vacuum leaks. To minimize these leaks, solder joints instead of fittings were used wherever possible, but even then the subsequent process of eliminating leaks was long and laborious. A constant source of problems was the seal around the tube sheets, this was finally solved with the installation of larger O-rings and a thicker outlet aluminum backing plate whose surface was milled flat to ensure a uniform seal of the teflon tube sheet.

The presence of noncondensable gases during the collection of data was a definite indicator of vacuum leaks. The data reduction software prompted the operator to check for the presence of noncondensables at the beginning and end of each data run. A mercury-in-glass manometer measured the absolute pressure in the test section and a thermocouple measured steam temperature. The saturation temperature corresponding to the measured pressure, and the Gibbs-Dalton ideal-gas-mixture relations were used to compute the noncondensable gas (assumed to be air) concentration. The data reduction software prompted the operator to check for the presence of noncondensables at each datum and issued a warning if the percentage exceeded programmed limits.

IV. SYSTEM OPERATION AND DATA REDUCTION

A. SYSTEM PROCEDURES

Copper has a tendency to condense steam in the dropwise mode. In order to ensure that only filmwise condensation takes place, previous investigators devised a procedure for the preparation of the tube surface. The tube's external and internal surfaces are first cleaned with a soft brush and tapwater. The tube is then suspended above a steam bath and a coating of a heated mixture containing 50% ethyl alcohol and 50% sodium hydroxide is applied to the tube surface. For an initial coating, the mixture is applied once every ten minutes for an hour. If a tube has been previously treated, the mixture is applied once every five minutes over a 20 minute period. This procedure deposits an ultra-thin, black oxide layer on the outside surface of the tube. The tube is then removed from the steam bath and thoroughly rinsed with distilled water prior to its installation in the test section. The oxide film gives the surface very high wetting characteristics and its thermal resistance is insignificant. System startup and general operating procedures are detailed in Appendix A.

System pressure, measured using a mercury-in-glass manometer, and temperature, measured with the voltage reading of the vapor thermocouple, were closely monitored in order to maintain the

desired operating conditions. Table 4.1 lists the operating conditions used during the investigation:

TABLE 4.1
OPERATING CONDITIONS

Pressure Condition	Thermocouple Reading (microvolts)	Measured Temperature (°C)	Measured Pressure (mm Hg)
Vacuum	1977	48	85
Atmospheric	4277	100	765

Once the operating temperature was established (about 45 minutes after start-up), sample data were taken to check for non-condensables and desired vapor velocity. Adjustments to system temperature were made by manually controlling the amount of cooling water through the auxiliary condenser. The viewing window allowed direct observation of the condensing process. Cooling water flow rate was manually entered for each data run. Eight different rates were employed to obtain the largest possible range of cooling water temperature rise. To demonstrate repeatability, multiple data runs were taken and results compared.

B. DATA REDUCTION

As discussed in Chapter I, the total resistance to heat transfer consists of the sum of the resistances of water-side, wall, and vapor-side. The water-side (inside) and vapor-side (outside) resistances are

convective in nature and can be represented as:

$$R_i = 1/(h_i A_i) \quad (4.1)$$

and

$$R_o = 1/(h_o A_o) \quad (4.2)$$

where

R_i = inside resistance to heat transfer (K/W),

and

R_o = outside resistance to heat transfer (K/W).

The calculation of A_i must include not only the inside surface area corresponding to the active condensing length, but also the inlet and outlet portions of the tube which lie inside the nylon bushings and act as fins to conduct heat away. Therefore,

$$A_i = \pi D_i (L + L_1 \eta_1 + L_2 \eta_2), \quad (4.3)$$

and

$$A_o = \pi D_o L, \quad (4.4)$$

A_i = effective inside area (m^2),

L_1 = length of inlet portion of tube (m),

η_1 = fin efficiency for inlet portion of tube,

L_2 = length of outlet portion of tube (m), and

η_2 = fin efficiency for outlet portion of tube.

Combining Equations (1.2), (4.1), and (4.2) gives the following expression:

$$1/U_o A_o = R_o + R_i + R_w \quad (4.5)$$

To determine the overall heat-transfer coefficient, the heat-transfer rate must be calculated. This was accomplished by measuring the inlet and outlet temperatures and the mass flow rate of the cooling water through the tube. A correction factor was applied to the outlet temperature to account for the effect of viscous heating of the cooling water due to mixing and to the induced swirl from the insert. Properties of the cooling water were calculated based on an average of the inlet and outlet temperatures. Quartz thermometer readings were used to determine the inlet and outlet temperatures. A calibrated flowmeter provided the mass flow rate. An energy balance gave:

$$Q = \dot{m} c_p \Delta T \quad (4.6)$$

where

\dot{m} = mass flow rate (kg/s) and

c_p = specific heat at constant pressure (J/kg·K).

The velocity of the cooling water through the tube was determined by the simple relationship:

$$V = \dot{m}/(\rho_c A_c) \quad (4.7)$$

where

V = test tube average cooling water velocity (m/s),

ρ_c = test tube cooling water density (kg/m³), and

A_c = cross-sectional flow area of tube (equal to $\pi D_i^2/4$) (m²).

With the value of the heat transfer rate known, and using Equations (1.1) and (1.4), the overall thermal resistance is found. Since, the wall resistance can be calculated by Equation (1.4), the two unknowns remaining in Equation (4.5) are the values for the inside and outside heat transfer coefficients, which appear in R_i and R_o , respectively. To obtain these values, a Modified-Wilson-Plot technique was employed. The alternative was the use of instrumented finned tubes fitted with wall thermocouples. Past investigations used instrumented smooth tubes and subtracted the measured inside resistance in order to get the outside resistance. A comparison of the various methods has shown that the Modified-Wilson-Plot method, when done properly, yielded results consistent with those obtained by the costlier, more time-consuming method of direct-reading, instrumented tubes.

The Modified-Wilson-Plot method requires that the form for both inside and outside heat transfer coefficients be known. To maximize

the accuracy, the inside and outside resistances should be of equal magnitude. A spiral insert was used to reduce the inside resistance. During this, and past, NPS studies, a Sieder-Tate relationship was used for the inside heat transfer coefficient:

$$h_i = C_i(k_c/D_i)Re^{0.8}Pr^{0.333}(\mu_c/\mu_w)^{0.14} = C_i\Omega \quad (4.8)$$

where

C_i = Sieder-Tate type coefficient,

k_c = thermal conductivity of cooling water (W/m·K),

Re = Reynolds number of cooling water ($\rho VD_i/\mu_w$),

Pr = Prandtl number of cooling water,

μ_c = dynamic viscosity of cooling water, evaluated at average cooling water temperature ($N\cdot s/m^2$), and

μ_w = dynamic viscosity of cooling water, evaluated at wall temperature ($N\cdot s/m^2$).

A Nusselt-type equation was used to determine the outside heat-transfer coefficient:

$$h_o = \alpha[(k_f^3 \rho_f^2 g h_{fg}) / (\mu_f D_o q)]^{1/3} = \alpha F^* \quad (4.9)$$

where

α = dimensionless coefficient, and

q = heat flux based on outside area (W/m^2).

$$q = Q/A_o \quad (4.10)$$

After the proper substitutions of Equations (4.8) and (4.9) into (4.5), the result becomes:

$$[(1/U_o) - R_w]F^* = [(A_o F^*)/(A_i C_i \Omega)] + (1/\alpha) \quad (4.11)$$

This is a linear equation with two unknowns; C_i and α . To solve for them we make the following substitutions:

$$Y = [(1/U_o) - R_w]F^* \quad (4.12)$$

$$X = [(A_o F^*)/(A_i \Omega)], \quad (4.13)$$

$$C_i = (1/m), \quad (4.14)$$

and

$$\alpha = (1/b), \quad (4.15)$$

to arrive at the following linear expression:

$$Y = mX + b \quad (4.16)$$

A least-squares fit of Equation (4.16) was then made to determine α and C_i simultaneously. An iterative procedure was required to calculate both F^* and Ω , because of their temperature dependences.

To calculate enhancement ratios, the following analysis was used,

starting with this relationship:

$$q = a\Delta T_f^n \quad (4.17)$$

After substituting

$$q = h_o \Delta T_f \quad (4.18)$$

the resulting relationship is:

$$h_o = a\Delta T_f^{n-1} \quad (4.19)$$

Nusselt theory predicts a value of 0.75 for n . Therefore, n was set to 0.75 so that the enhancement ratio, based on constant heat flux could be determined:

$$\epsilon_q = (h_{of}/h_{os}) = (a_f/a_s) = [(\alpha_f F_f^*)/(\alpha_s F_s^*)] \quad (4.20)$$

where subscripts f and s denote finned tube and smooth tube, respectively.

h_{of} = outside heat-transfer coefficient for finned tube (W/m^2K),

and

h_{os} = outside heat-transfer coefficient for smooth tube (W/m^2K).

If the heat flux across the condensate film is held constant for both finned and smooth tubes then their values of F^* will be equal, reducing Equation (4.20) to:

$$\epsilon_q = (\alpha_f/\alpha_s) \quad (4.21)$$

The values for α_f and α_s were taken directly from the Modified-Wilson-Plot analysis to calculate the enhancement ratio. For constant vapor-side temperature drop, Equation (4.21) can be replaced by:

$$\epsilon_{\Delta T} = (\alpha_f/\alpha_s)^{3/4} \quad (4.22)$$

Once determined, by using Equation (4.14), the value for the Sieder-Tate coefficient was used to calculate the inside heat-transfer coefficient and the outside heat-transfer then was calculated as:

$$h_o = \{1/[(1/U_o) - A_o/(h_i A_i) - A_o R_w]\} \quad (4.23)$$

When graphically presenting the data, least-squares fits of Equation (4.19), using values of h_o calculated by Equation (4.23), were utilized.

The effect of tube diameter appears only in F^* and therefore α should be independent of the tube diameter. Previously, Van Petten [Ref. 6] calculated enhancements for both medium and small tubes based on an α he obtained for a medium smooth tube. He did recommend that a small smooth diameter be manufactured to confirm the theoretical conclusion. A small smooth tube was fabricated during this thesis, and after testing, an α which differed slightly from the medium tube was obtained. Specific results are presented in the following chapter.

The additional calculations required for the inundation data were

minimal. In order to calculate the dimensionless parameter, K , with which Honda et. al. [Ref. 35] predicted flow mode transition, the inundation flow rate and the mass condensation rate were required. Inundation flow rate, as measured with calibrated condensate pump controller settings, was manually entered into the program. The mass condensation rate was evaluated as:

$$\dot{m}_c = Q/h_{fg} \quad (4.24)$$

where

\dot{m}_c = mass condensate rate (kg/s).

Γ could then be calculated:

$$\Gamma = (\dot{m}_c + \dot{m}_i)/(2L) \quad (4.25)$$

where

\dot{m}_i = inundation flow rate (kg/s).

K could then be calculated using Equation (2.26). Visual observations were made as inundation rate was increased in an attempt to observe the predicted flow modes of droplet, column, column-sheet, and sheet.

C. PROGRAM MODIFICATIONS

The modifications to the program utilized by Van Petten [Ref. 6] included.

1. additional tube diameter variable was added for the QMC tube

2. exponent for Reynolds number in the Sieder-Tate equation was allowed to vary at operator's discretion
3. an alternate relationship for the inside heat-transfer coefficient was provided as an option to the operator
4. α for small smooth tube was added and used to calculate enhancement ratios for small, QMC, and QMCNPS tubes
5. required inundation inputs and calculations were incorporated
6. comments were liberally added to make the program more user-friendly

V. RESULTS AND DISCUSSION

A. SINGLE TUBE

1. Repeatability

Data were obtained for those tubes described in Chapter III and detailed in Tables 3.1 and 3.2. Investigation began with testing of the medium diameter tubes. As data were collected, comparisons were immediately made with Van Petten [Ref. 6], which ensured validity as well as repeatability. The curves on all figures of outside heat-transfer coefficient vs. wall temperature difference are a least-squares fit of:

$$h_o = a\Delta T_f^{0.25} \quad (5.1)$$

Figures 5.1, 5.2, and 5.3 compare selected data for medium diameter tubes under vacuum conditions and Figures 5.4, 5.5, and 5.6 show similar data under atmospheric conditions.

Figure 5.2 also shows typical uncertainty bands associated with the data. Uncertainty is much greater for the low cooling water flow rates. As cooling water flow rate is increased, the difference between vapor and wall temperature increases, the outside heat-transfer coefficient decreases, and the uncertainty decreases. Appendix B gives a brief description of the uncertainty analysis employed.

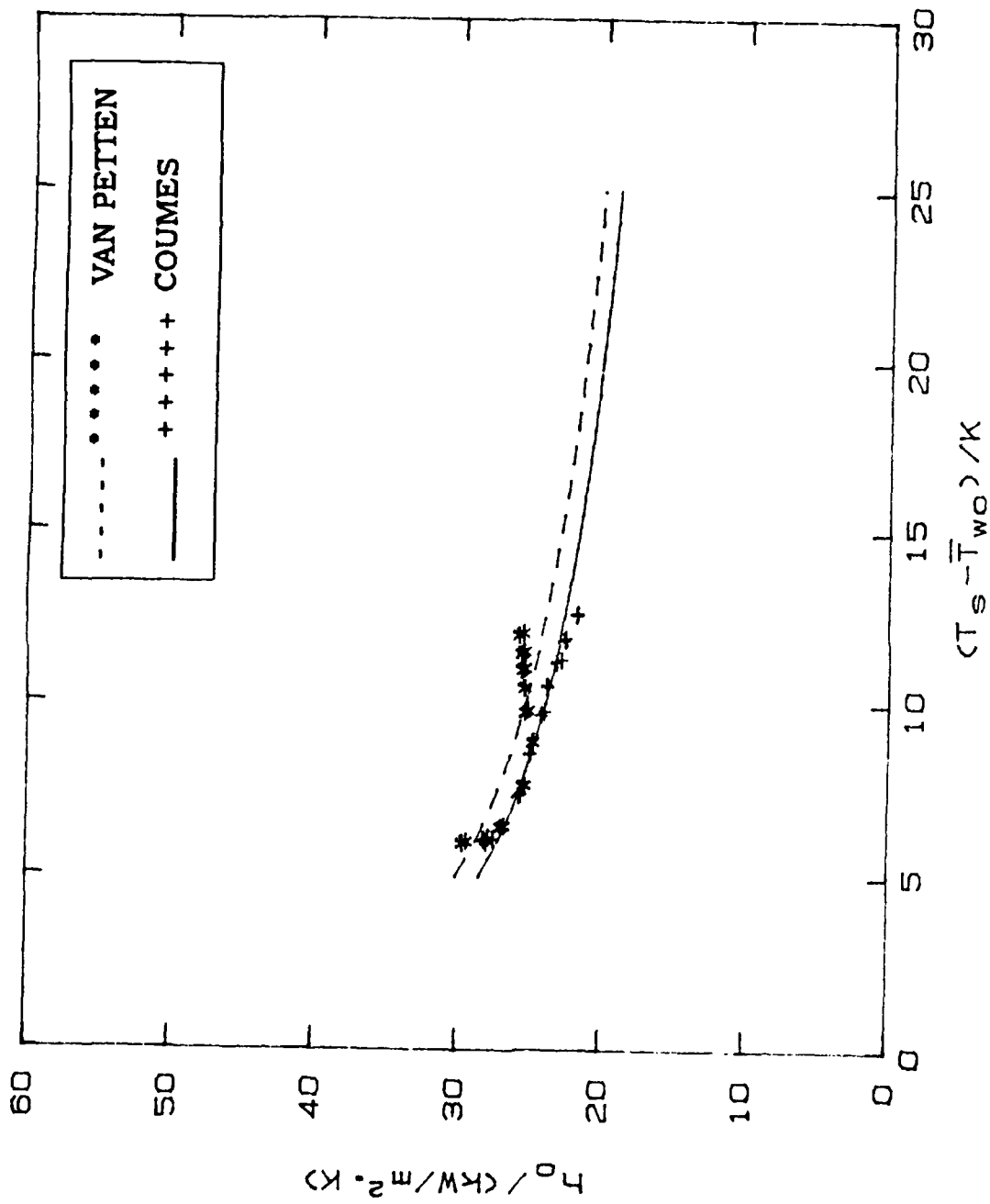


Figure 5.1 Repeatability of Tube 8 Under Vacuum Conditions

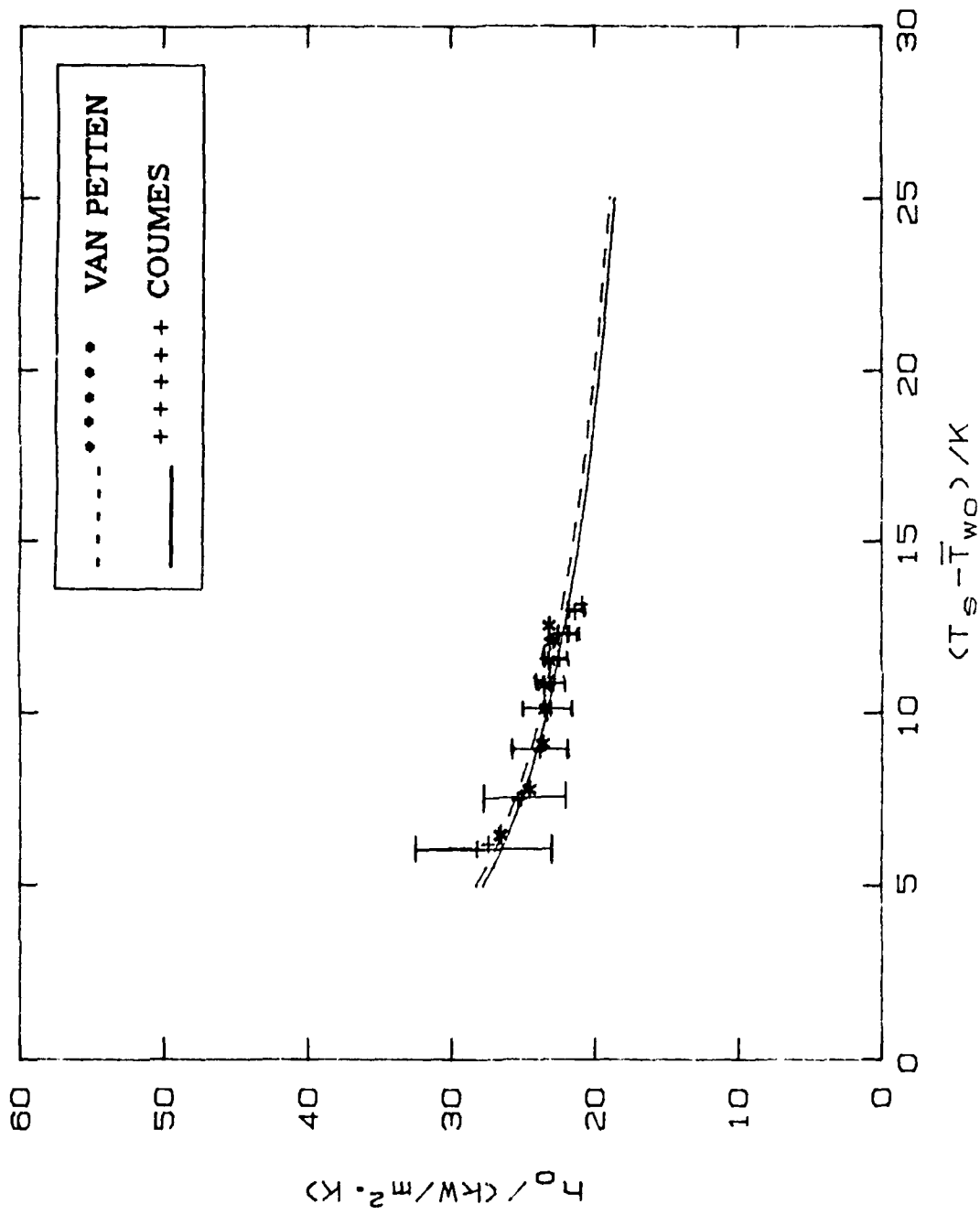


Figure 5.2 Repeatability of Tube 9 Under Vacuum Conditions Showing Uncertainty Bands

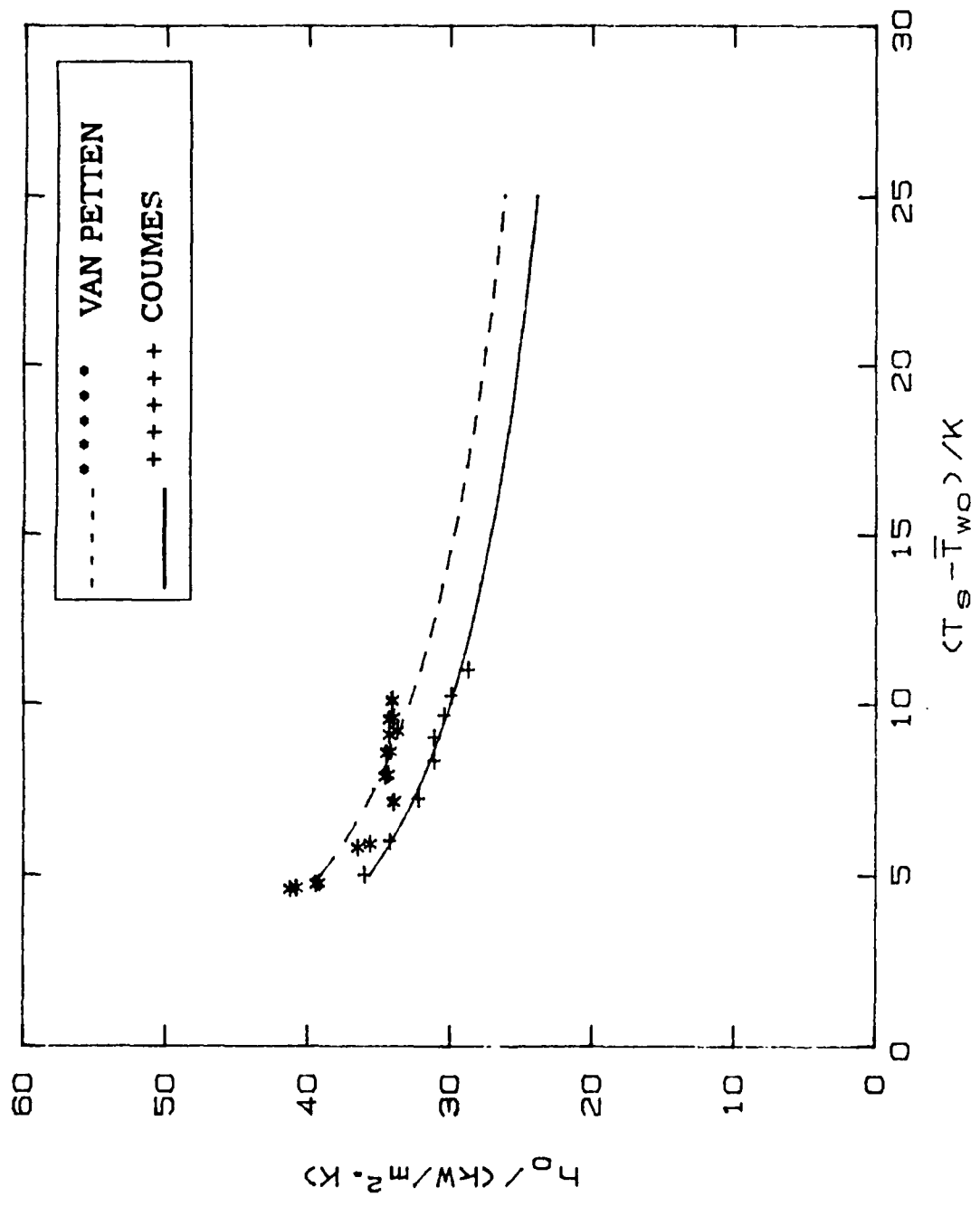


Figure 5.3 Repeatability of Tube 12 Under Vacuum Conditions

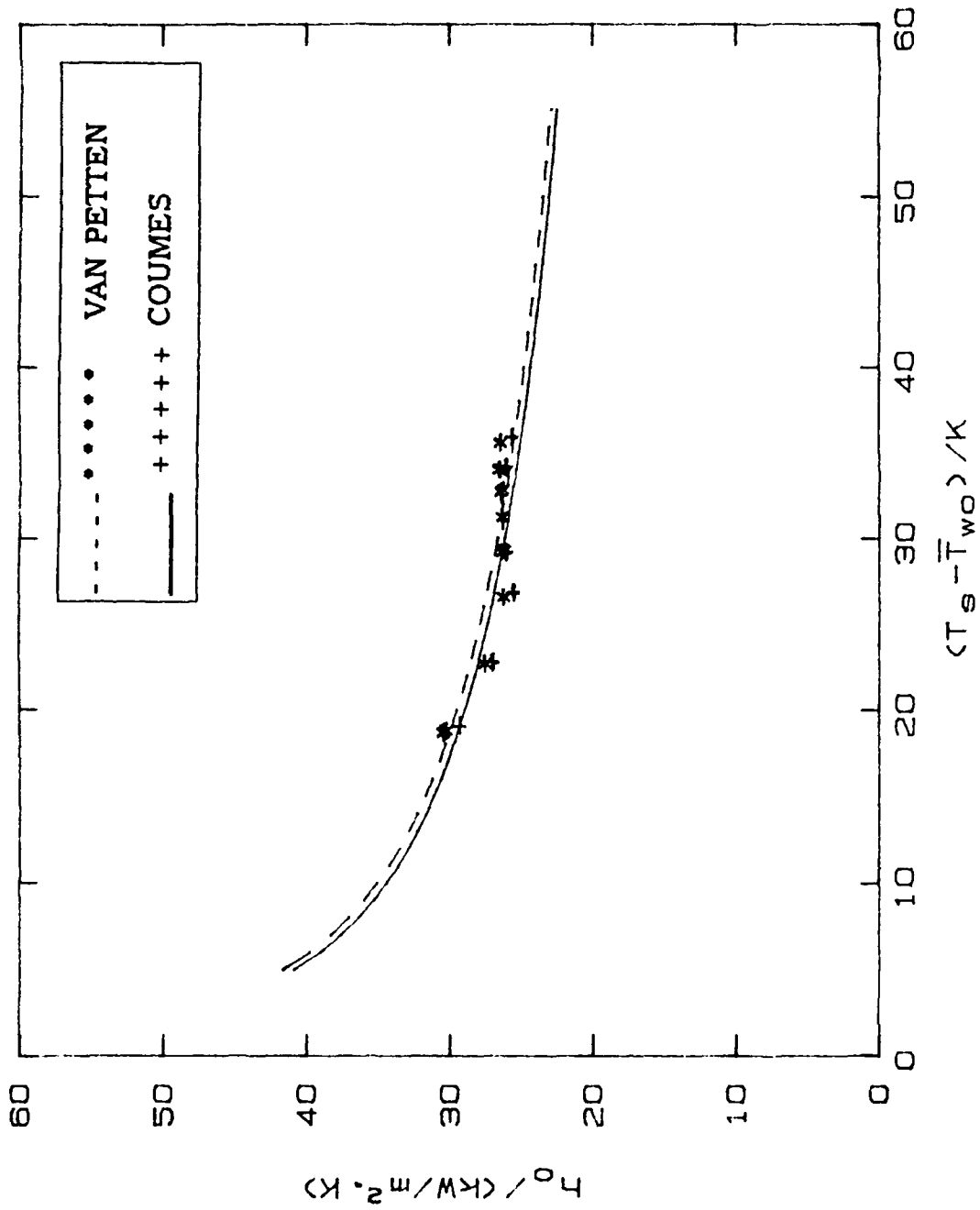


Figure 5.4 Repeatability of Tube 9 at Atmospheric Conditions

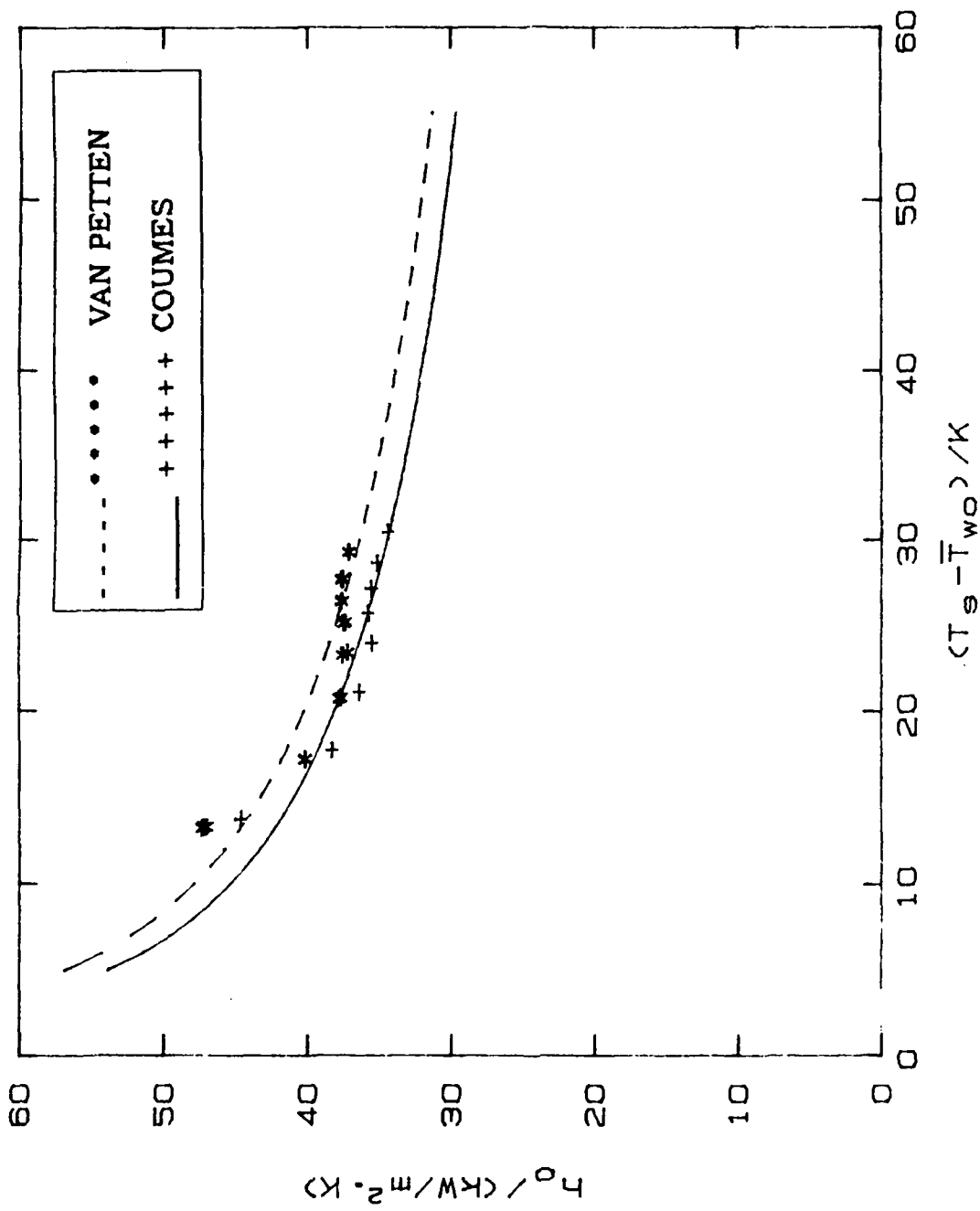


Figure 5.5 Repeatability of Tube 11 at Atmospheric Conditions

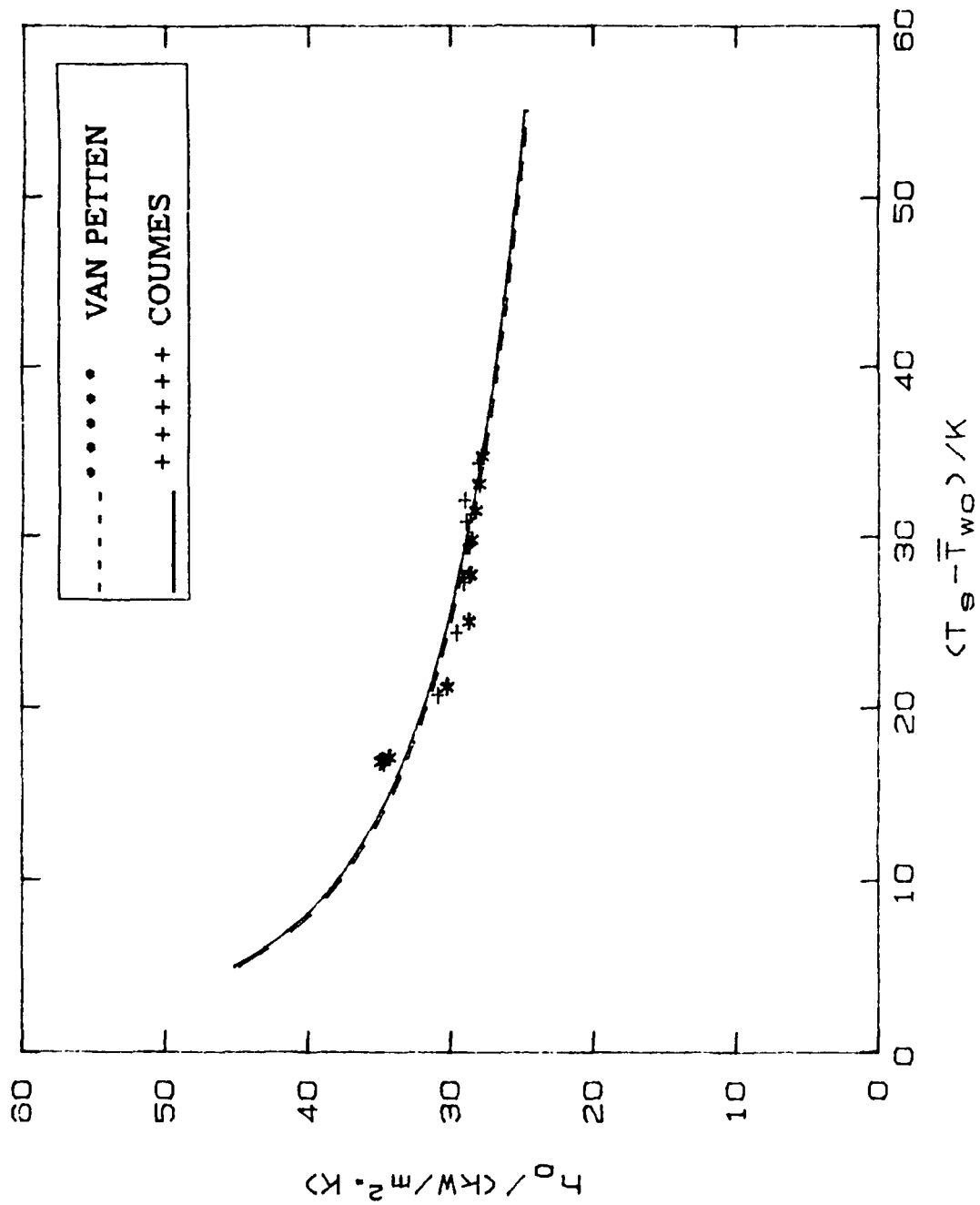


Figure 5.6 Repeatability of Tube 13 at Atmospheric Conditions

While collecting data, any sudden variations (from expected trend) in the outside coefficient could have been indications of either dropwise condensation or the presence of noncondensables. To avoid dropwise condensation, cooling water flow rate was initially maximized so that condensate fully wetted the tube surface before any data were taken. This method seemed to be critical when taking data for the small tubes, and especially the small smooth tube. Several runs were conducted for the small smooth tube and if the tube surface had not been initially wetted by using the maximum cooling water rate, 'dry' patches (potential dropwise sites) on the tube surface were clearly visible and the heat-transfer coefficients calculated were higher than expected. Figures 5.7, 5.8, and 5.9 compare selected data for small tubes at vacuum and Figures 5.10, 5.11, and 5.12 compare small tubes at atmospheric pressure. Van Petten collected data for the QMCNPS tube only at atmospheric conditions. Figure 5.13 is a comparison of that data with that of this investigation.

Table 5.1 summarizes the repeatability of data with that obtained by Van Petten. Comparisons were based on the difference between the least-squares-fit calculations of the heat transfer coefficient of the two investigations ($\% \text{ difference} = [(h_{o, \text{ Coumes}} - h_{o, \text{ Van Petten}}) / h_{o, \text{ Coumes}}] \times 100$). With the exception of tubes 2, 3 and the QMCNPS tube at atmospheric conditions (note, all are small

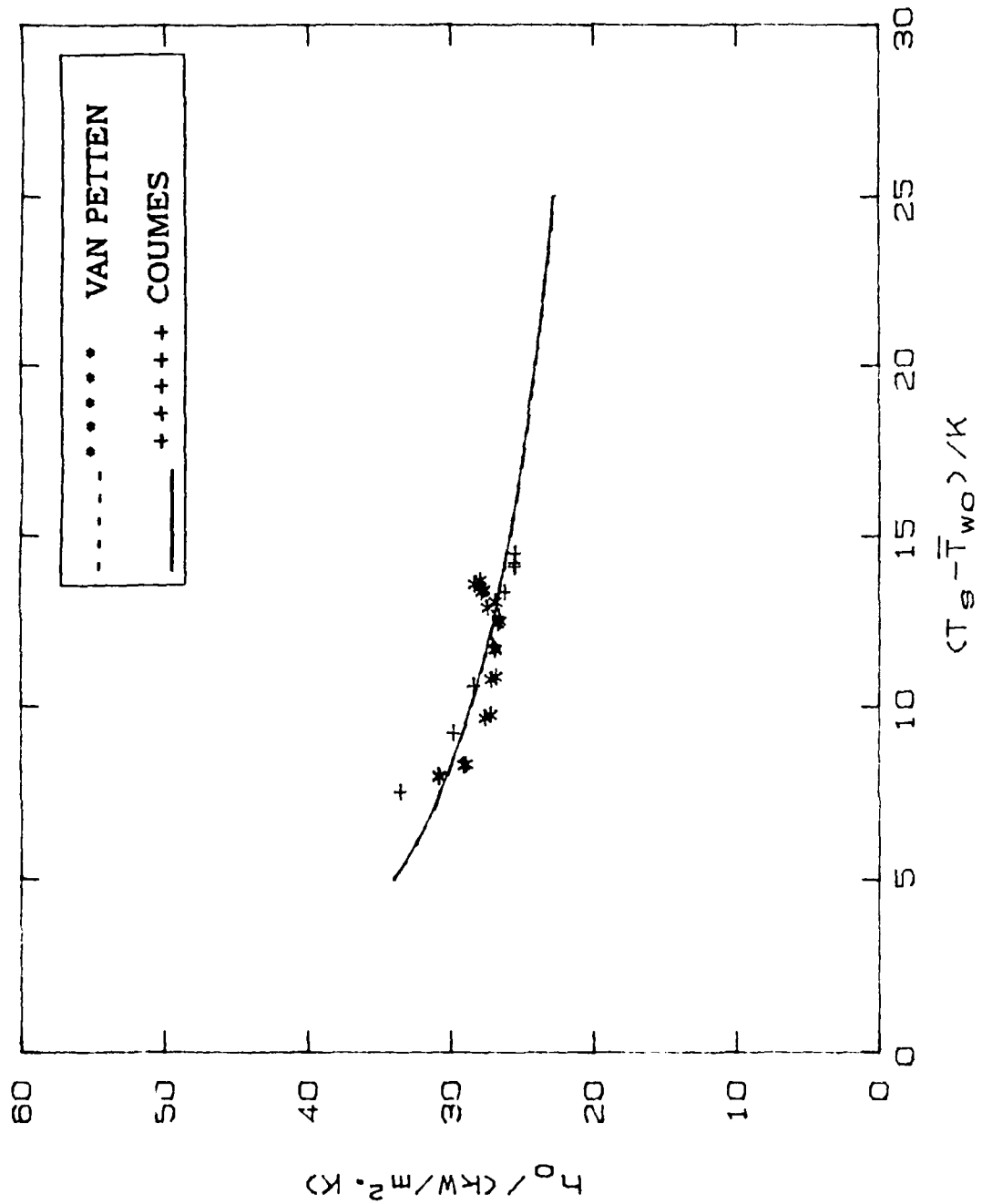


Figure 5.7 Repeatability of Tube 2 Under Vacuum Conditions

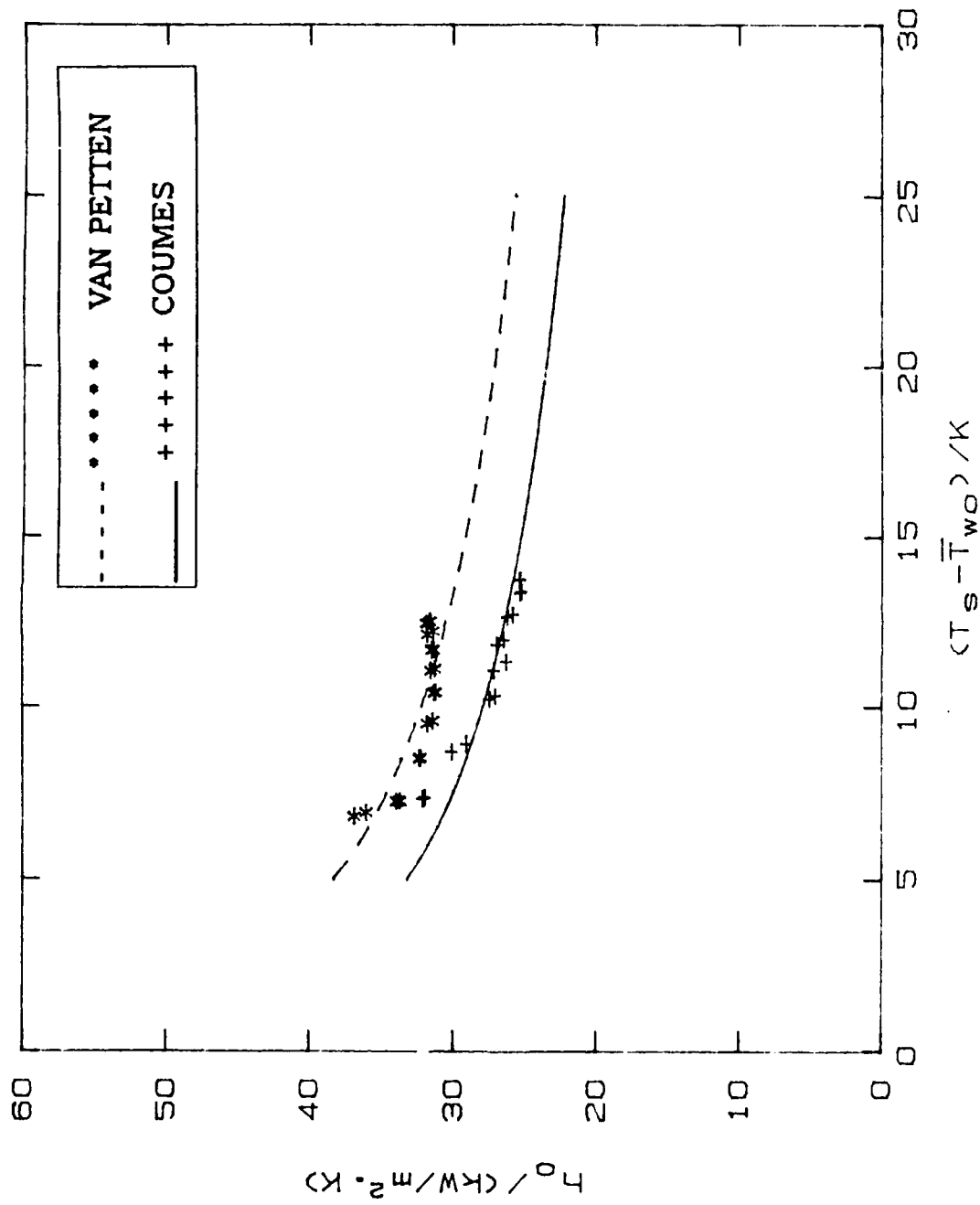


Figure 5.8 Repeatability of Tube 4 Under Vacuum Conditions

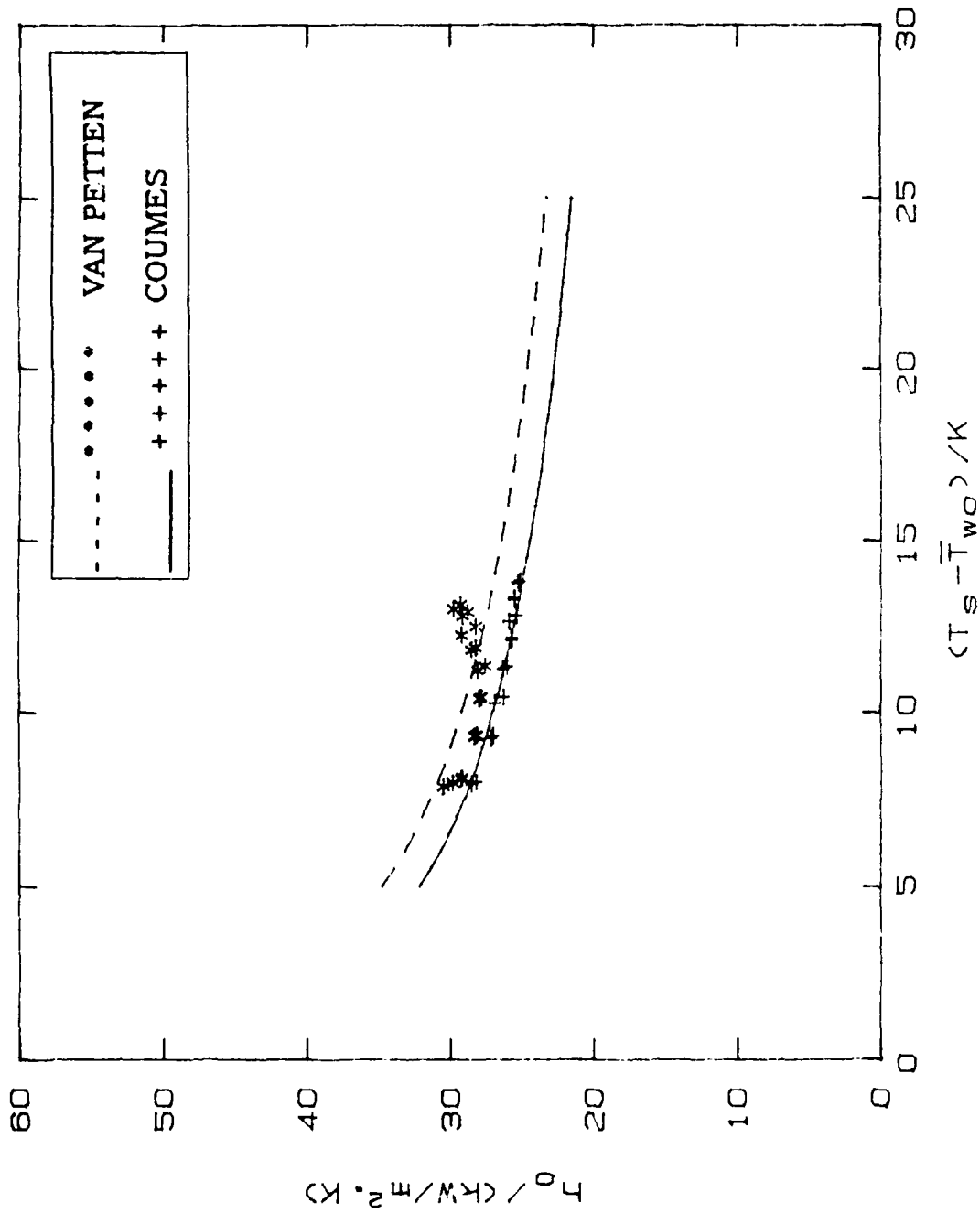


Figure 5.9 Repeatability of Tube 6 Under Vacuum Conditions

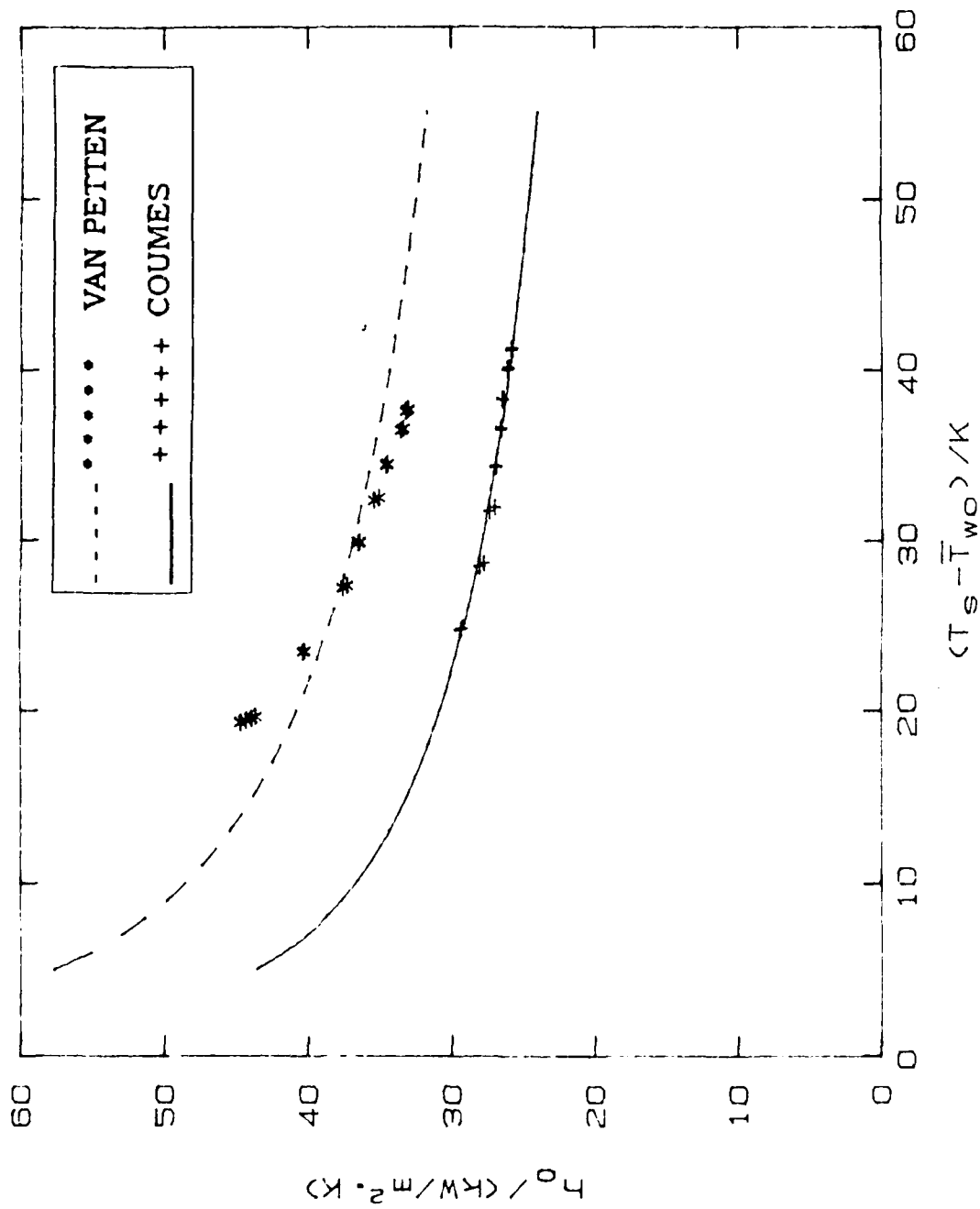


Figure 5.10 Repeatability of Tube 3 at Atmospheric Conditions

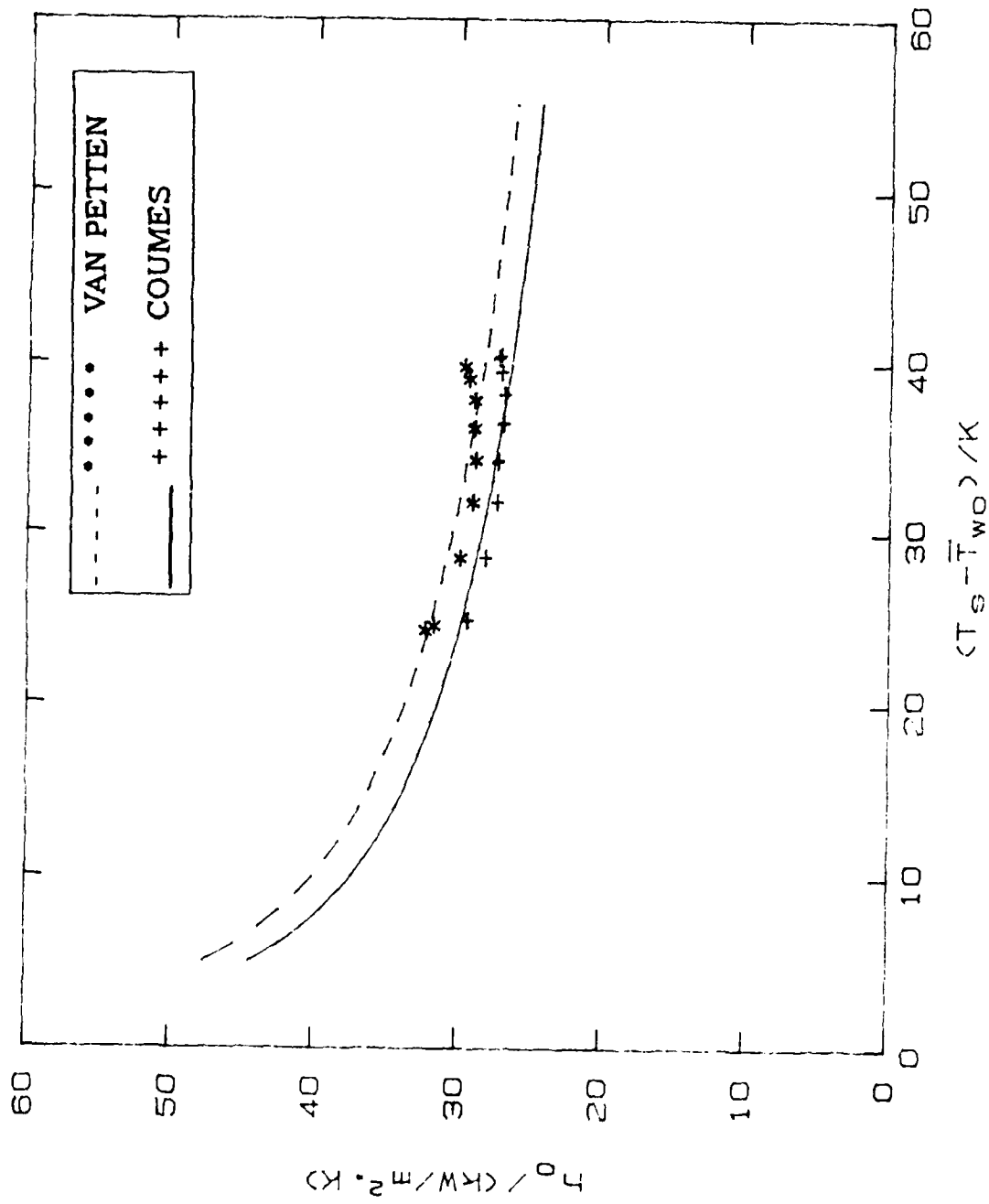


Figure 5.11 Repeatability of Tube 5 at Atmospheric Conditions:

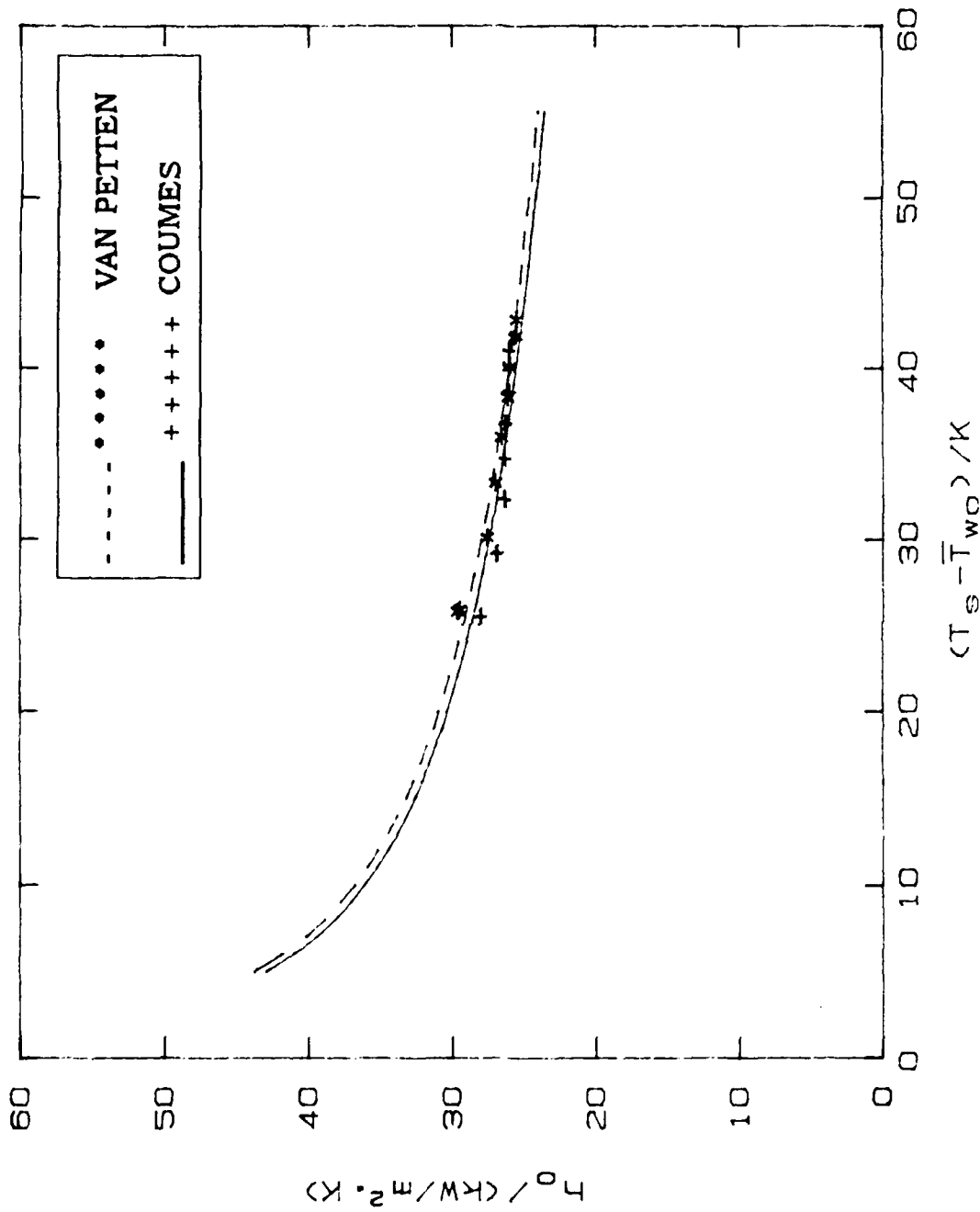


Figure 5.12 Repeatability of Tube 7 at Atmospheric Conditions:

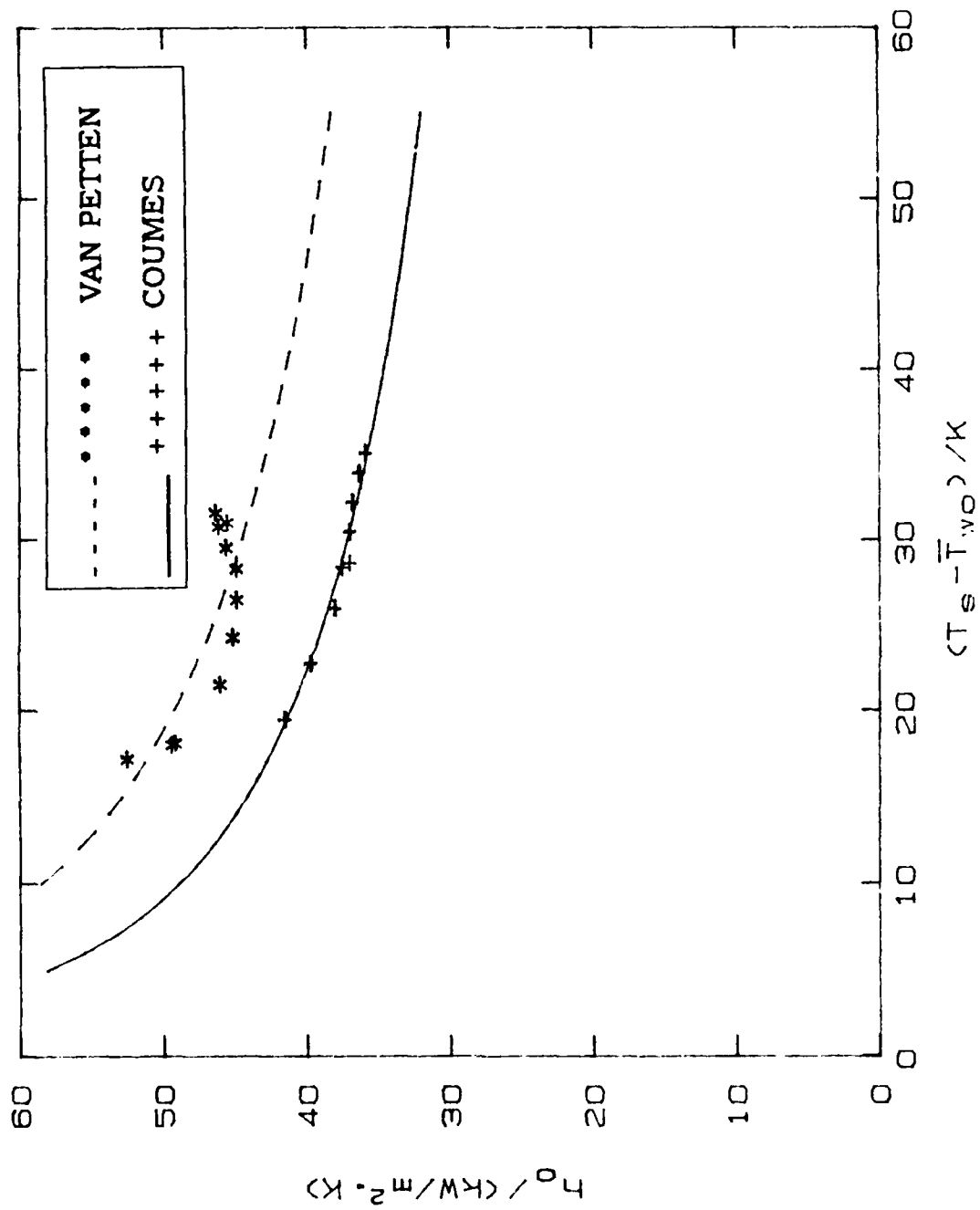


Figure 5.13 Repeatability of QMCNPS Tube at Atmospheric Conditions

Table 5.1

REPEATABILITY

Tube	Vacuum	Atmospheric
	(%)	(%)
Small		
Smooth	---	---
Finned		
2	+ 2.7	-24.6
3	- 2.0	-31.0
4	-12.3	+10.1
5	- 0.6	-5.9
6	- 5.3	+7.1
7	-11.9	-1.0
QMC	---	---
QMCNPS	---	-18.7
Medium		
Smooth	---	---
Finned		
8	-2.2	+3.3
9	-1.9	-0.7
10	---	---
11	-7.5	-4.3
12	-7.3	-9.8
13	-5.5	+1.9

diameter tubes), the data are in good agreement. The discrepancies for these tubes may be attributable to the possible presence of dropwise condensation during Van Petten's investigation. As mentioned previously, small diameter tubes were more susceptible to the dropwise condensation problem.

2. Inside Heat-Transfer Coefficient

The Sieder-Tate type coefficients calculated by the Modified-Wilson-Plot technique are tabulated in Table 5.2. Theoretically, the value of C_i for tubes with the same internal diameter should be equal, unless the external condensation process on different finned tubes influences the circumferential heat flux distribution. However, with the exception of the QMC tube, the variation observed is certainly within the combined experimental error and least-squares approximation of the Modified-Wilson Plot technique. The relatively large difference exhibited by the QMC tube is probably due to the insert. Because the QMC tube has a larger internal diameter (see Table 3.2), the insert, which was designed for the QMCNPS tube, did not fit as tightly, therefore, the enhancement which the insert provided was not as great. Table 5.3 shows the calculated averages of C_i for small and medium diameter tubes, which compare favorably with those of Van Petten [Ref. 6].

Table 5.2

SIEDER-TATE COEFFICIENTS

Tube	Vacuum	Atmospheric
Small		
Smooth	0.047	0.048
Finned		
2	0.053	0.050
3	0.053	0.045
4	0.051	0.047
5	0.048	0.044
5A*	0.048	0.048
6	0.045	0.044
7	0.047	0.048
QMC	0.040	0.038
QMCNPS	0.047	0.040
Medium		
Smooth	0.070	0.068
Finned		
8	0.066	0.064
9	0.067	0.061
10	0.067	0.067
11	0.064	0.065
12	0.065	0.061
13	0.064	0.064

* Additional data set collected for Tube 5

TABLE 5.3

AVERAGE VALUES OF C_1

Small	0.047 ± 0.003 (Van Petten; 0.051 ± 0.003)
Medium	0.065 ± 0.002 (Van Petten; 0.066 ± 0.002)

* excludes values of QMC tube

When performing calculations to determine the outside heat-transfer coefficient, the average values of Table 5.3 were used. The variation is small, and if the Modified-Wilson Plots for a typical tube are compared, there is very little difference between the results obtained by using the values of Table 5.2 and Table 5.3. Figure 5.14 shows the plots of a randomly selected tube, where the two values of C_i have been used. The circles are representative of the 'best fit' value (Table 5.2), whereas the triangles are representative of the 'average' value (Table 5.3). The X and Y values which appear as axis values are those which appear in Equations (4.13) and (4.12), respectively.

When working with instrumented smooth tubes, Wanniaracchi et. al. [Ref. 7] found that data were better correlated when a constant term (B) was added to the assumed Sieder-Tate type relationship for the inside heat-transfer coefficient:

$$Nu = C_i Re^{0.8} Pr^{0.333} (\mu_c/\mu_w)^{0.14} + B \quad (5.2)$$

Equation (5.2) should therefore be utilized when conducting the Modified-Wilson plot technique. It would entail an additional iteration loop (to zero in on B), but might improve the data fit significantly.

3. Outside Heat-Transfer Coefficient

The outside heat-transfer coefficients were calculated, as previously stated, using Equation (4.17). Figures 5.15 and 5.16 depict

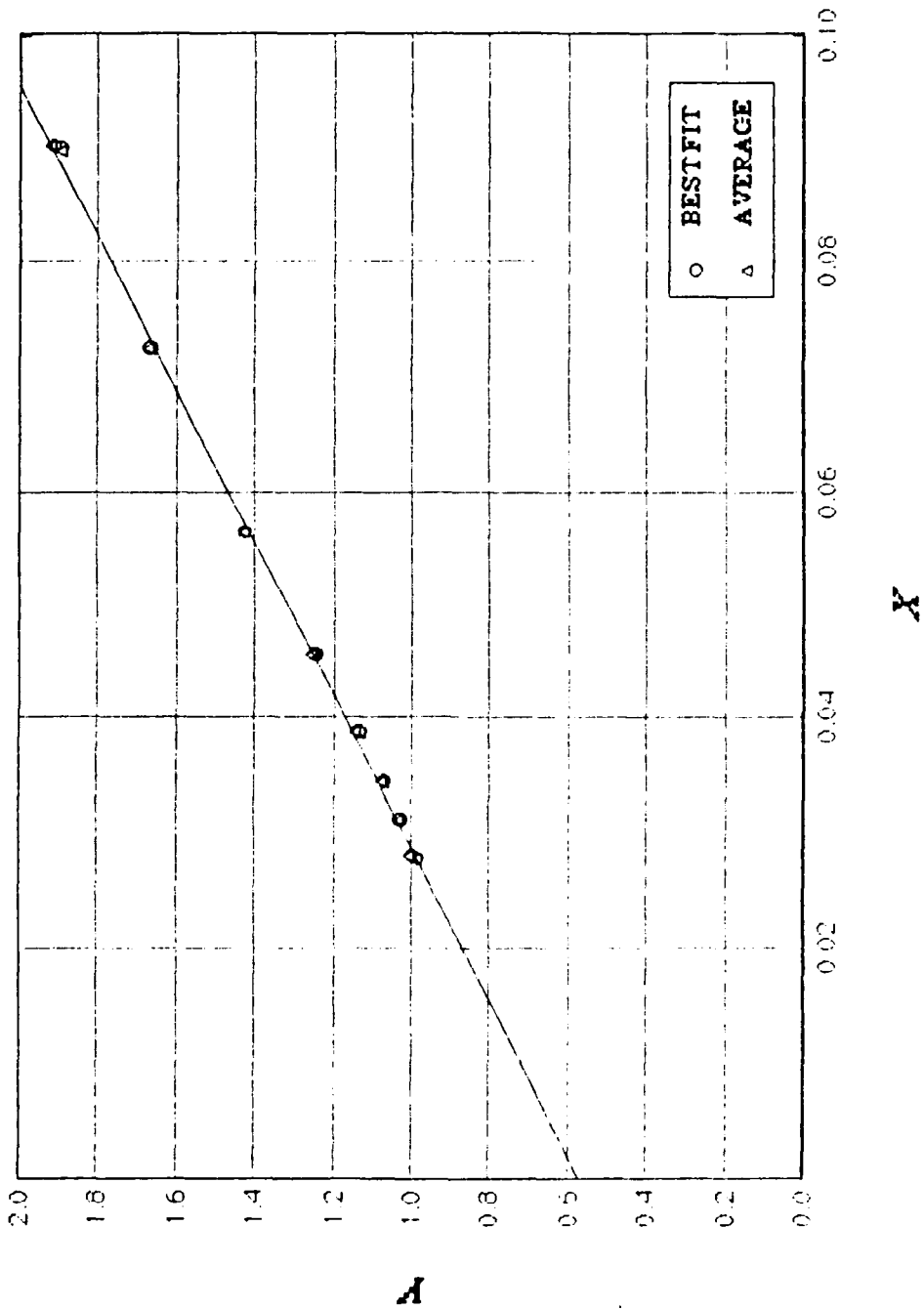


Figure 5.14 Modified - Wilson - Plot,
 'BestFit' Versus 'Average' C_i 's for Tube 9 at Vacuum

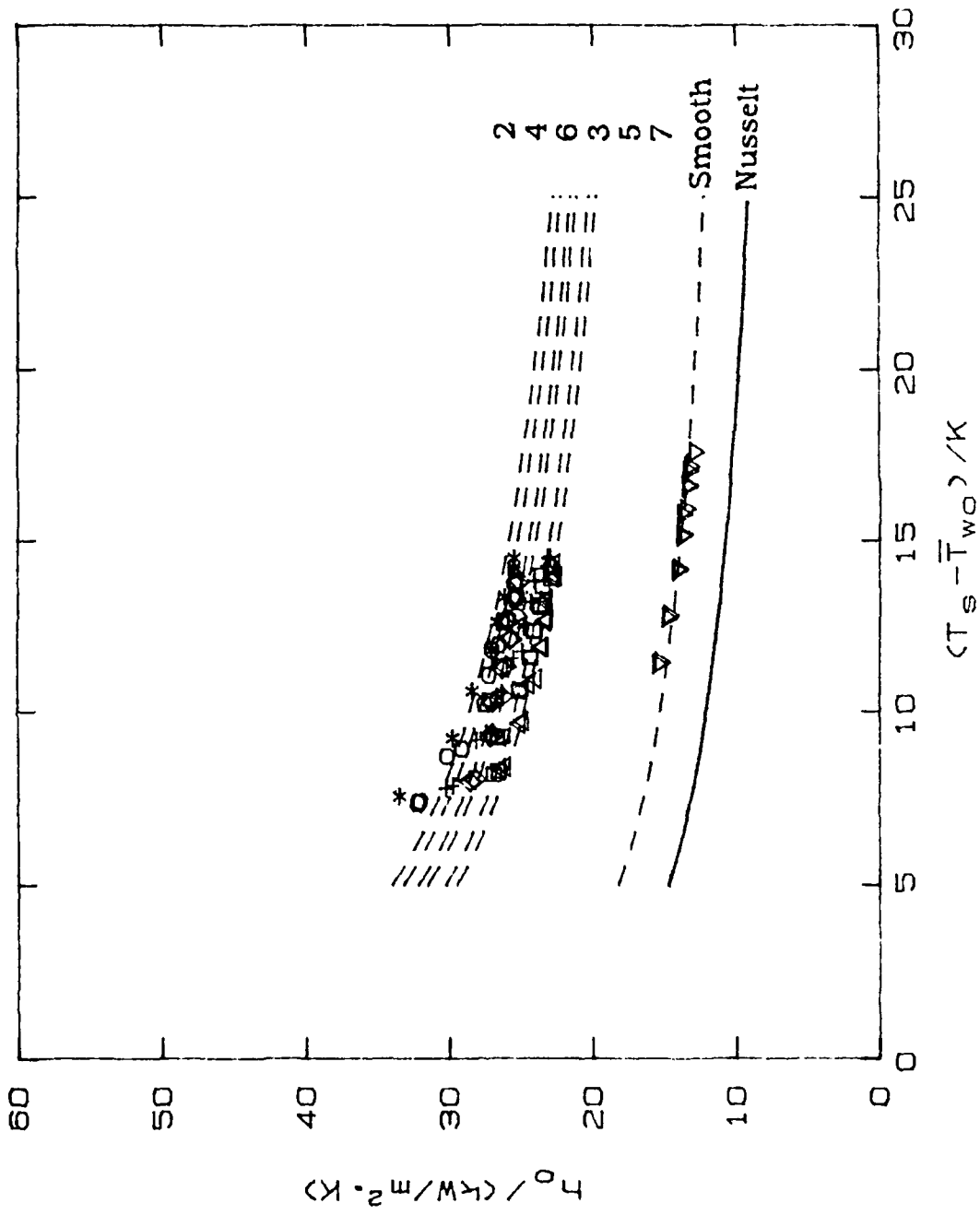


Figure 5.15 Heat-Transfer Coefficients for Small Tubes at Vacuum Conditions

outside heat-transfer coefficient data versus vapor-side temperature drop for small tubes at vacuum and at atmosphere, respectively. Figures 5.17 at vacuum conditions, and 5.18 at atmospheric conditions, show results for the QMC and QMCNPS tubes. An average C_i , from Table 5.3, was used to obtain the QMCNPS curves while the 'best fit' value of Table 5.2 was used for the QMC curves. The large spread in the data can probably be traced to the determination of h_i . Because the insert did not appear to enhance the tube-side of the QMC tube as efficiently as it did the QMCNPS tube (the larger QMC D_i argument), the QMC h_i was then smaller, therefore, recalling Equation (4.23), its h_o would then be larger.

Figures 5.19 and 5.20 are the vacuum and atmospheric data for the medium diameter tubes. Also plotted on all the figures, and appearing as a solid line below the tube data, is the Nusselt theory prediction for a smooth tube.

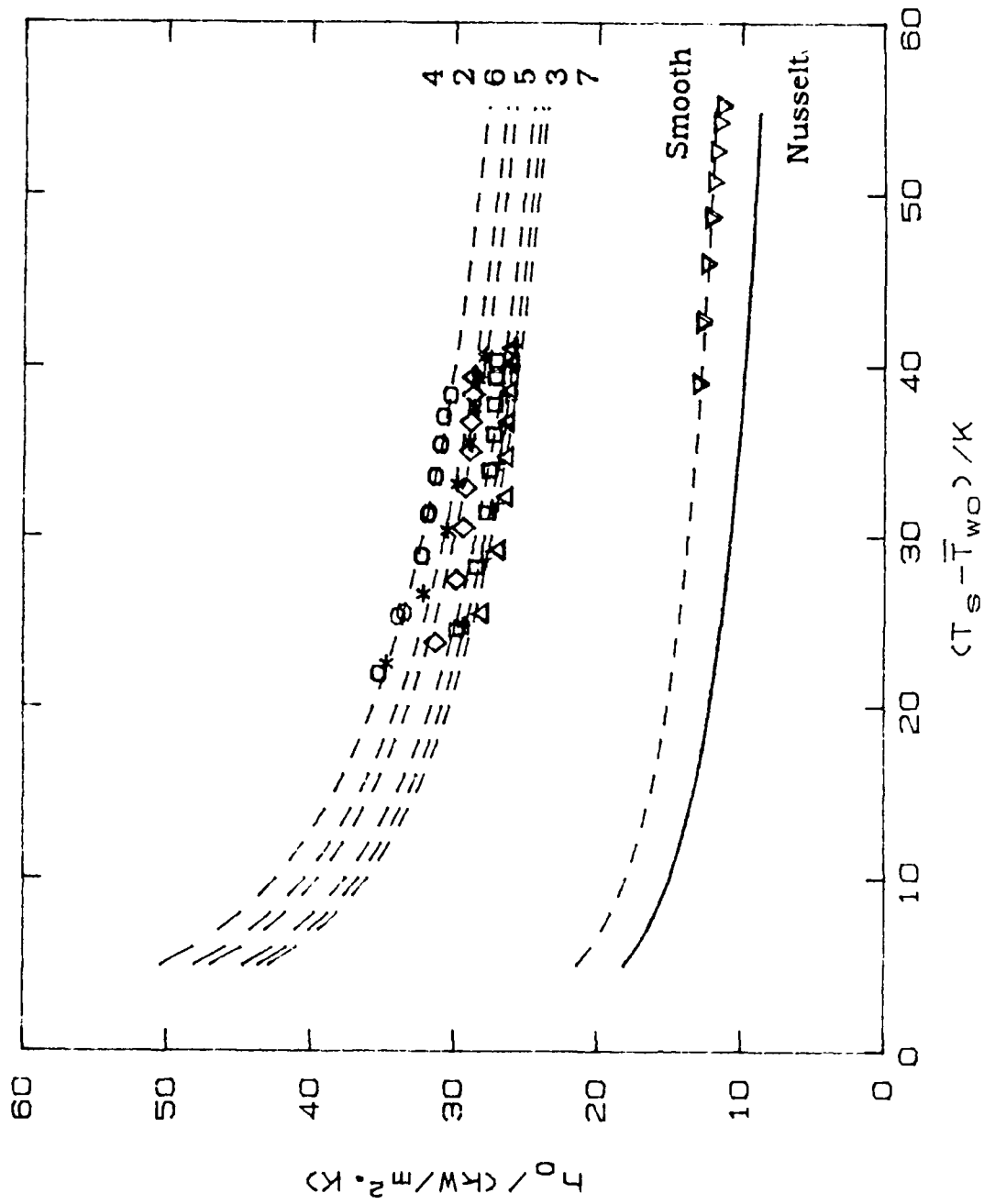


Figure 5.16 Heat-Transfer Coefficients for Small Tubes at Atmospheric Conditions

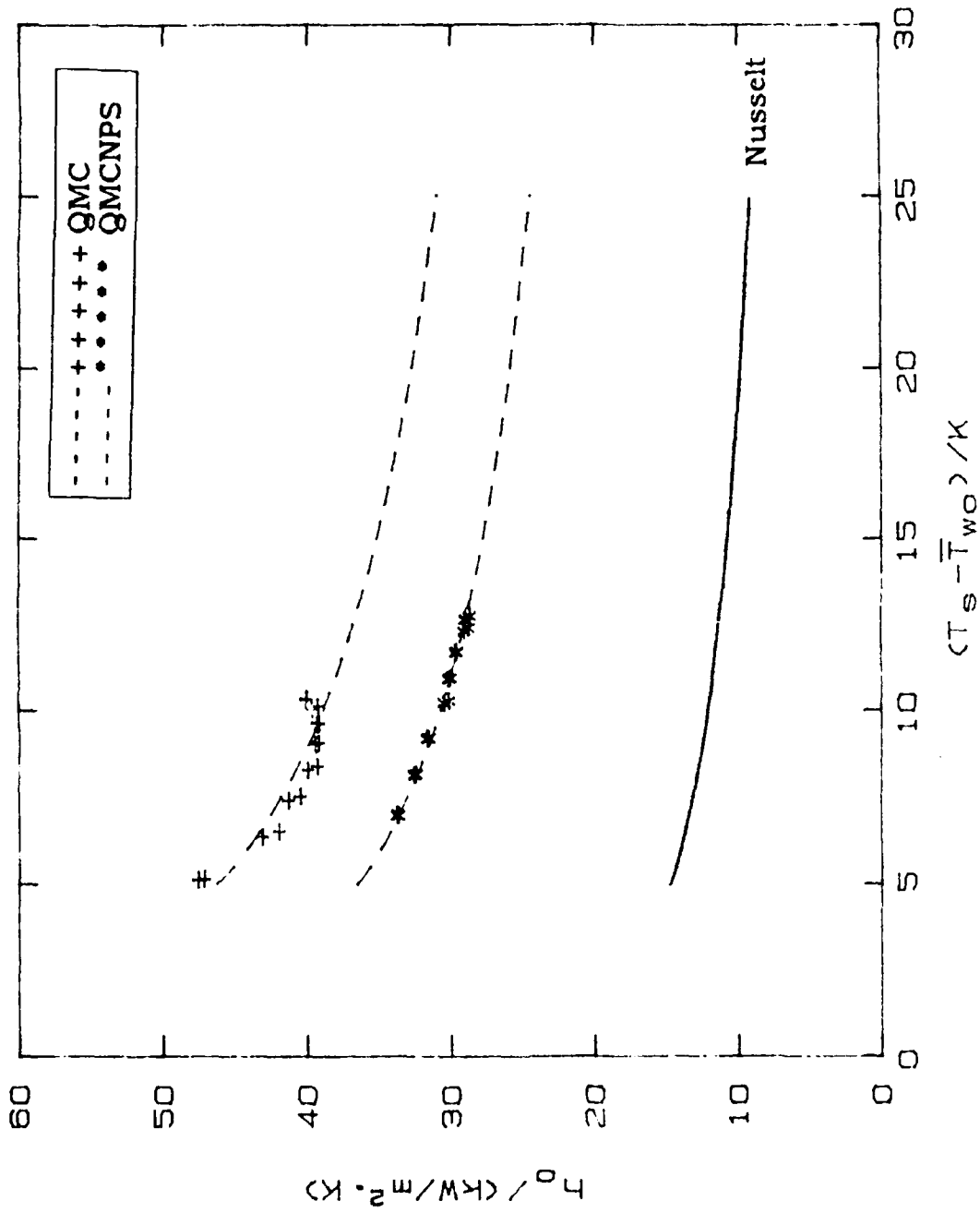


Figure 5.17 Heat - Transfer Coefficients for QMCNPs and QMC Tubes at Vacuum Conditions

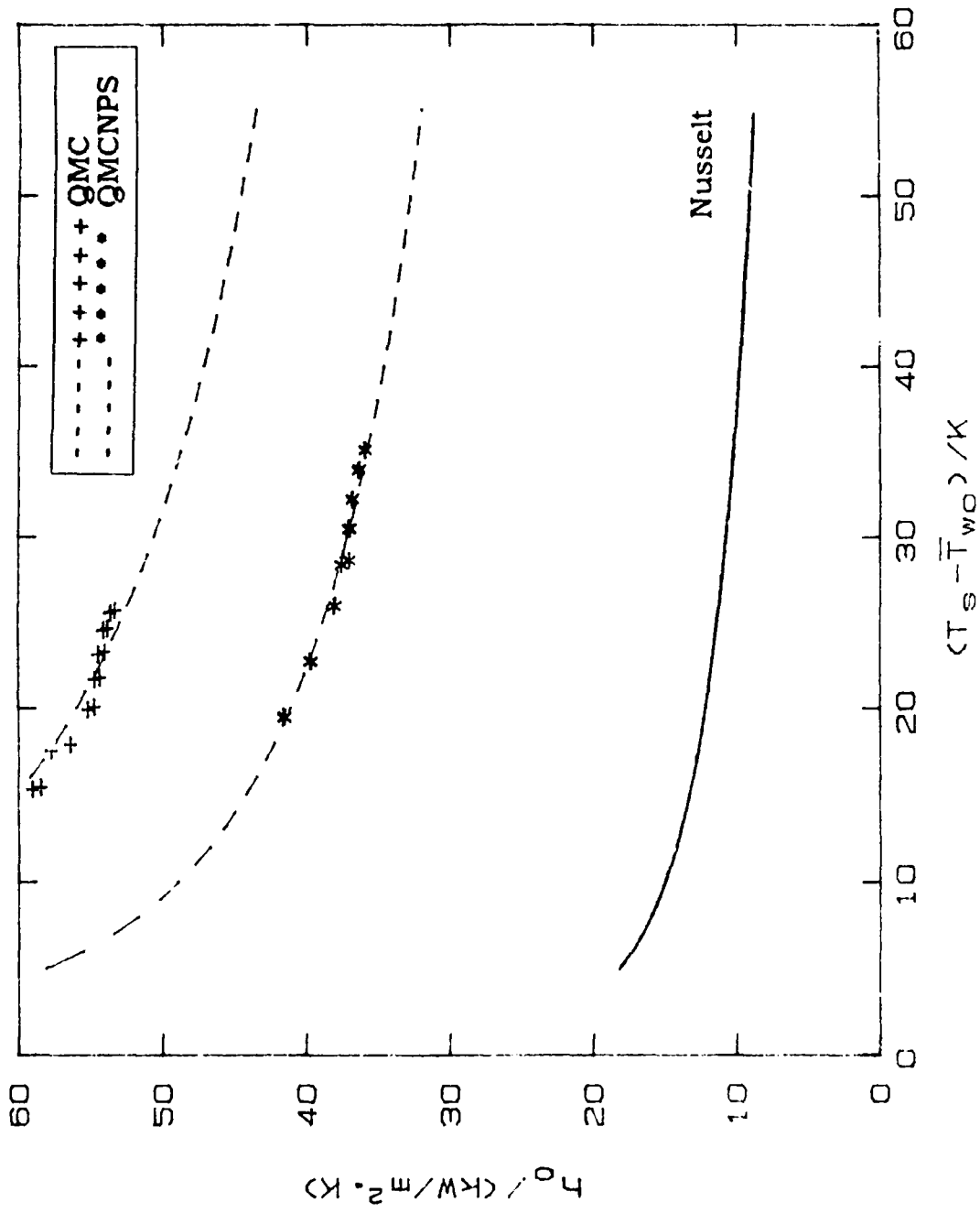


Figure 5.18 Heat-Transfer Coefficients for QMCNPS and QMC Tubes at Atmospheric Conditions

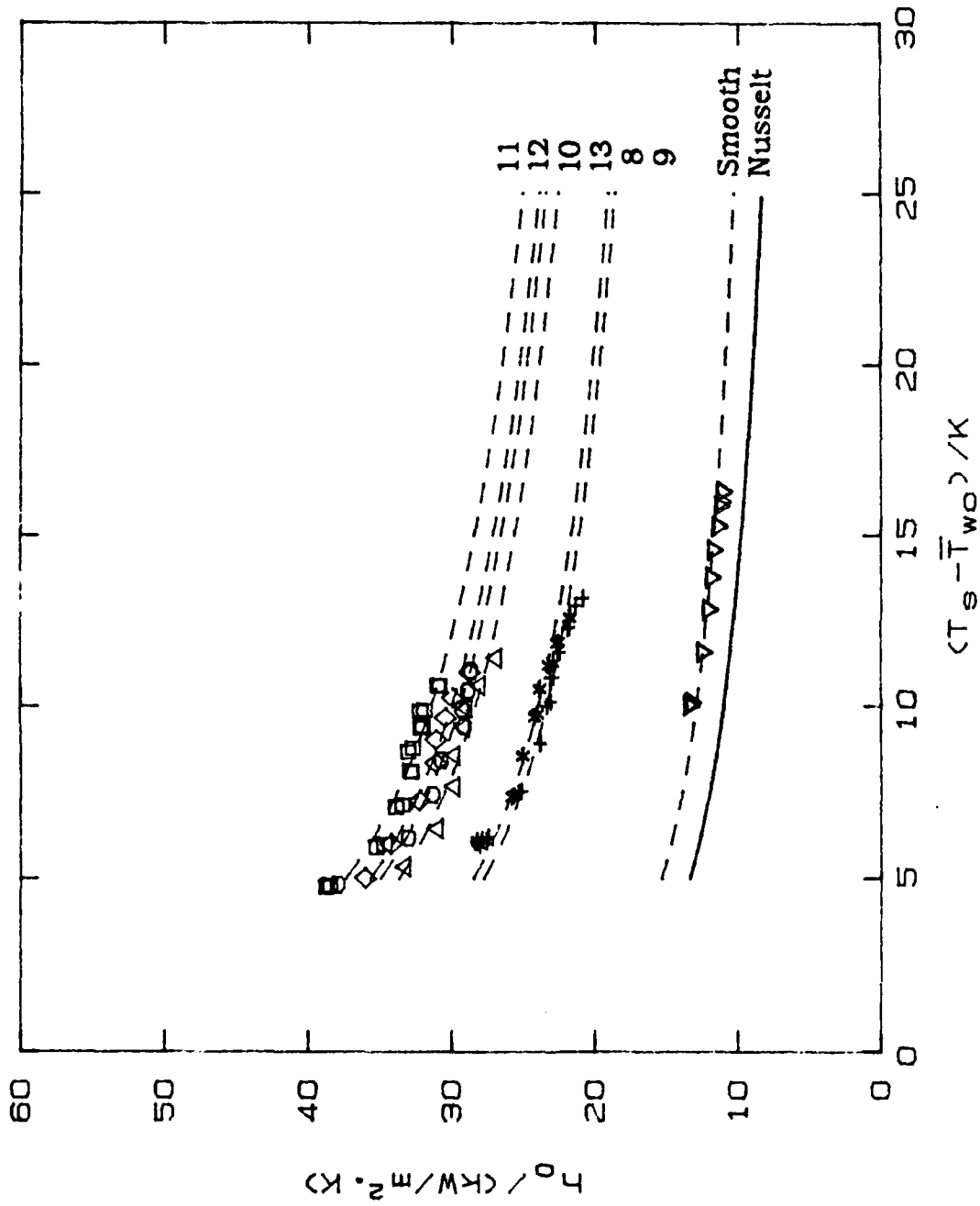


Figure 5.19 Heat-Transfer Coefficients for Medium Diameter Tubes Under Vacuum Conditions

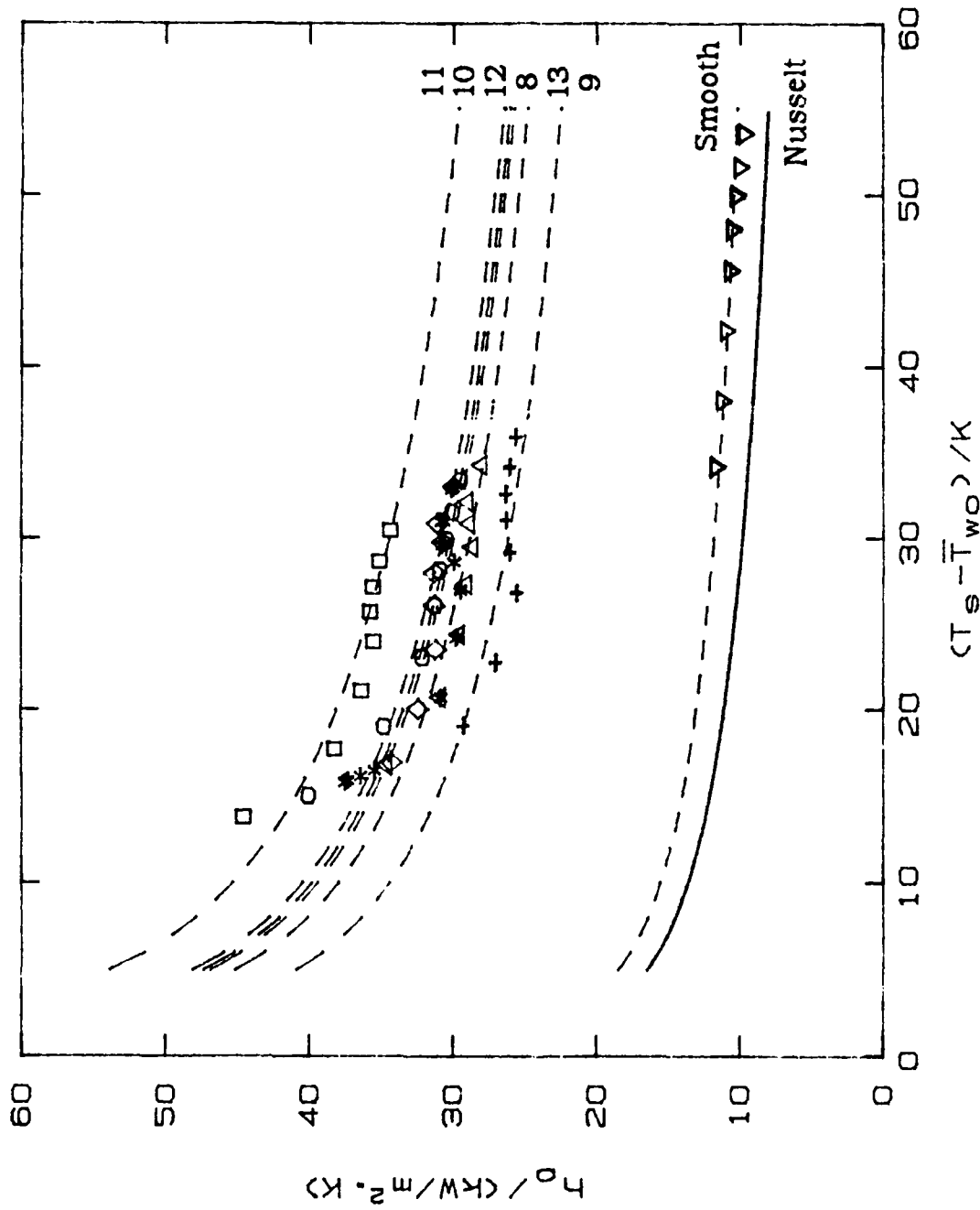


Figure 5.20 Heat-Transfer Coefficients for Medium Diameter Tubes at Atmospheric Conditions

4. Enhancement Ratios

Once the average C_i values were determined all data were reprocessed. Using an average C_i , α 's were calculated both for the smooth tubes (α_s) and for the finned tubes (α_f). Enhancement ratios were then determined using Equations (4.21) and (4.22).

To validate the accuracy of the smooth tube data it was compared to Nusselt theory, and also to the empirical correlation of Fujii et al. [Ref. 22]. Figures 5.21 and 5.22 show small smooth tube data at vacuum and at atmosphere, respectively. Figures 5.23 and 5.24 show medium smooth tube data for vacuum and at atmosphere, respectively. The smooth tube data is consistently higher than that of the Fujii correlation, ranging from 8 % (medium diameter tubes) to 19 % (small diameter tubes) greater.

Tables 5.4 and 5.5 summarize the enhancements calculated, as well as the retention angle, determined by Equation (2.6), and the area enhancement. The area enhancement is the ratio of the total surface area of the finned tube to that of the smooth tube. As shown, heat-transfer enhancement is greater than area enhancement, with the exception of the closely spaced fins (fully flooded conditions). However, even at fully flooded conditions, significant heat-transfer enhancement is realized. Additionally, atmospheric conditions simultaneously yield greater enhancements and smaller retention

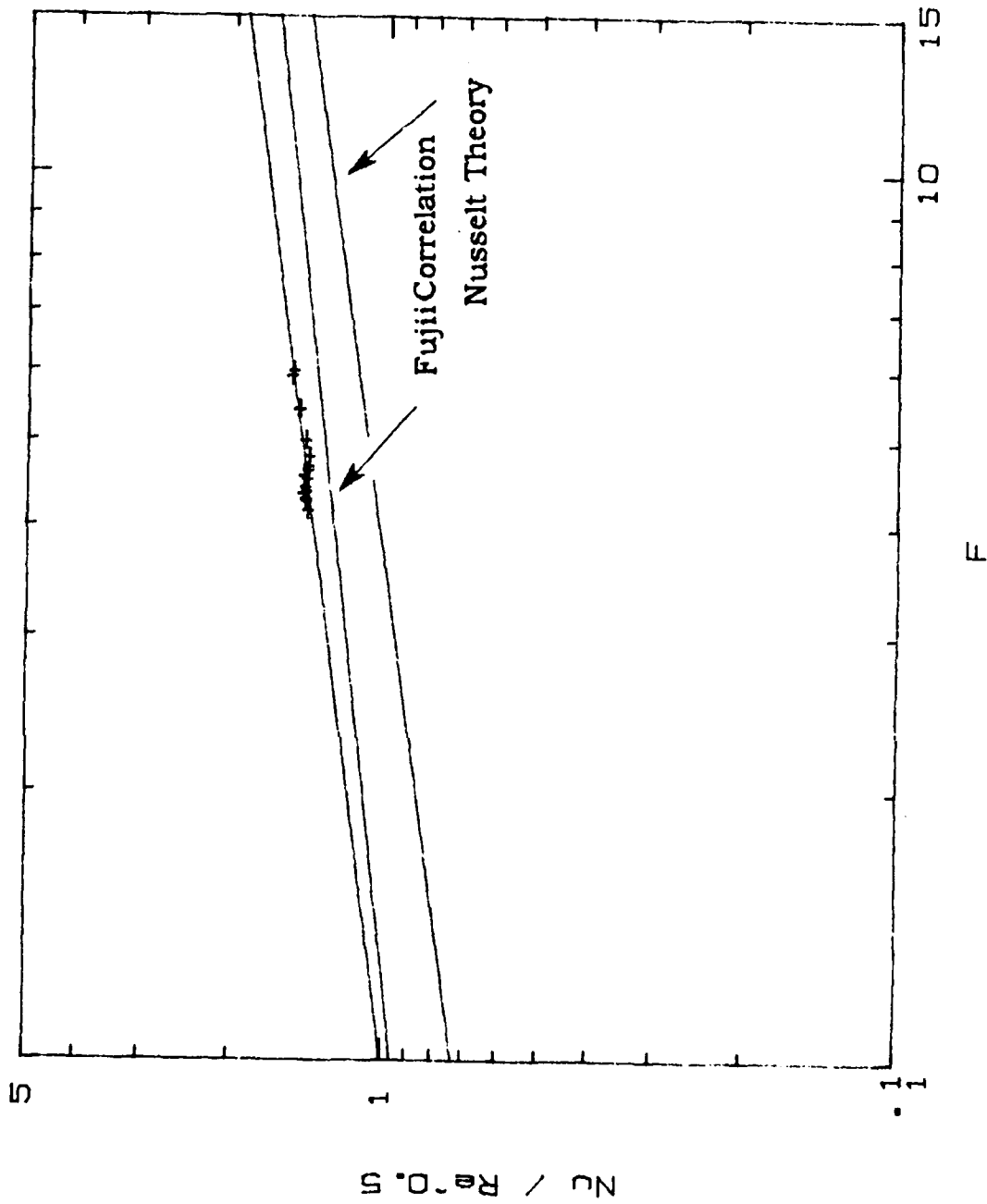


Figure 5.21 The Influence of Vapor Velocity on Small Smooth Tube Data Under Vacuum Conditions

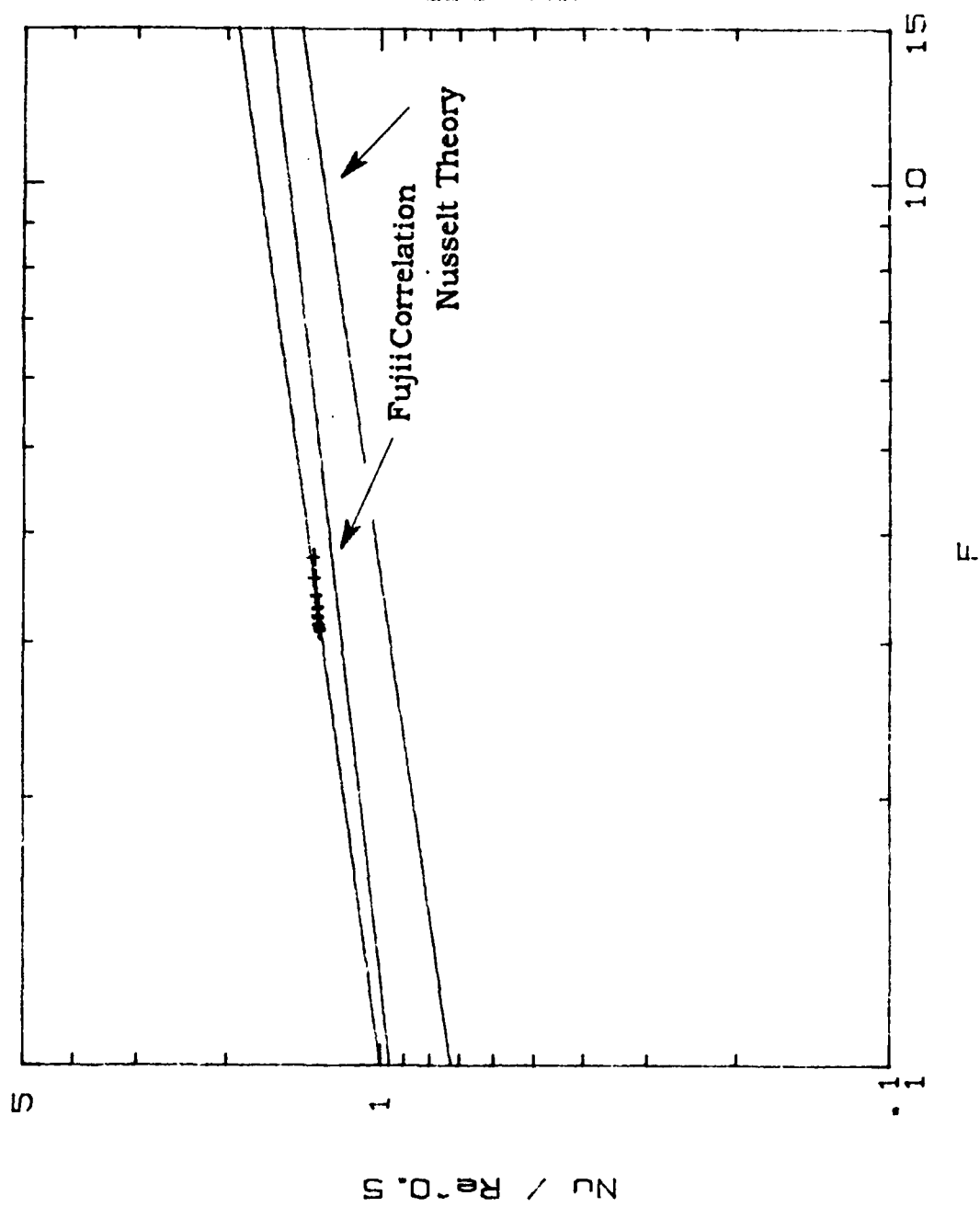


Figure 5.22 The Influence of Vapor Velocity on Small Smooth Tube Data at Atmospheric Conditions

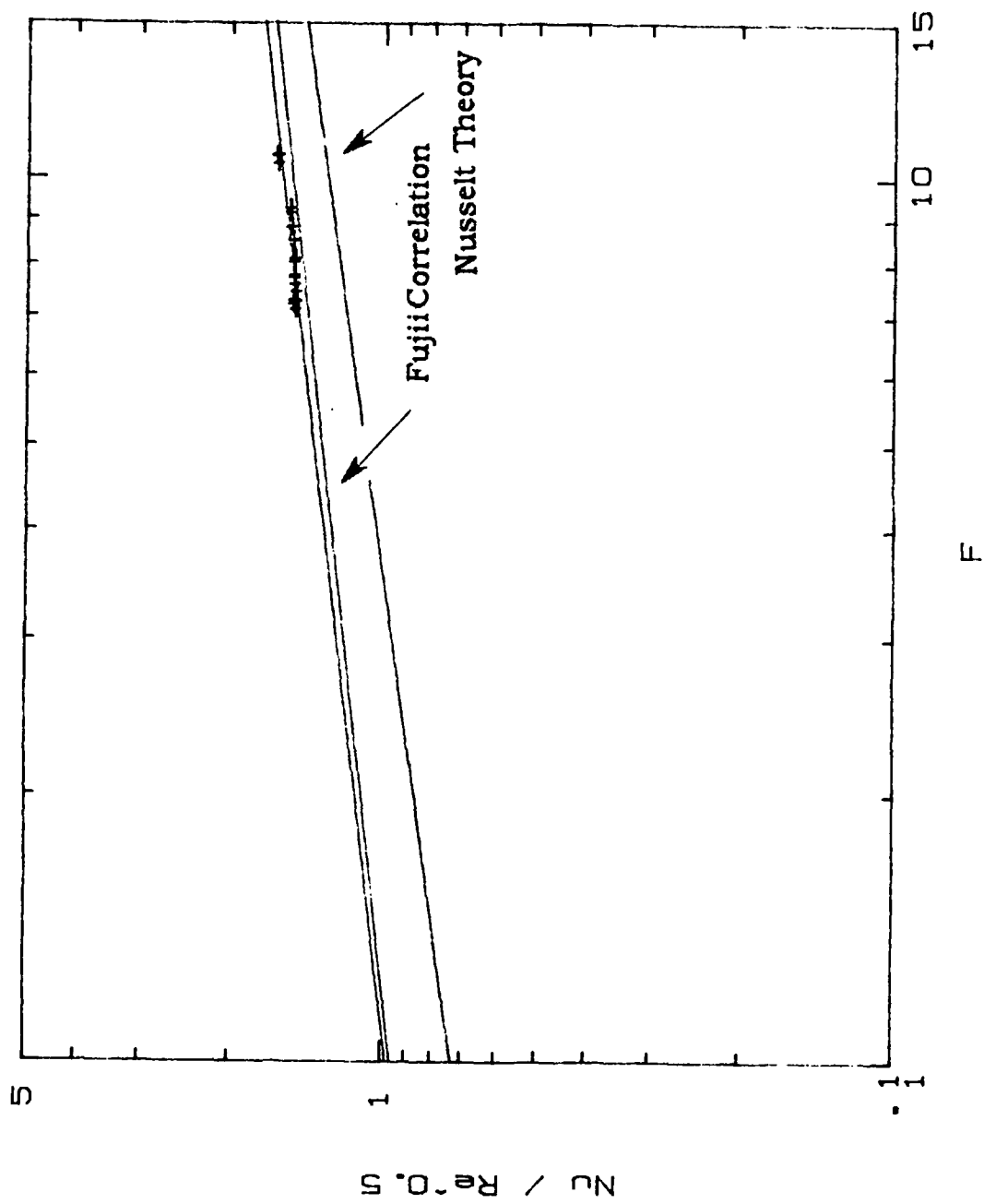


Figure 5.23 The Influence of Vapor Velocity on Medium Smooth Tube Data Under Vacuum Conditions

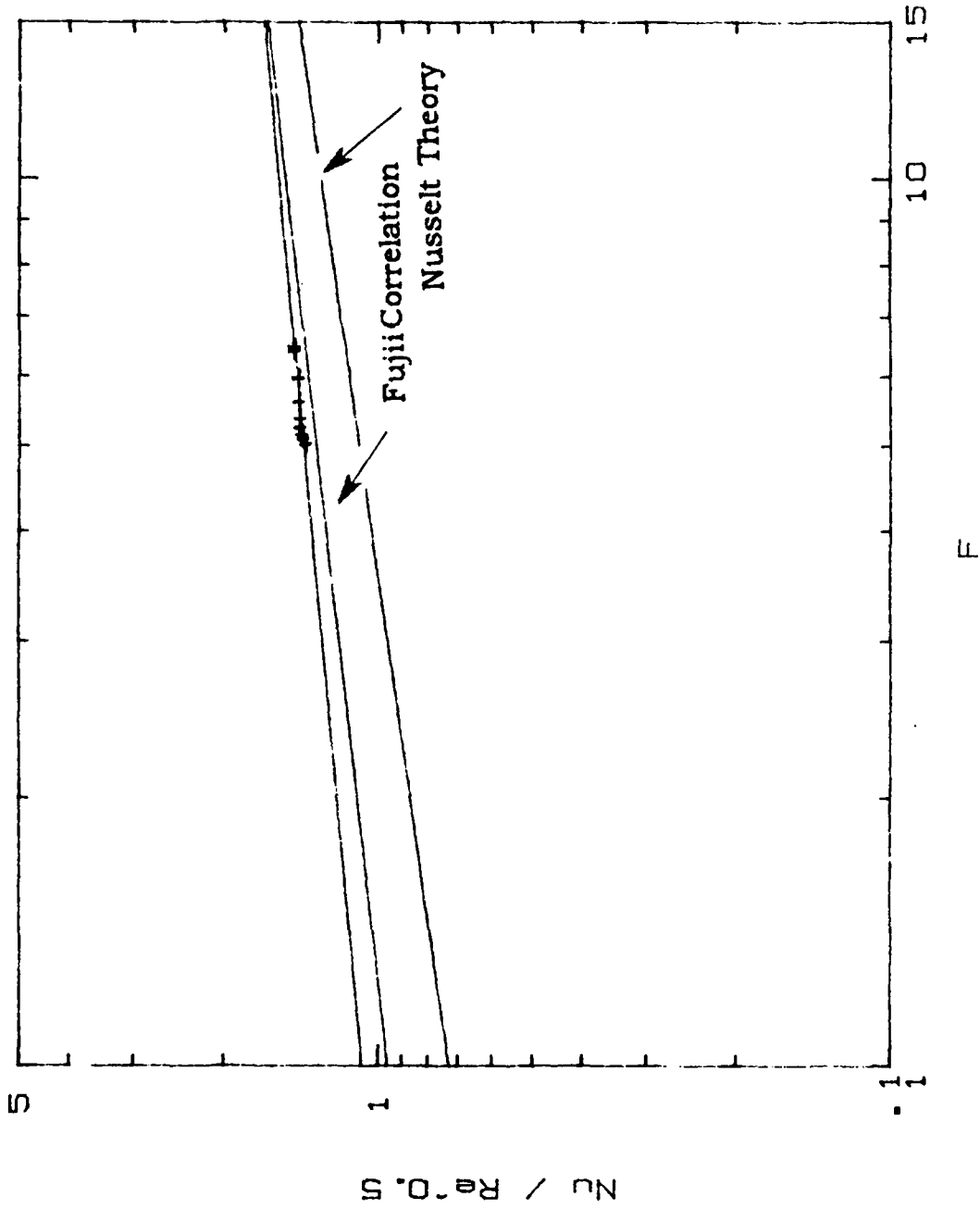


Figure 5.24 The Influence of Vapor Velocity on Medium Smooth Tube Data at Atmospheric Conditions

TABLE 5.4

SUMMARY OF ENHANCEMENTS AT VACUUM CONDITIONS

Tubes	Retention Angle	Fin Spacing (degrees)	Area Enhancement (mm)	Heat Transfer Enhancement
Small				
2	180 ^a	0.25	2.85	1.85
3	180 ^a	0.50	2.54	1.71
4	156	1.00	2.15	1.80
5	106	1.50	1.93	1.64
5A [*]	106	1.50	1.93	1.69
6	88	2.00	1.77	1.75
7	59	4.00	1.46	1.60
Medium				
8	180 ^b	0.25	2.77	1.83
9	180 ^b	0.50	2.47	1.79
10	110	1.00	2.10	2.24
11	84	1.50	1.88	2.39
12	71	2.00	1.74	2.29
13	48	4.00	1.44	2.16

* Additional data set taken for Tube 5

a fully flooded condition for this small tube occurs at a fin spacing of 0.96 mm

b fully flooded condition for this medium tube occurs at a spacing of 0.67 mm

TABLE 5.5

SUMMARY OF ENHANCEMENTS AT ATMOSPHERIC CONDITIONS

	Retention Angle	Fin Spacing (degrees)	Area Enhancement (mm)	HeatTransfer Enhancement
Tubes				
Small				
2	180 ^c	0.25	2.85	2.17
3	180 ^c	0.50	2.54	1.98
4	135	1.00	2.15	2.27
5	98	1.50	1.93	2.02
5A ^a	98	1.50	1.93	2.01
6	82	2.00	1.77	2.12
7	55	4.00	1.46	1.94
Medium				
8	180 ^d	0.25	2.77	2.43
9	180 ^d	0.50	2.47	2.14
10	101	1.00	2.10	2.50
11	78	1.50	1.88	2.79
12	66	2.00	1.74	2.47
13	45	4.00	1.44	2.36

^a Additional data set taken for Tube 5

^c fully flooded condition for this small tube occurs at a fin spacing of 0.85 mm

^d fully flooded condition for this medium tube occurs at a spacing of 0.60 mm

angles than do vacuum conditions.

Figures 5.25 and 5.26 are plots of enhancement ratio versus fin spacing for vacuum and atmospheric conditions, respectively. Small diameter tubes become fully flooded as the fin spacing reduces to ~ 0.9 mm, whereas medium tubes become fully flooded at about ~ 0.6 mm. Once the tube is fully flooded, enhancement should increase as fin spacing is decreased further because metal heat-transfer surface (with a high thermal conductivity) is replacing a liquid film (with a relatively low thermal conductivity). This trend may be observed for the medium tubes in both Figures 5.25 and 5.26. Consistent with Van Petten [Ref. 6], Wanniarachchi et. al. [Ref. 7], and Yau et. al. [Ref. 8], an optimum fin spacing of 1.50 mm for the medium diameter tubes was observed.

The small tube behavior is apparently more complicated. Considering the fully flooded region (between fin spacings of 0.25 - ~ 0.9), we would expect, as we saw for the medium diameter tubes, to see enhancement increasing as fin spacing was decreased. However, what we observe is a decrease in enhancement between fin spacings of 1.0 - 0.5 mm before an increase is seen from 0.5 - 0.25 mm. The second area of interest is the data at a fin spacing of 1.5 mm. As noted in Tables 5.4 and 5.5 an additional set of data was taken for Tube 5. This was an effort to confirm the dip which the small tube enhancement makes at a fin spacing of 1.50 mm. This dip was also

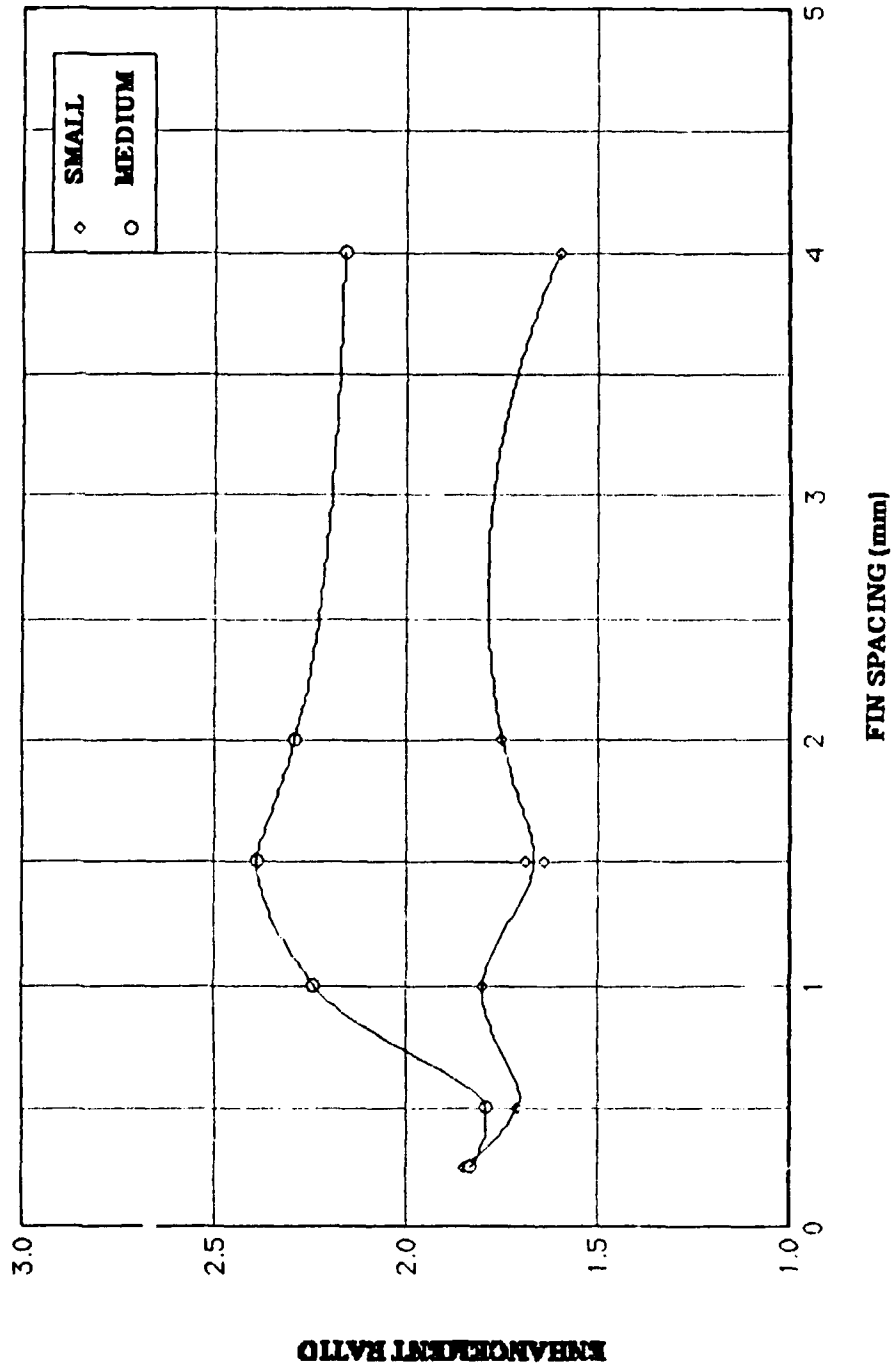


Figure 5.25 Heat - Transfer Enhancement Ratios Under Vacuum Conditions

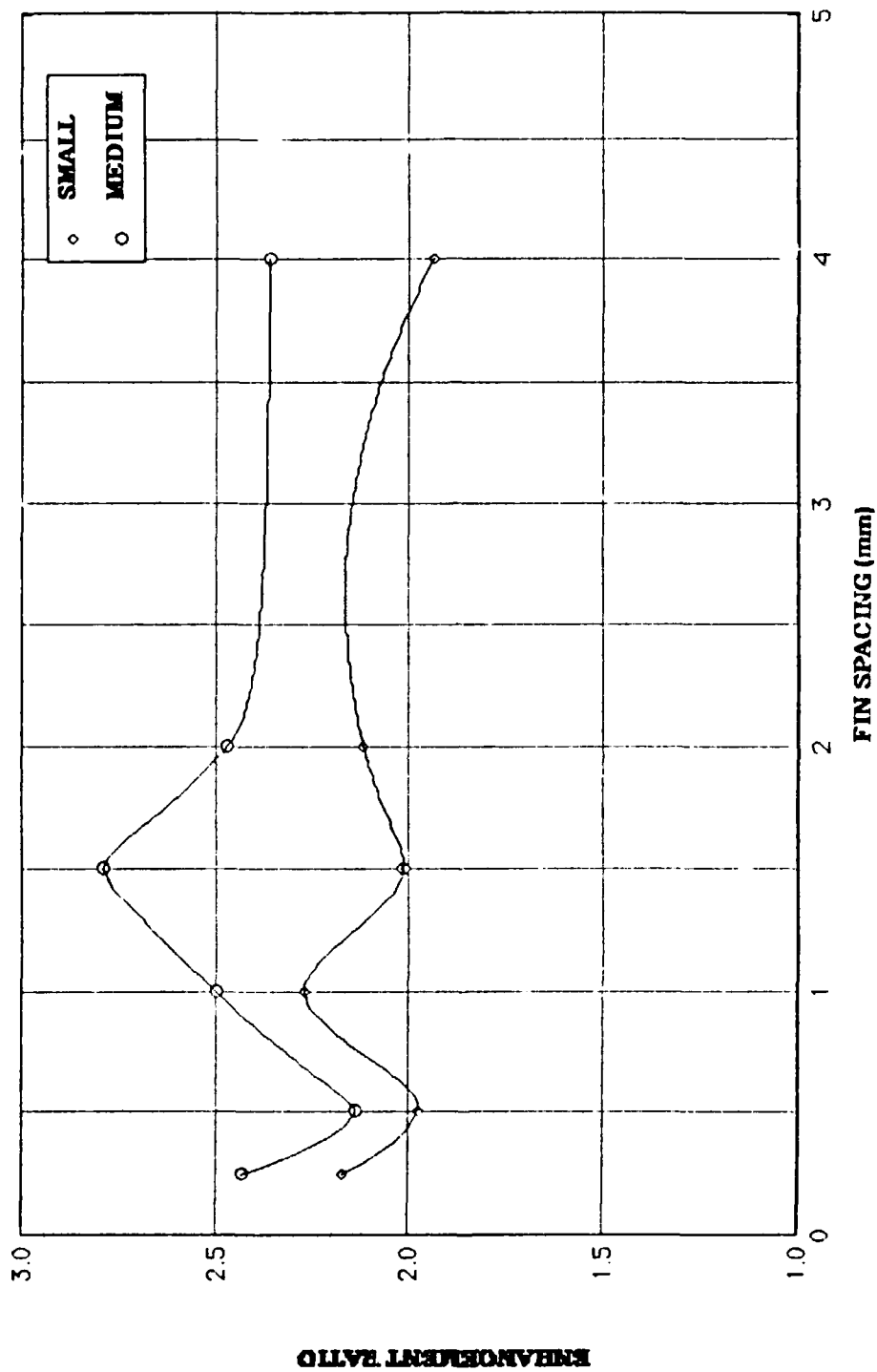


Figure 5.26 Heat-Transfer Enhancement Ratios at Atmospheric Conditions

recorded by Van Petten. When an uncertainty of about 10% is affixed to the small tube enhancement ratios, as in Figures 5.27 and 5.28, an argument could be made that the dip is insignificant/nonexistent, and that optimum fin spacing for the small tube is the same as that of medium and large diameter tubes, namely 1.5 mm. However, Figures 5.29 and 5.30 show the excellent agreement between the two data sets so the dip may be real. Similar dip phenomena have been observed for R-113, by Marto et. al [Ref. 42], and for steam, by Yau et. al. [Ref. 8]. A possible solution may be provided by the three-dimensional model which Honda et. al [Ref. 27] have proposed. They theorize that the dip may correspond to a change in the condensate film profile on the fin root tube surface in the unflooded region in going from large spacings to small spacings. Further investigation, both experimental and theoretical, is therefore required to understand this small tube performance characteristics.

A direct comparison of the enhancement ratios obtained by Van Petten [Ref. 6] can be somewhat misleading. Although he performed a similar reprocessing of data, he used average C_i 's. to reprocess and calculate α 's for his finned tubes, but did not use those average C_i 's to calculate new α 's for his smooth tube. Additionally, because he did not have a small smooth tube he used the medium smooth tube data to calculate his small tube enhancements. The

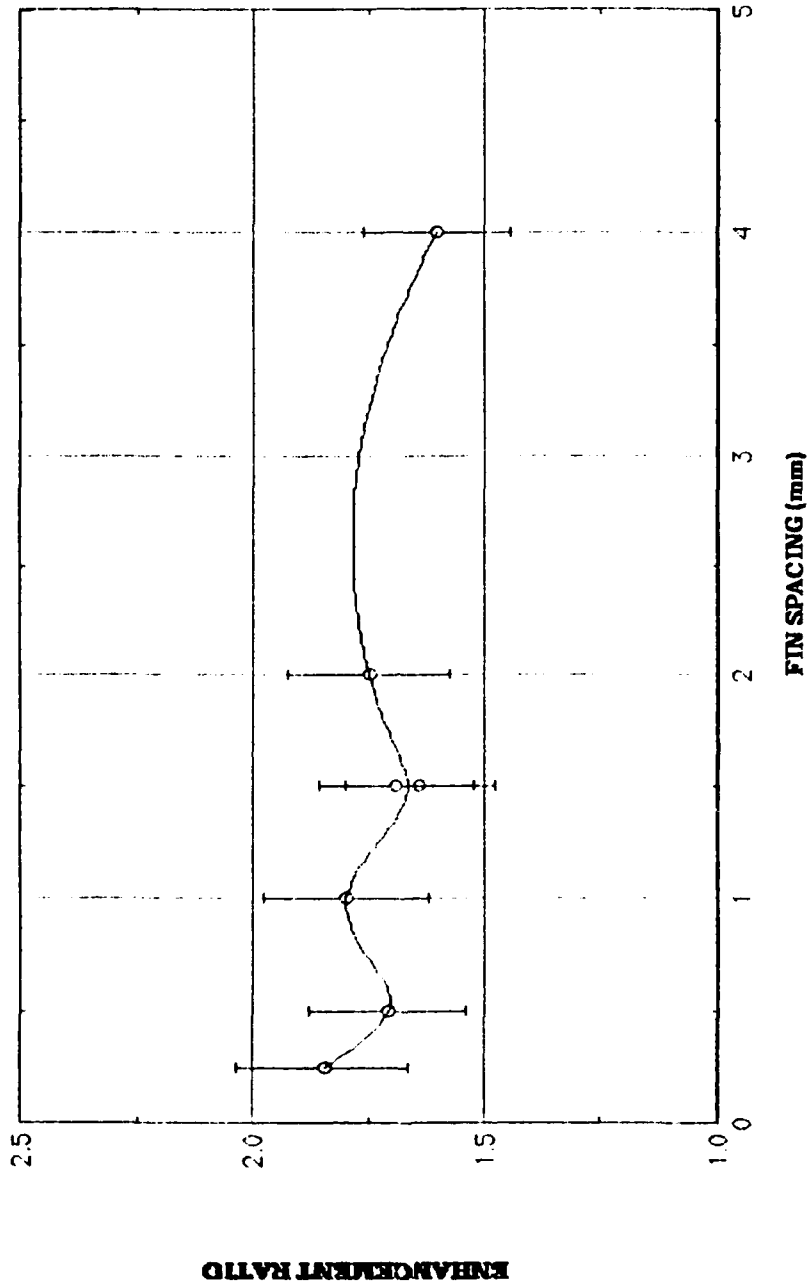


Figure 5.27 Small Tube Enhancements with Uncertainties Under Vacuum Conditions

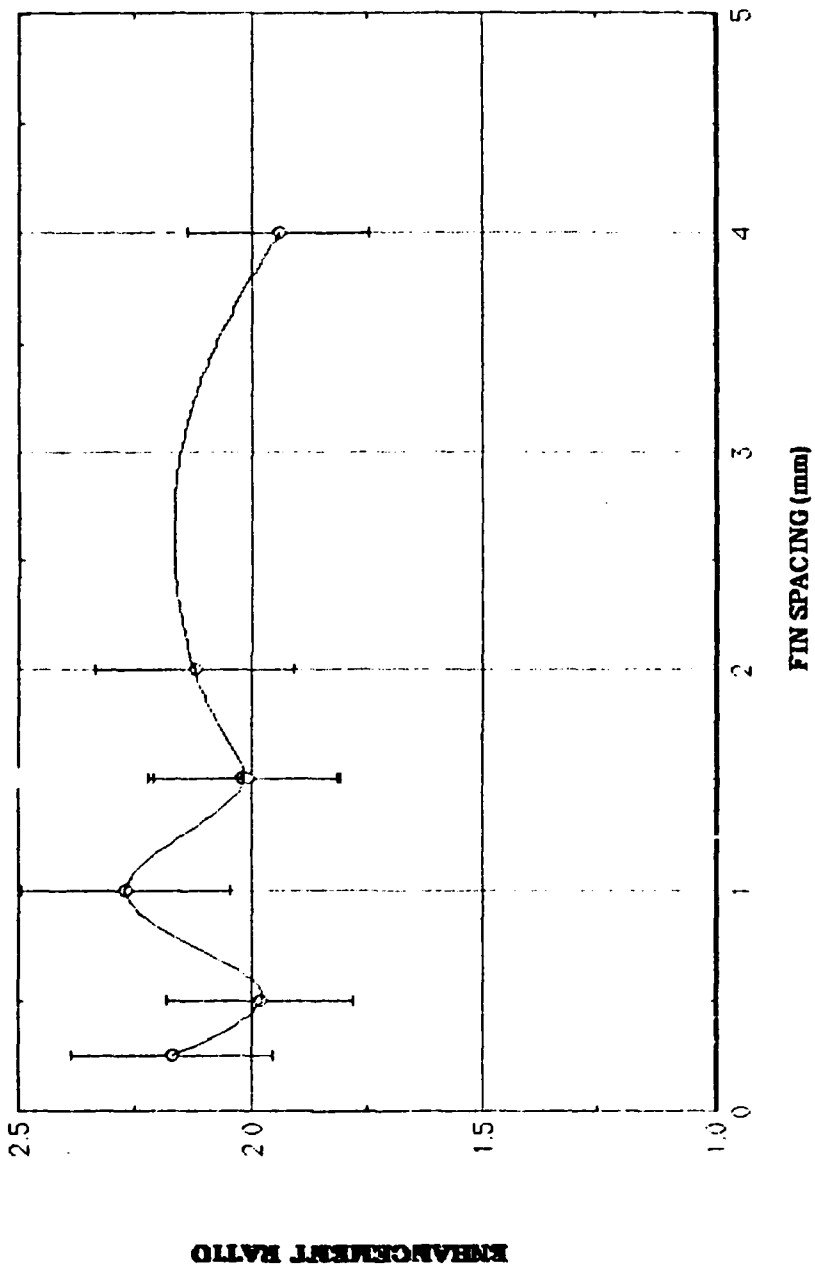


Figure 5.28 Small Tube Enhancements with Uncertainties at Atmospheric Conditions

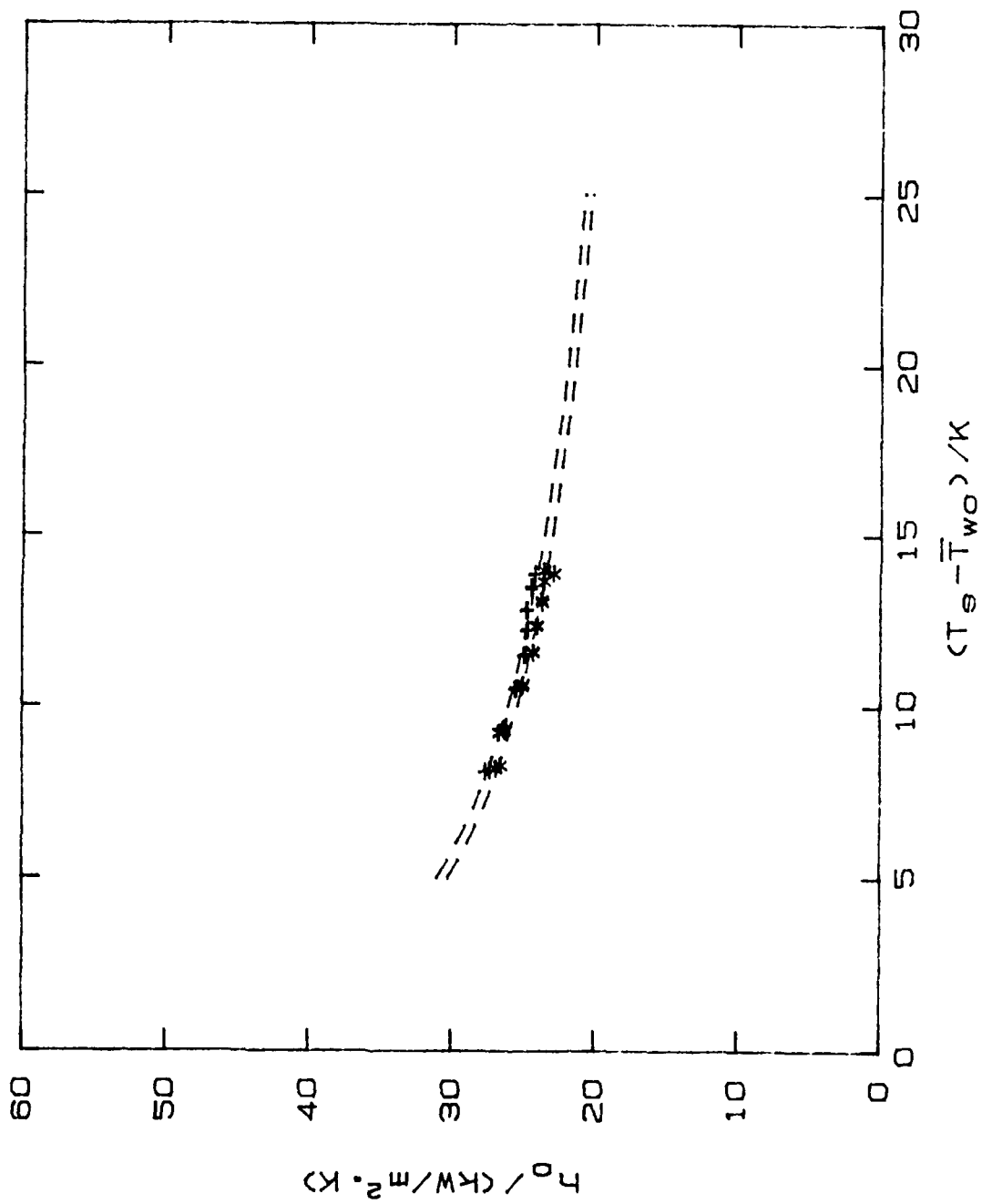


Figure 5.29 Repeatability of Tube 5 Data Under Vacuum Conditions

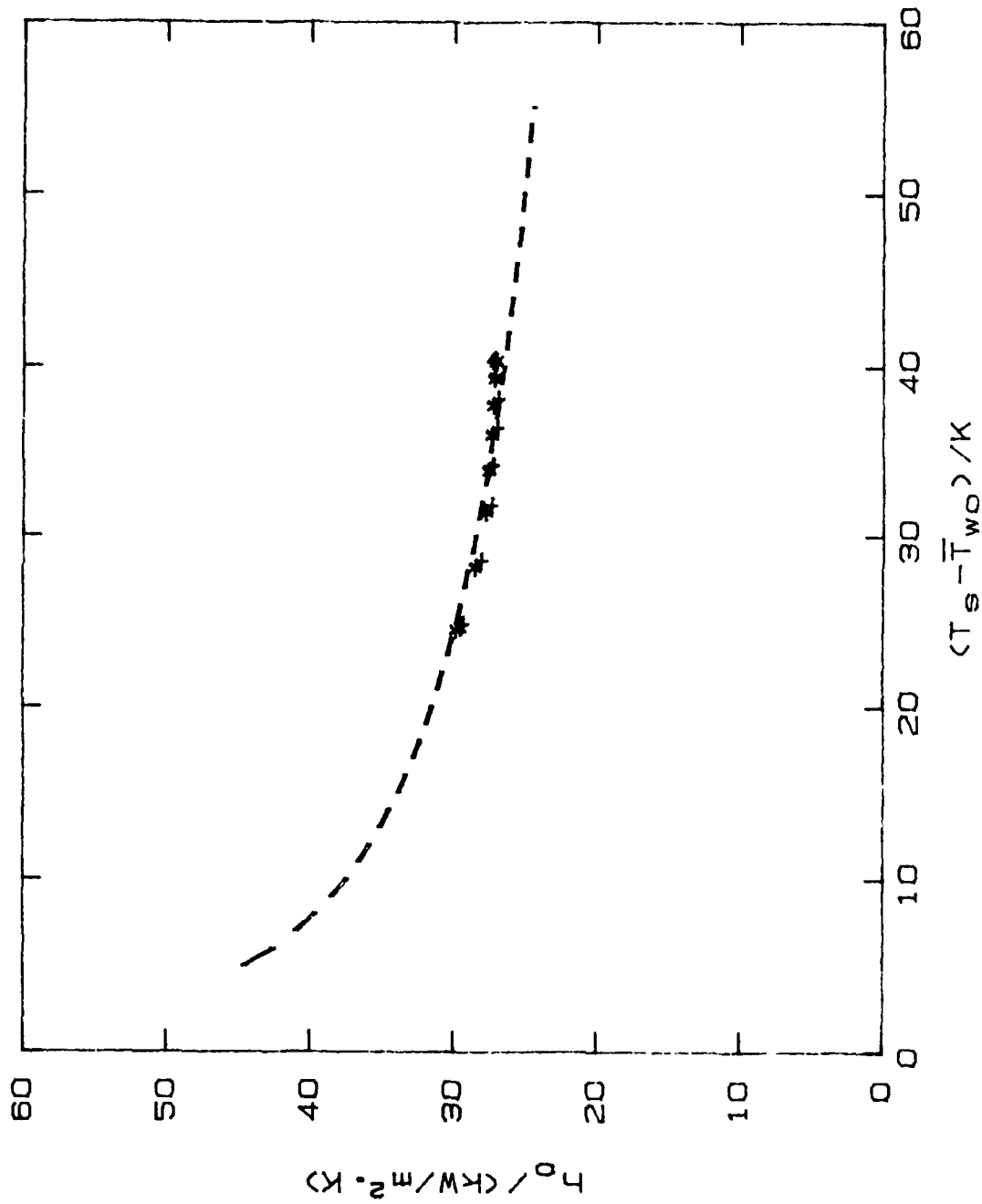


Figure 5.30 Repeatability of Tube 5 Data at Atmospheric Conditions

the calculated heat-transfer enhancement ratios are lower.

TABLE 5.6

SUMMARY OF SMOOTH TUBE α 'S

	Vacuum		Atmospheric	
	Small	Medium	Small	Medium
Van Petten	0.803	0.803	0.867	0.867
Coumes	0.933	0.838	0.952	0.876
% Difference	13.9	4.2	8.9	1.0

Theoretically, as Equation (4.9) shows, the effect of tube diameter appears only in the value of F^* , and α should therefore be independent of tube diameter. The higher value obtained for the small tube, both when compared to the medium tube data and to the Fujii correlation could be attributed to undetected dropwise condensation, or perhaps simply to the uncertainty of the data.

When the results obtained by Van Petten [Ref.6] for large tubes are combined with results presented in Figures 5.25 and 5.26, it can be clearly seen that the enhancement ratio increases as tube diameter increases, as shown in Figures 5.31 and 5.32.

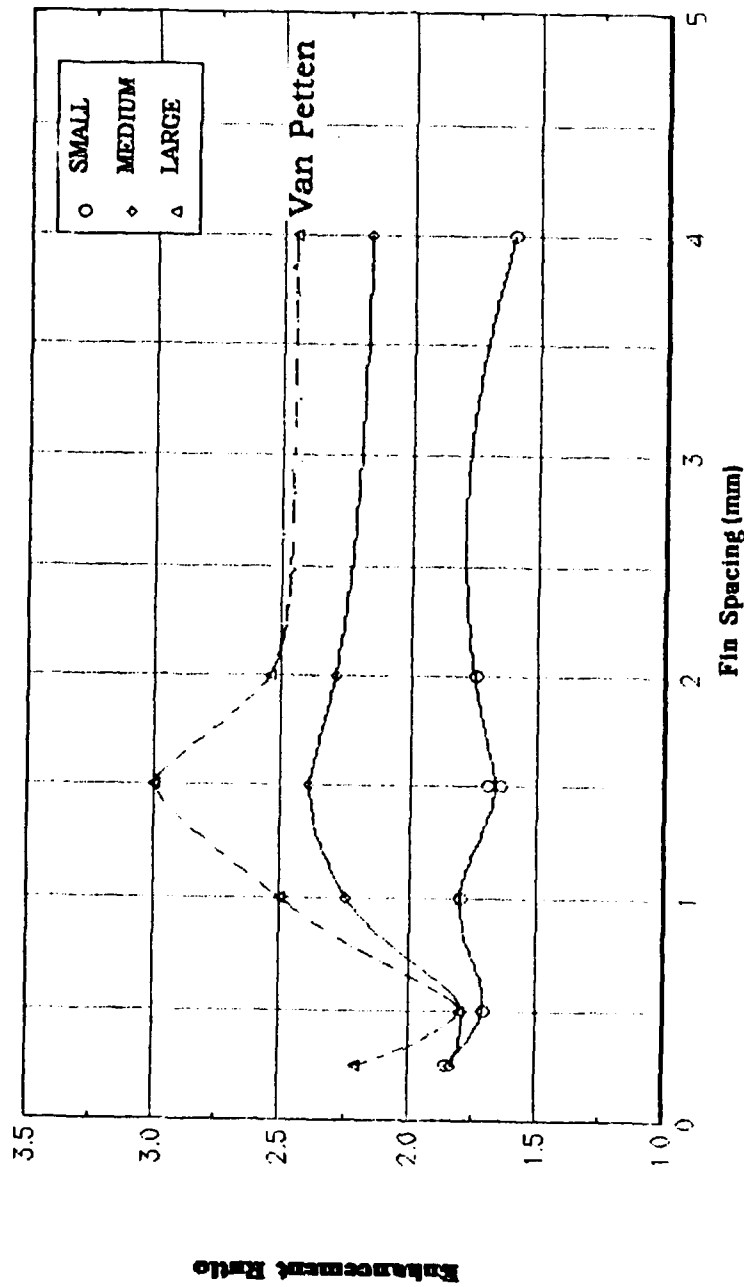


Figure 5.31 Heat-Transfer Enhancement Ratios for the Small, Medium and Large Tubes Under Vacuum Conditions

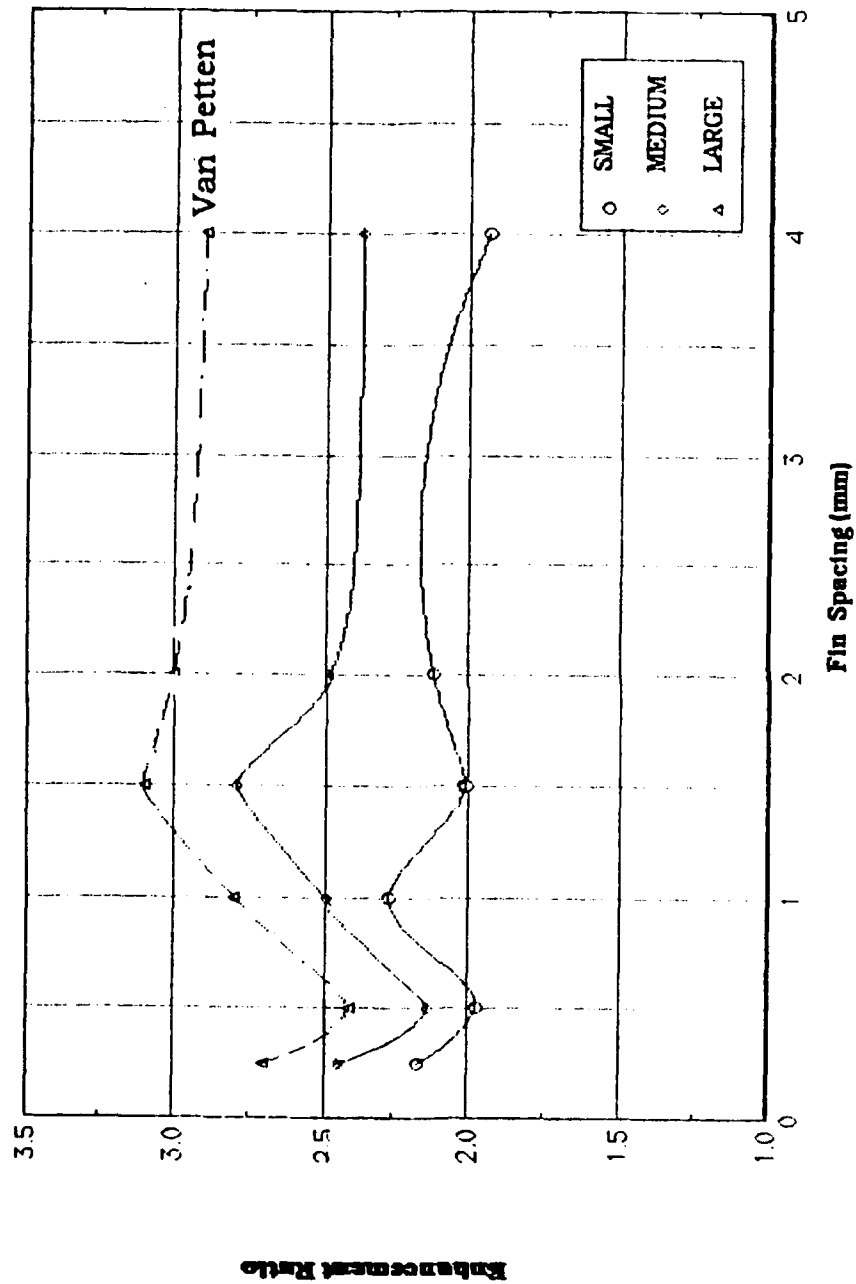


Figure 5.32 Heat - Transfer Enhancement Ratios for the Small, Medium and Large Tubes at Atmospheric Conditions

5. QMC and QMCNPS Tubes

Specific discussion of these results has been previously deferred. One of the thesis' objectives was to attempt to resolve differences in data collected during a concurrent research project being conducted by Queen Mary College (QMC) of the University of London.

Marto [Ref. 5] compares data taken at NPS for R-113 and steam with the data taken at QMC. The NPS data was gathered for tubes with fin heights of 1 mm, fin thicknesses of 1 mm, and a fin root diameter of 12.7 mm, while the QMC data were for tubes with a fin height of 1.59 mm, fin thicknesses of 0.5 mm, and a fin root radius of 12.6 mm. As expected, and shown in Figure 5.33, because of the increased heat-transfer area (due to larger fin height and fin density), for R-113, the QMC data showed enhancements greater than the NPS data. However, for steam, just the opposite trend was unexplicably observed.

In order to more closely correlate the data, and to attempt to resolve the conflicting trends, a tube was manufactured for testing at NPS (termed the QMC.NPS tube). Its geometric parameters of fin height, thickness, and spacing, internal diameter and fin root diameter were to match those of a tube being used in the QMC investigation. Van Petten [Ref. 6] reported preliminary results for R-113 and steam. The R-113 data point appears on Figure 5.33,

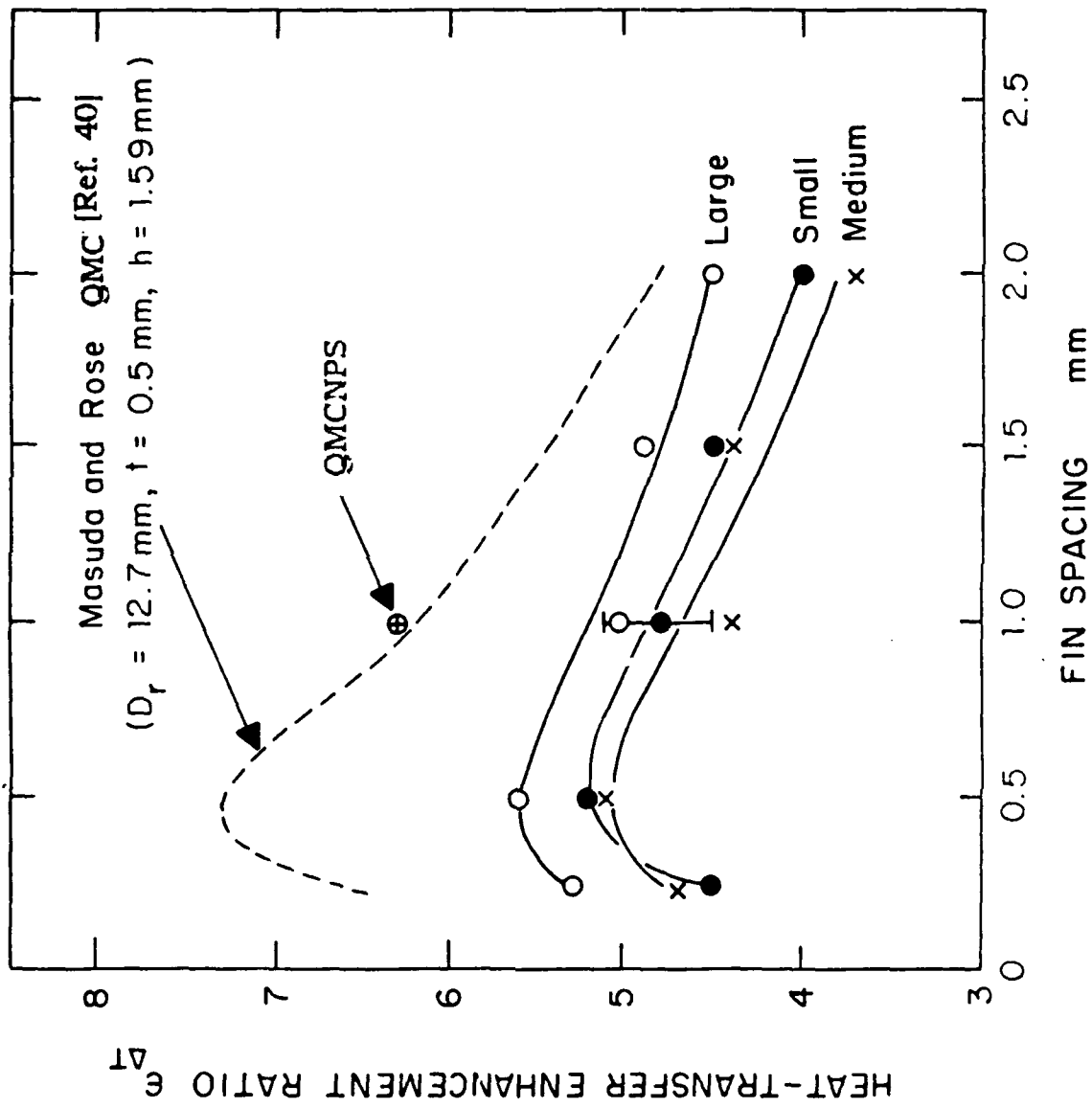


Figure 5.33 Comparison of NPS and QMC Data for R-113 [Ref. 42]

denoted as QMCNPS, and is in excellent agreement with the QMC data of Masuda and Rose [Ref. 40]. However, with the steam data point, there was no agreement.

During this study, a tube actually used in the QMC study was also modified and then tested (termed the QMC tube). A detailed geometric comparison between that tube and the QMCNPS tube was previously given in Table 3.2. Figures 5.17 and 5.18 show comparisons of the two tubes' data.

When calculating the enhancement ratios for the tubes, several methods were considered. Table 5.2 lists the Sieder-Tate coefficients for all tubes tested. Because the coefficients for the QMC tube were considerably lower than that of the QMCNPS tube (and the other small tubes), two different enhancements were calculated and are reported here. One ratio was based on the 'best fit' coefficient of Table 5.2, while the other used the 'average' coefficient of Table 5.3. Figures 5.34 and 5.35 show the data plotted using the 'best fit' and 'average' coefficients, under vacuum and at atmospheric conditions. As can be observed, the 'average' coefficient with the least-squares-fit distorts the data considerably, when compared to the 'best fit' curve. Table 5.7 lists the enhancement ratios determined using both schemes.

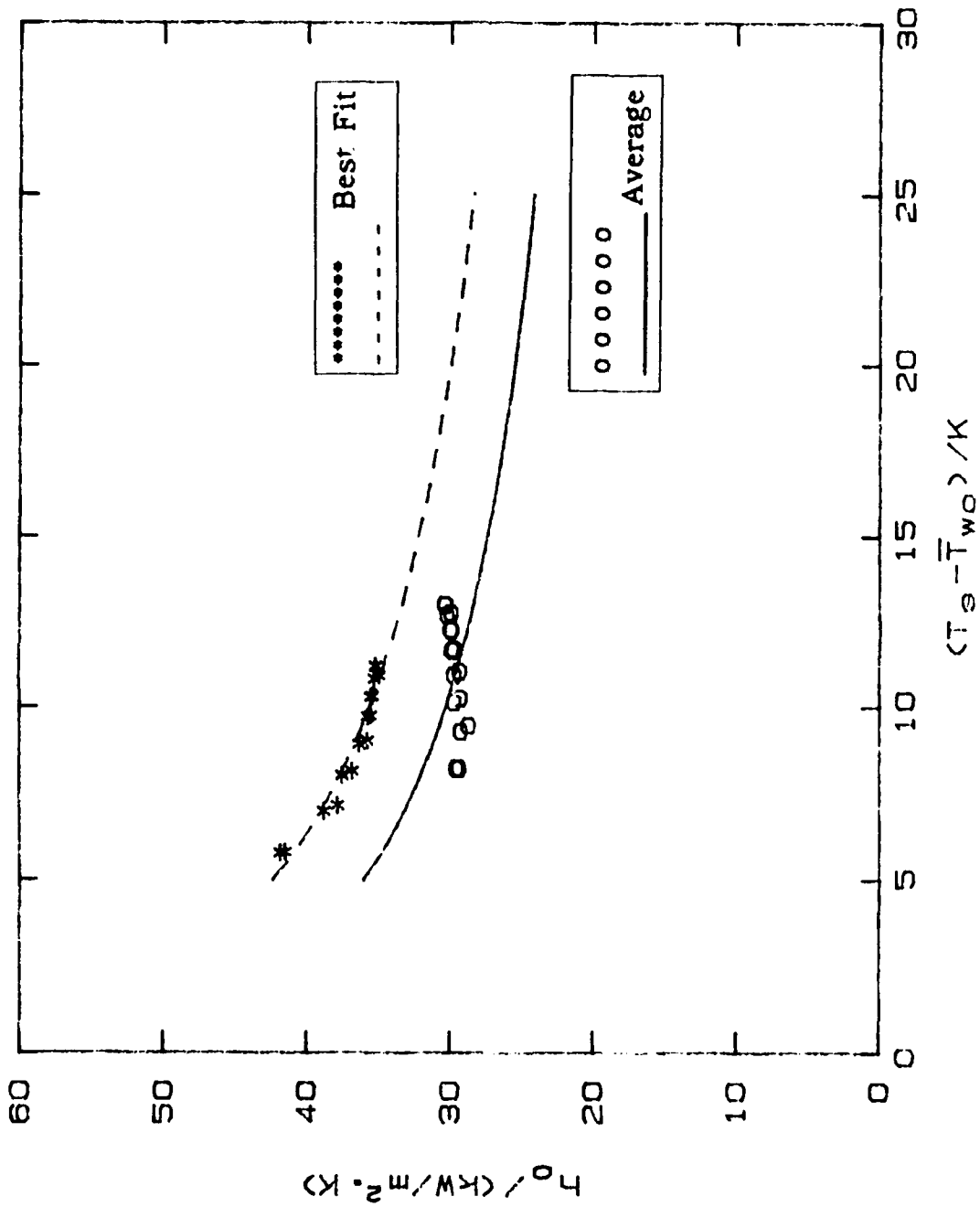


Figure 5.34 Data for the QMC Tube Under Vacuum Conditions Using 'Best Fit' Versus 'Average' Values of C_i

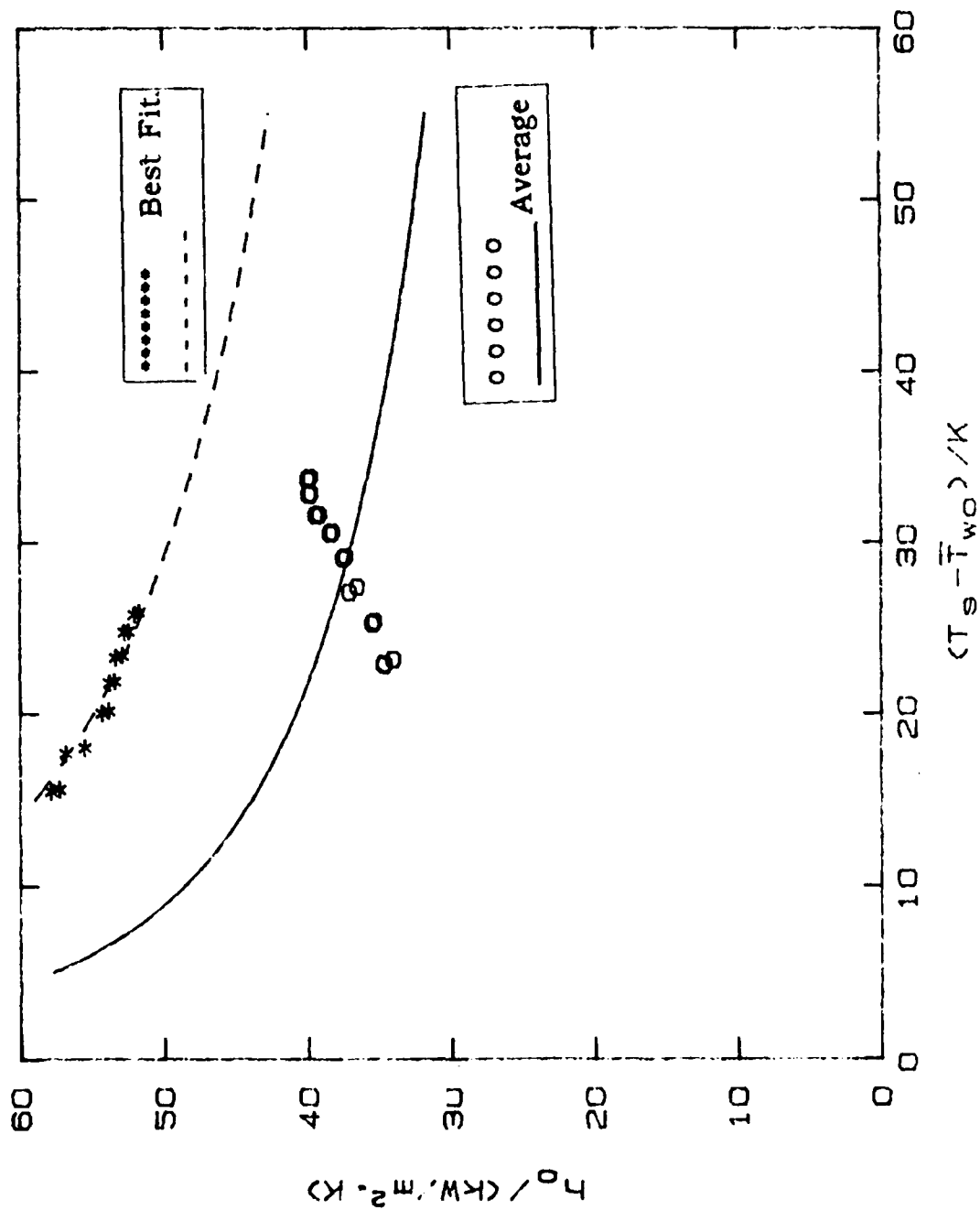


Figure 5.35 Data for the QMC Tube Under Vacuum Conditions Using 'Best Fit' Versus 'Average' Values of C_i

TABLE 5.7

ENHANCEMENT RATIOS FOR QMC AND QMCNPS TUBES

	Vacuum		Atmospheric	
	QMC	QMCNPS	QMC	QMCNPS
Best Fit	2.59	1.98	3.54	2.68
Average	2.05	2.05	2.64	2.61

Although the 'average' method gives enhancement ratio results that are in close agreement, Figures 5.34 and 5.35 graphically demonstrate the reason why it should not be done. Figure 5.36 shows the enhancement ratios for the 'best fit' scheme at atmospheric conditions, also included are actual QMC data [Ref. 43] for steam. The inconsistency of the different data is clearly seen, but is still not fully understood. Possible causes could include:

1. discrepancies in geometry of tubes, detailed in Table 3.2 and Figures 3.11 and 3.12
2. calculation of enhancements
3. use of spiral insert and its effect on the value of the inside heat-transfer coefficient

The last item appears to be the most obvious starting place to begin a systematic review of the difference in the two investigations. The QMC data for steam was obtained without using an insert. Therefore, α 's for both smooth and finned tubes could be significantly different. Also, the good agreement for R-113 may be due to the fact that the data obtained at NPS was also without an insert.

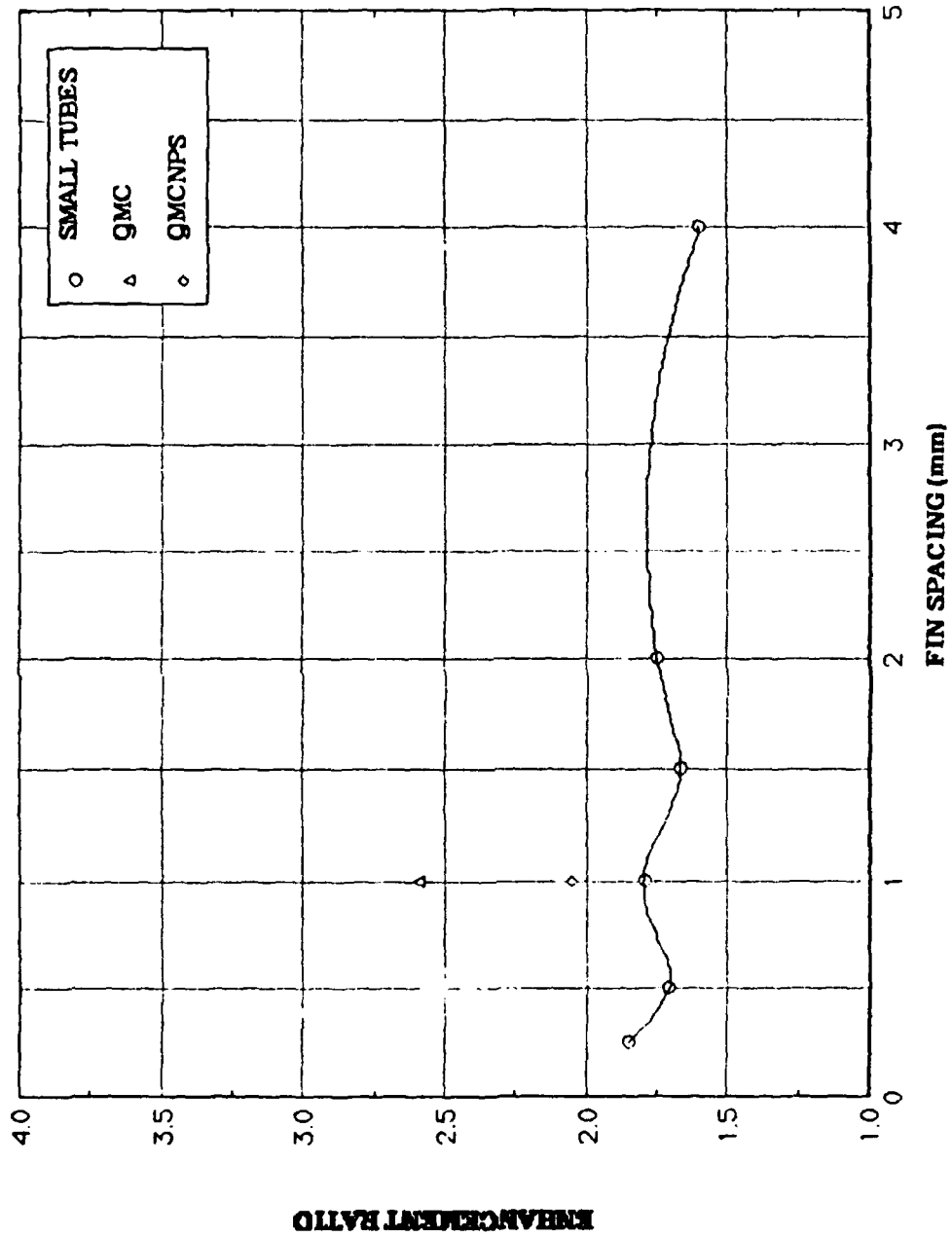
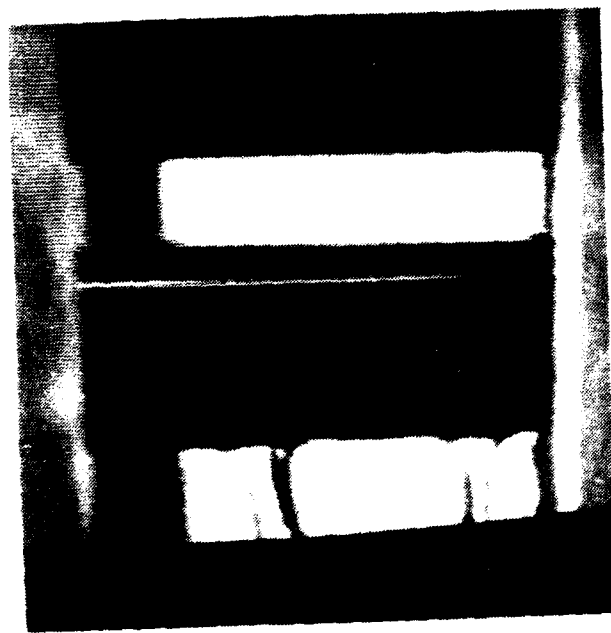


Figure 5.36 'Best Fit' Enhancement Ratios at Atmospheric Conditions for QMC Tubes and QMCNPS Tube

B. INUNDATION EFFECT

Flow visualization studies of the effect of condensate inundation were conducted for both smooth and finned tubes. Preliminary static (i.e., non-condensing) studies with water had demonstrated that the design of the inundation tubes, Figures 3.6 and 3.7, would support the inundation rates required to observe the full range of flow modes which Honda et. al [Ref. 33] had described.

The condensate return system, in its original design was unable to maintain a constant inundation rate, because of pump cavitation. A modified system was temporarily installed to provide recirculated condensate to a single inundation tube in order to obtain photographs for the initial phase of flow-visualization. Two medium smooth tubes, one in the dummy tube position, the other in the active tube position, were placed in the test section and atmospheric operating conditions were reached. Visual observations, made as inundation rate was increased, revealed the four falling modes. A video camera was used to record the condensate flow patterns as the inundation rate was varied. Figures 5.37 through 5.42 are Polaroid snapshots showing the various modes, as well as a value for the dimensionless parameter, K , described in Equation (2.26). In the droplet and column modes, the condensate falls at regularly spaced intervals (corresponding to the Taylor wavelength, Yung et. al [Ref. 44]), and spreads axially over the entire surface of the smooth tube. At the maximum inundation



**Figure 5.37 Inundation of Smooth Tube,
Droplet Mode, $K = 0.017$**

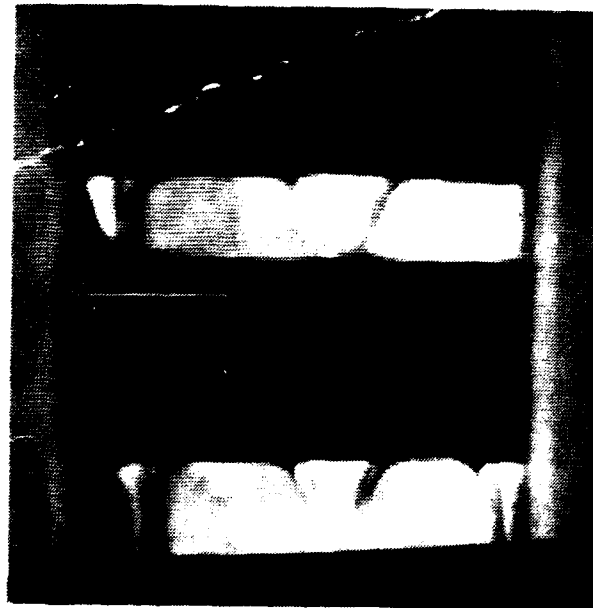


**Figure 5.38 Inundation of Smooth Tube,
Droplet Mode, $K = 0.045$**

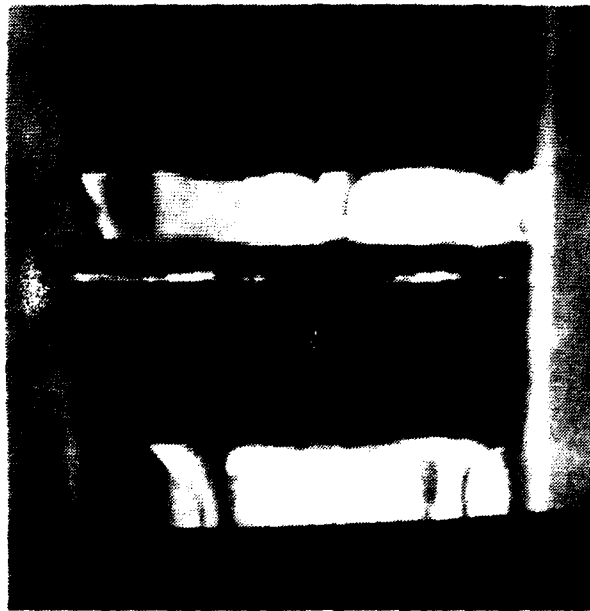


**Figure 5.39 Inundation of Smooth Tube,
Droplet - Column Mode, $K = 0.095$**



**Figure 5.40 Inundation of Smooth Tube,
Column Mode, $K = 0.15$**

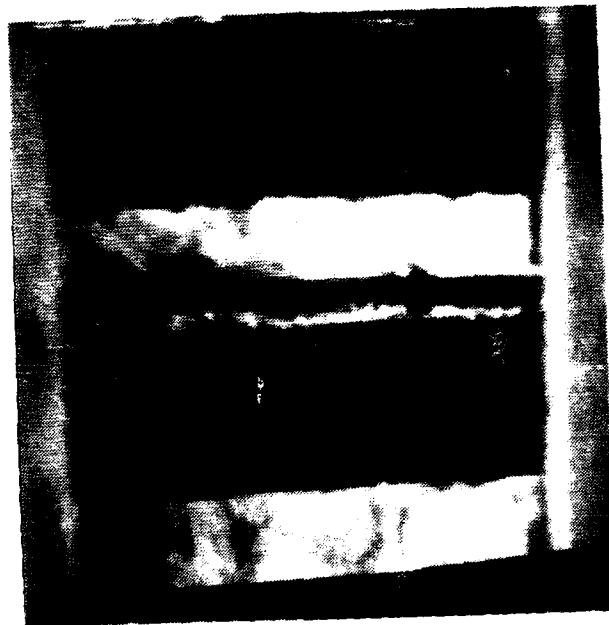
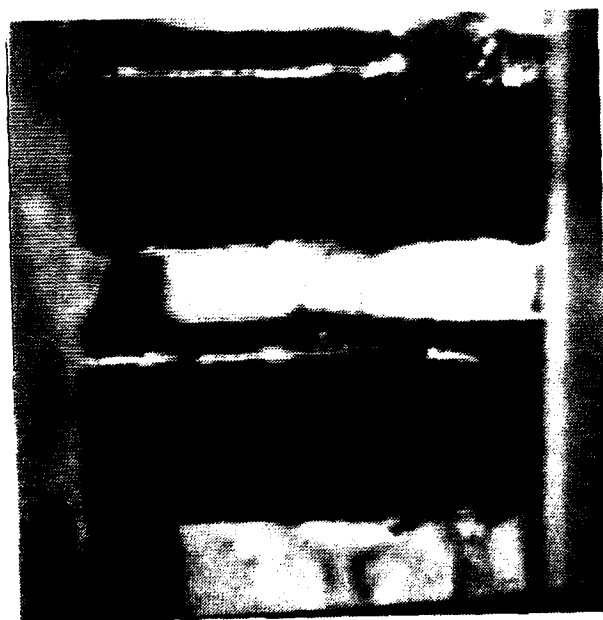


Figure 5.41 Inundation of a Smooth Tube,
Column Mode, $K = 0.21$



**Figure 5.42 Inundation of Smooth Tube,
Column - Sheet Mode, $K = 0.27$**

rate, flow has nearly transitioned completely to the sheet mode.

The smooth tubes were removed and a pair of medium diameter finned tubes (1 mm fin spacing, thickness and height) were installed in their places. Atmospheric conditions were achieved and visual observations were again made. Both 35mm and video cameras were employed to record the falling modes. Figures 5.43 through 5.52 are 35mm prints which show the flow pattern and the corresponding value of K . Just as in the smooth tube case, in the droplet and column modes the condensate falls at regularly spaced intervals. However, as the photographs clearly show the condensate falls to the tube below and then flows circumferentially down the grooves between several adjacent fins. This is in contrast to the smooth tubes where the condensate has a tendency to flow axially as well as circumferentially around the tube. The space between these condensate inundated regions is unaffected, and therefore a significantly enhanced heat-transfer performance is expected when compared to the smooth tube, whose entire surface is wetted by the axial migration of the falling condensate.

Honda et. al [Ref. 33] reported K values for falling mode transitions. A comparison of those reported values (for low surface tension fluids) with those observed during this preliminary investigation are recorded in Table 5.8.

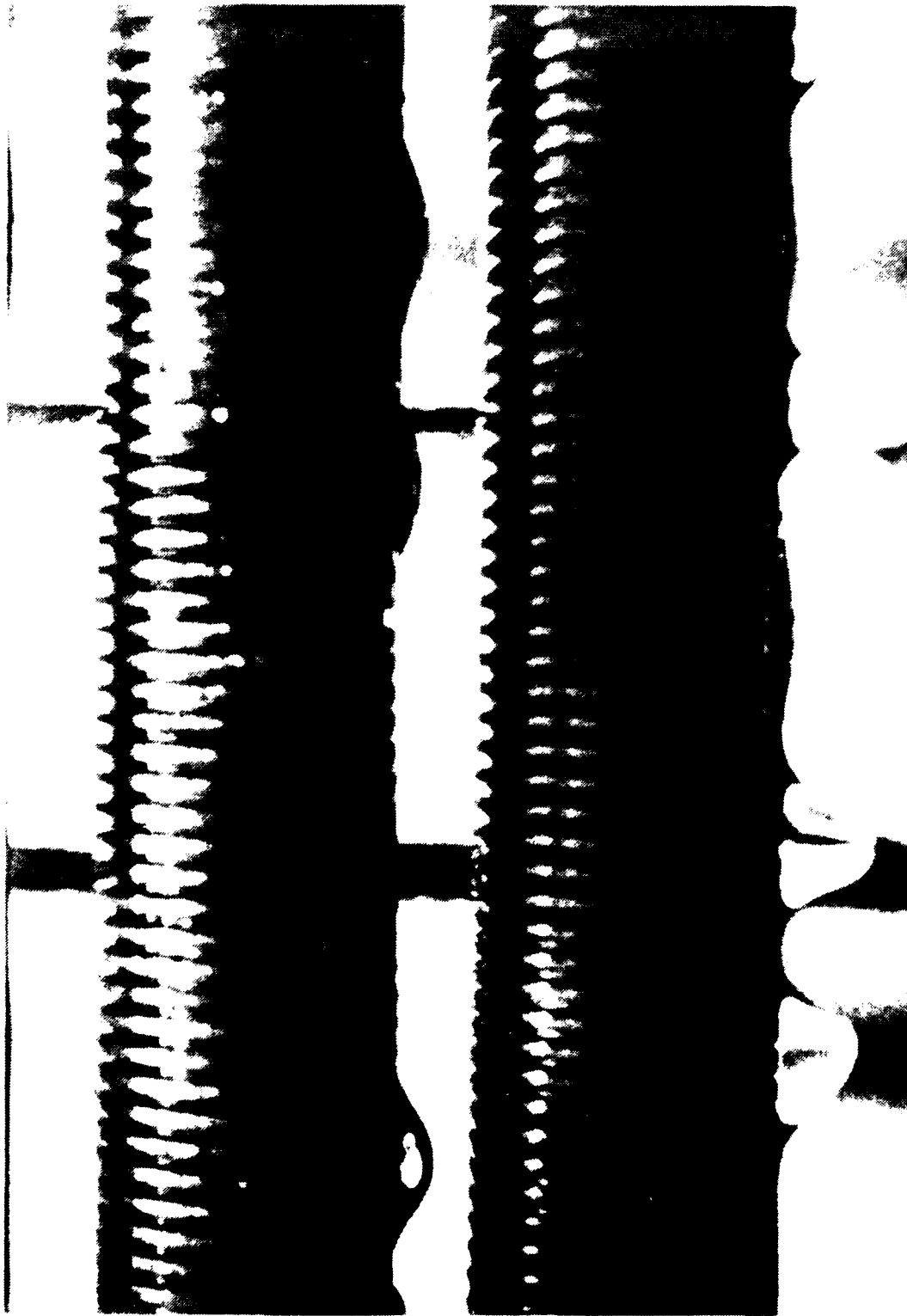


**Figure 5.43 Inundation of Finned Tube
Droplet Mode, $K = 0.030$**

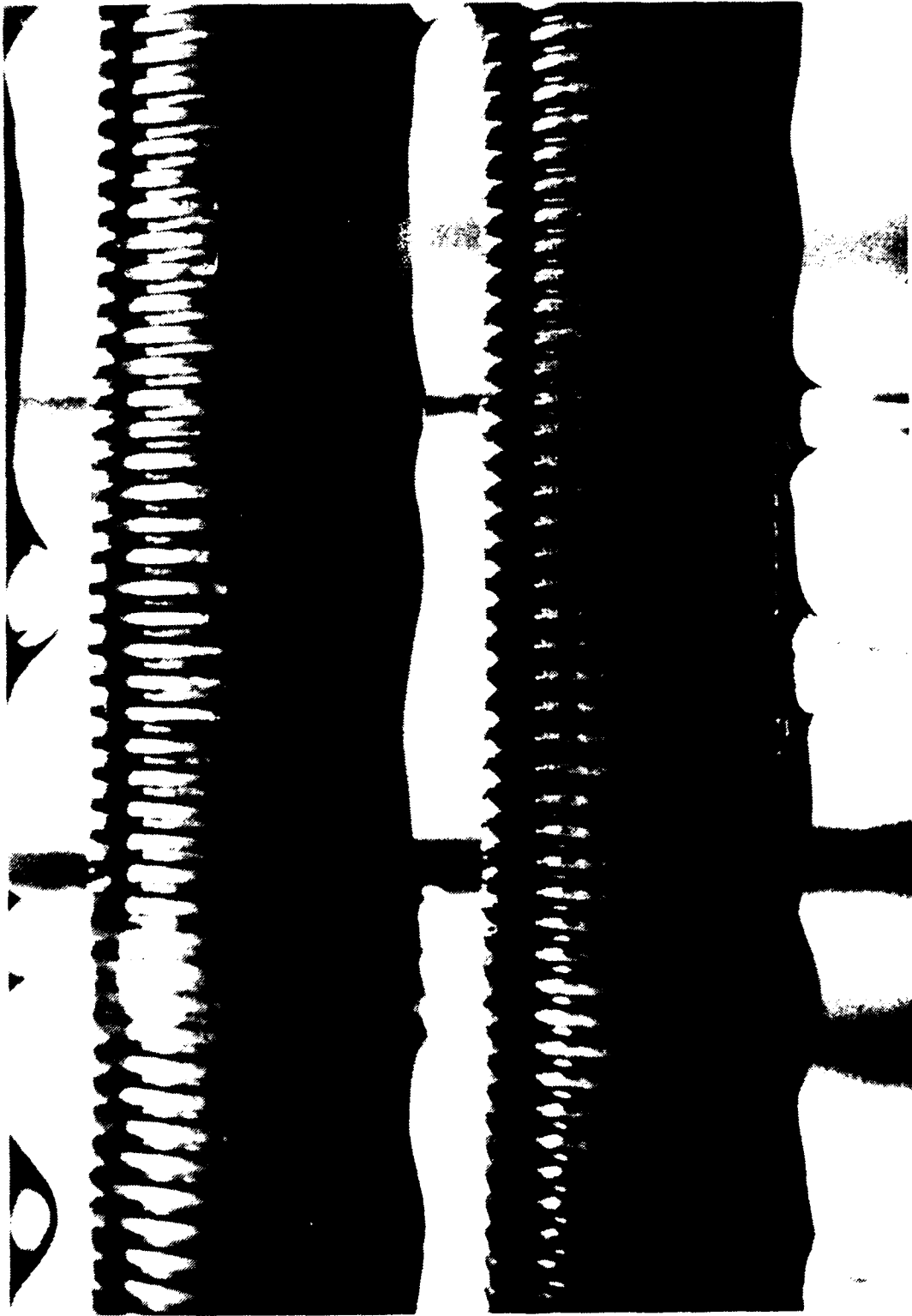
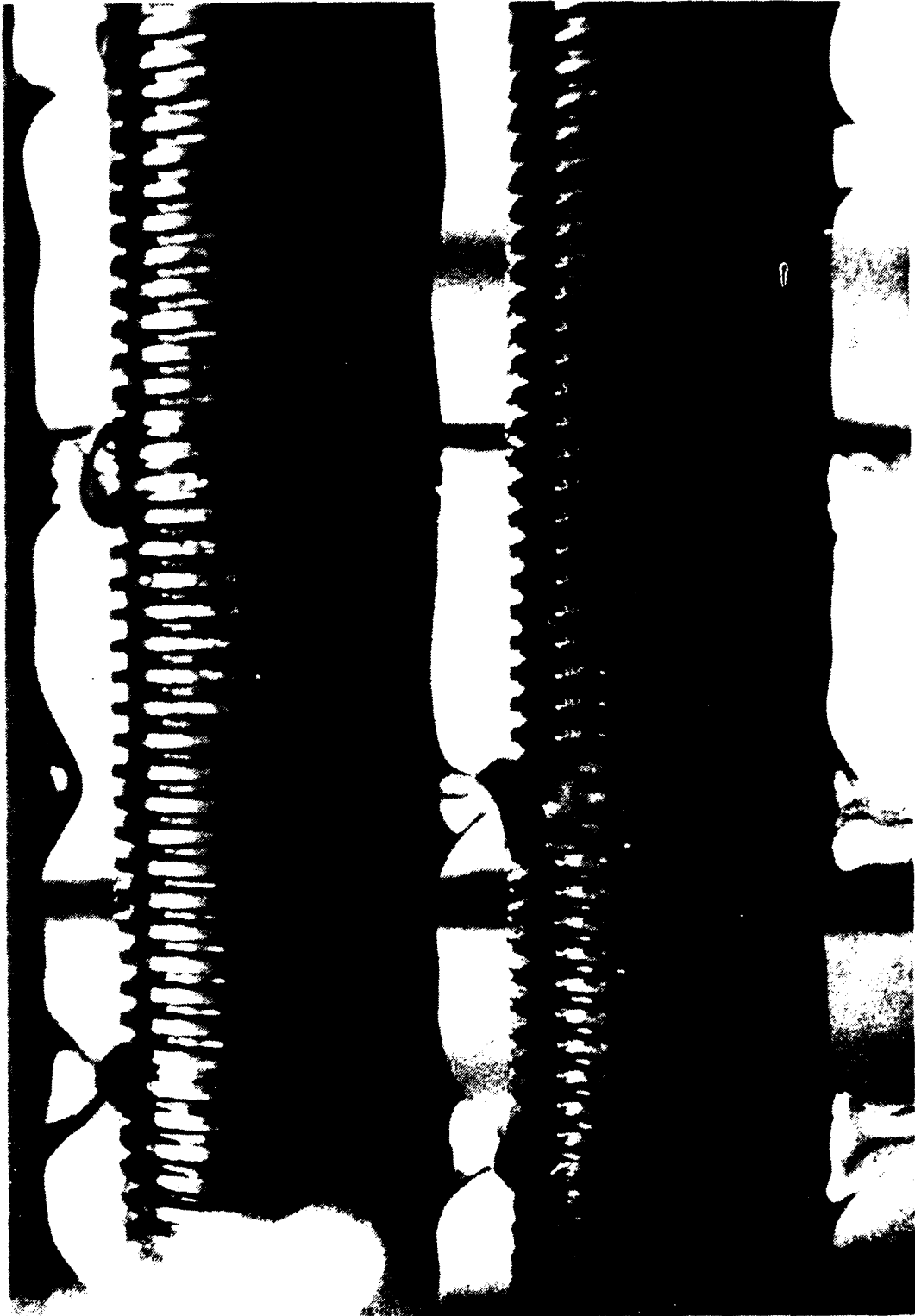
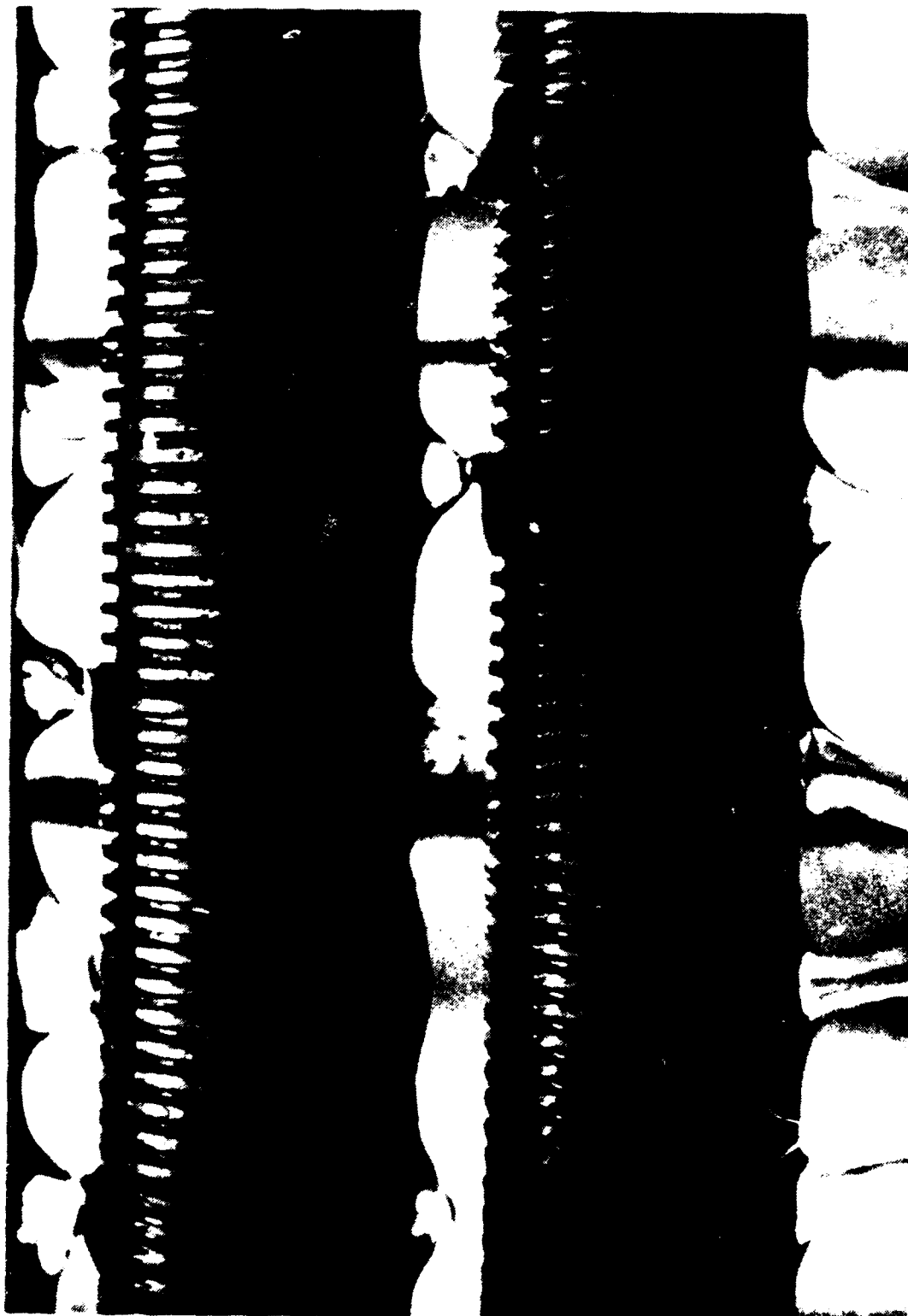


Figure 5.44 Inundation of Finned Tube,
Droplet Mode, $K = 0.065$



**Figure 5.45 Inundation of Finned Tube,
Droplet - Column Mode, $K = 0.100$**



**Figure 5.46 Inundation of Finned Tube,
Column Mode, $K = 0.14$**

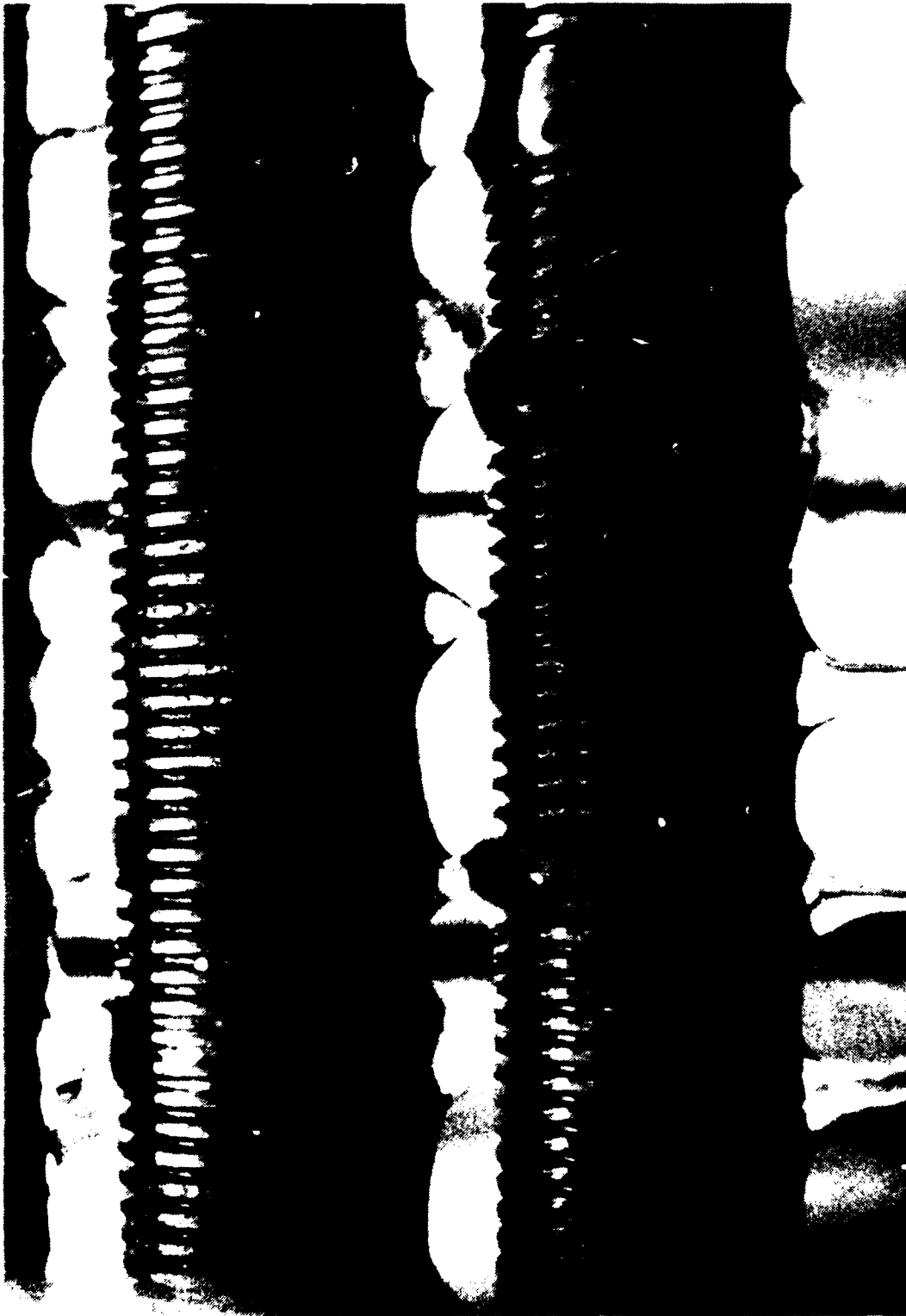


**Figure 5.47 Inundation of Finned Tube
Column Mode, $K= 0.17$**

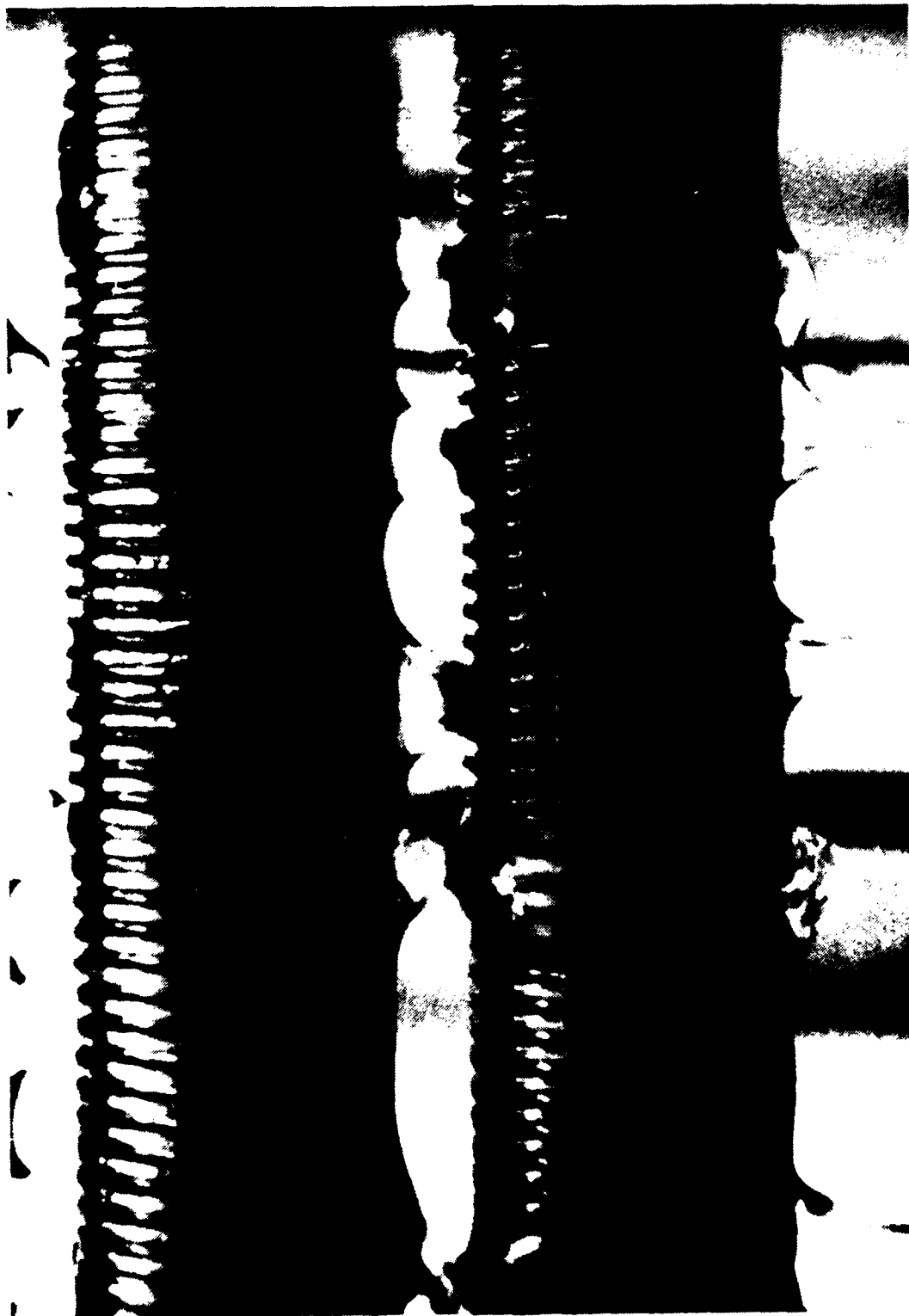


**Figure 5.48 Inundation of Finned Tube
Column Mode, $K = 0.20$**

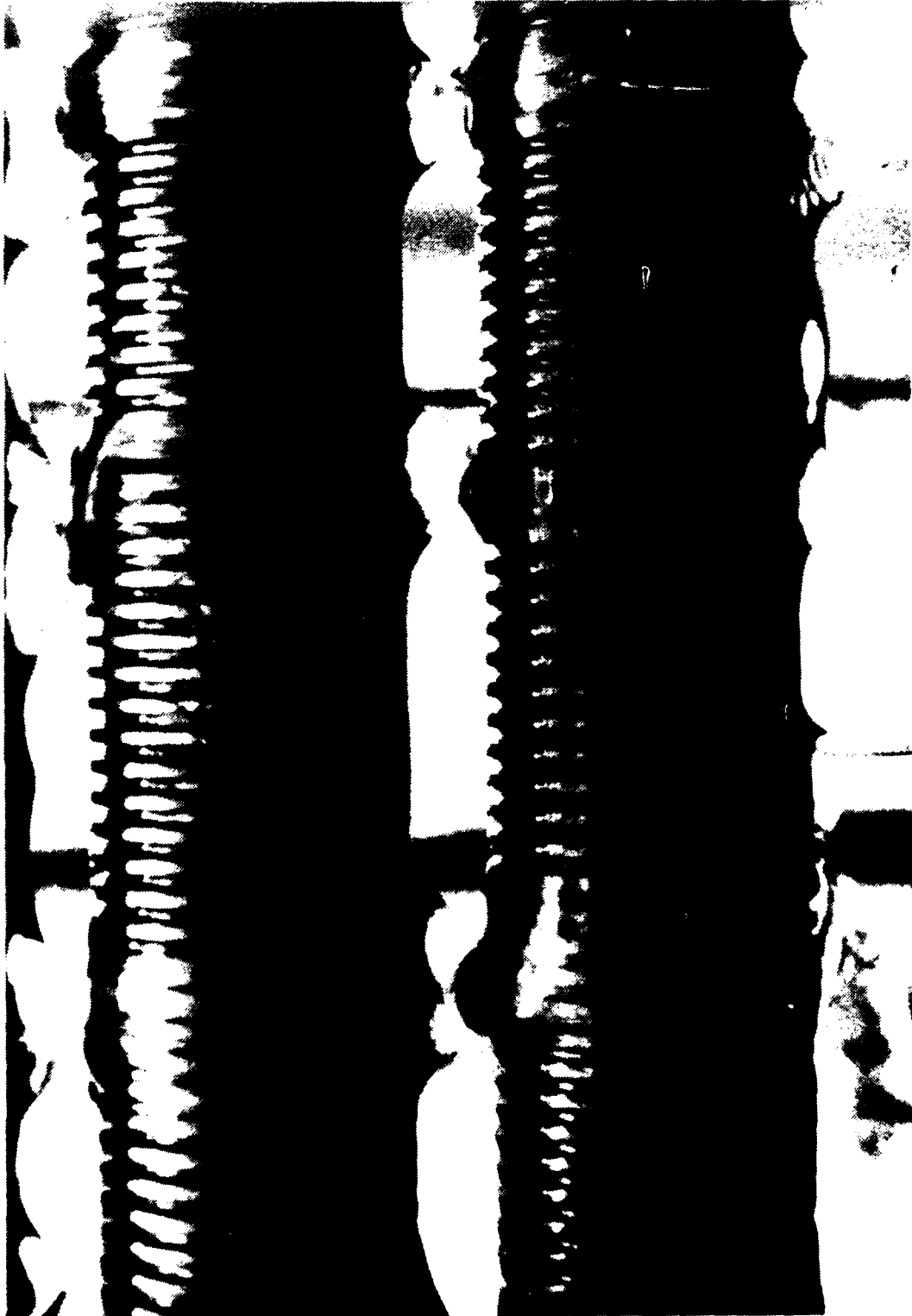


**Figure 5.49 Inundation of Finned Tube
Column Mode, $K = 0.24$**



**Figure 5.50 Inundation of Finned Tube
Column Mode, $K = 0.27$**



Figure 5.51 Inundation of Finned Tube
Column Mode, $K = 0.31$



**Figure 5.52 Inundation of Finned Tube
Column - Sheet Mode, $K = 0.34$**

TABLE 5.8

DIMENSIONLESS PARAMETER, K

	Honda	Smooth Tubes	Finned Tubes
Falling Modes			
Droplet - Droplet/Column	0.06-0.13	0.045	0.065
Droplet/Column - Column	0.06-0.13	0.095	0.10
Column - Column/sheet	0.37-0.47	0.27	0.34

VI. CONCLUSIONS AND RECOMMENDATIONS

A. CONCLUSIONS

1. The heat transfer enhancement of integral-fin tubes is affected by root diameter. Enhancement increases as root diameter increases.
2. The optimum fin spacing is near 1.5 mm for the medium tube, as found in previous published investigations.
3. Small tube behavior deviates from the standard optimum fin spacing, and appears to exhibit an optimum fin spacing of 1 mm.
4. Data taken for the QMC tube is unexplainably higher than that obtained by the joint project at Queen Mary College. The utilization of a spiral insert during the tests at NPS may be the cause .
5. Condensate inundation flow modes were correlated to the dimensionless parameter K .
6. Photographic and visual observations clearly demonstrated axial migration of condensate for smooth tubes, resulting in a totally wetted surface. For finned tubes, circumferential migration (limited to several channels between adjacent fins) was observed, leaving unaffected portions of the finned tube free of inundation.

B. RECOMMENDATIONS

1. Obtain small tubes with fin spacings of 1.25 and 1.75 mm in order to determine an optimum fin spacing for this small diameter tube.

2. Re-examine all the differences between the tubes used in the joint program with Queen Mary College and then repeat measurements in an effort to clear up the inconsistencies in the steam data.

3. Take data with and without the spiral insert and process the resulting data with the new form of the Sieder-Tate relationship (i.e. $B \neq 0$).

4. Replace the mercury-in-glass manometer with direct reading pressure gage.

5. Relocate the pressure and temperature probes in the inundation test section so they are upstream of the test tubes instead of downstream as presently located.

6. Obtain additional finned tubes to support further condensate inundation studies.

7. Conduct condensation studies with condensate inundation effects for various fluids, including steam and R-113.

APPENDIX A

SYSTEM START - UP AND SHUT - DOWN PROCEDURES

The system is started in the following manner:

1. Fill the boiler with distilled water to a level of four to six inches above the top of the heating elements.
2. Check purge pump system; oil level, drain valves, system vent valve.
3. Turn on data acquisition program and load software program entitled DRP12S.
4. Open fill valve for cooling water sump supply.
5. Turn on cooling water supply pumps and adjust tube flow rate to approximately 45%.
6. Open valve from tap water system to auxiliary condenser and adjust flow rate to approximately 40%.
7. Check system for water leaks.
8. Energize heaters and adjust voltage to ~50 volts for system warm-up.
9. If conducting vacuum run, energize vacuum purge pump, then open system vent valve (single turn).
10. Monitor system temperature (via thermocouple voltage reading) and pressure (mercury-in-glass manometer) carefully.
11. If conducting vacuum run wait until system pressure reaches

~120 mm Hg (left hand column) and then gradually increase voltage in 10 volt increments to 90 volts. Obtain desired operating condition by manually controlling flow through auxiliary condenser.

12. If conducting atmospheric run, open system vent valve and purge system drain valve. After ~1/2 hour warm-up begin increasing voltage in 10 volt increments until ~95 volts is reached. Wait until system pressure drops (just as hot vapor bubble makes its 180° turn at the top of the apparatus), then close system vent valve and purge system drain valve. Energize vacuum pump and open the system vent valve ~1/3 turn. Simultaneously raise voltage in 20 volt increments to 175 volts while throttling flow through the auxiliary condenser to obtain desired operating conditions.

13. Adjust cooling water flow meter setting to proper % for initial data run.

14. Allow the vacuum pump to operate continuously, monitor oil level through sight-glass.

The system is secured in the following manner:

1. Secure power to the boiler elements.
2. Isolate and secure the purge system.
3. Slowly open the system vent valve and purge drain valve in order to allow the system to come to atmospheric pressure.

4. Continue to circulate cooling water through the tube and auxiliary condenser to assist in cooling down the system.
5. Monitor system temperature, and when cool turn off data aquisition system.
5. Secure the cooling water systems.
6. Check oil level (and quality) in purge pump.
7. Periodically change distilled water in boiler.

APPENDIX B

UNCERTAINTIES AND ASSUMPTIONS

Uncertainties are unavoidably introduced whenever taking measurements. They are dependent upon the accuracy of measuring equipment and the operator's skill in using them. Although uncertainties associated with single measurements may be small, when combined with others in the data reduction scheme, they can quickly propagate into a rather large uncertainty. The uncertainties of the measured quantities in this investigation were determined by using the follow relationship proposed by Kline and McClintock [Ref. 45]:

$$W_r = \{ [(\delta R/\delta X_1)W_1]^2 + [(\delta R/\delta X_2)W_2]^2 + \dots + [(\delta R/\delta X_n)W_n]^2 \}^{1/2} \quad (B.1)$$

where

R = the result of the calculation,

W_r = the uncertainty of the result,

X_i = the measured independent variables ($i=1,2,3,\dots,n$),

W_i = the uncertainty in the measured variable ($i=1,2,3,\dots,n$).

Georgiadis [Ref. 35] provides a detailed account of the development of the uncertainty analysis. Mitrou [Ref. 46] created a program which calculated uncertainties. Sample outputs follow:

DATA FOR THE UNCERTAINTY ANALYSIS:

File Name: 25V
 Pressure Condition: Vacuum (11 kPa)
 Vapor Temperature = 48.40 (Deg C)
 Water Flow Rate (%) = 66.00
 Water Velocity = 6.49 (m/s)
 Heat Flux = 2.359E+05 (W/m^2)
 Tube-metal thermal conduc. = 385.0 (W/m.K)
 Sieder-Tate constant = 0.0470

UNCERTAINTY ANALYSIS:

VARIABLE	PERCENT UNCERTAINTY
Mass Flow Rate, Md	0.95
Reynolds Number, Re	1.28
Heat Flux, q	1.28
Log-Mean-Tem Diff, LMTD	.73
Wall Resistance, Rw	2.63
Overall H.T.C., Uo	1.47
Water-Side H.T.C., Hi	6.48
Vapor-Side H.T.C., Ho	6.91

DATA FOR THE UNCERTAINTY ANALYSIS:

File Name: 125A
 Pressure Condition: Atmospheric (101 kPa)
 Vapor Temperature = 100.05 (Deg C)
 Water Flow Rate (%) = 54.00
 Water Velocity = 2.99 (m/s)
 Heat Flux = 8.792E+05 (W/m^2)
 Tube-metal thermal conduc. = 385.0 (W/m.K)
 Sieder-Tate constant = 0.0650

UNCERTAINTY ANALYSIS:

VARIABLE	PERCENT UNCERTAINTY
Mass Flow Rate, Md	1.16
Reynolds Number, Re	1.42
Heat Flux, q	1.25
Log-Mean-Tem Diff, LMTD	.16
Wall Resistance, Rw	2.67
Overall H.T.C., Uo	1.27
Water-Side H.T.C., Hi	3.30
Vapor-Side H.T.C., Ho	5.98

Perhaps just as important as uncertainties in the final evaluation of collected data is considering the assumptions used throughout the data reduction analysis. A partial list of the assumptions used during this investigation follows:

- no partial dropwise condensation occurs
- fouling not included as thermal resistance
- noncondensable gases not included as thermal resistance
- strictly radial conduction through the tube wall(i.e. concentric isotherms were assumed)
- no circumferential variation in wall temperature profile considered
- thermal properties of tube material considered uniform and constant
- thermal resistance of black oxide layer considered negligible
- modelling of inlet and outlet portions of tube as fins
- evaluation of cooling water properties at bulk average temperature
- use of Modified-Wilson-Plot technique
- assumption of Sieder-Tate type relationship for inside heat-transfer coefficient with swirl-type insert
- assumption of Nusselt-type relationship for outside heat-transfer coefficient

- calculation of condensate film temperature as

$$(2/3)T_{\text{wall}} + (1/3)T_{\text{sat}}$$

APPENDIX C

RAW DATA

Table C.1 contains the names of the raw data files with the corresponding tube designation. A sample file follows the table.

TABLE C.1

SUMMARY OF RAW DATA FILES

SINGLE TUBE STUDY

Tube	Vacuum	Atmospheric
Small Tubes		
Smooth	SMV	SMA
2	2SV	2SA
3	3SV	3SA
4	4SV	4SA
5	5SV	5SA
5A	5ASV	5ASA
6	6SV	6SA
7	7SV	7SA
QMCNPS	QNPSV	QNA
QMC	QMCV	QMCA
Medium Tubes		
Smooth	MEDV	MEDA
8	8SV	8SA
9	9SV	9SA
10	10SV	10SA
11	11SV	11SA
12	12SV	12SA
13	13SV	13SA

Tube Number: 08
File Name: BSA
Pressure Condition: Atmospheric
Steam Velocity: 1.0 (m/s)

Data #	Vw (m/s)	Tin (C)	Tout (C)	Ts (C)
1	1.16	23.17	30.77	99.91
2	1.16	23.22	30.87	99.94
3	1.48	23.17	29.67	99.98
4	1.48	23.21	29.70	99.93
5	1.97	23.09	28.62	99.97
6	1.97	23.05	28.58	99.90
7	2.51	22.97	27.76	99.96
8	2.51	22.97	27.78	100.22
9	2.99	22.89	27.23	99.92
10	2.99	22.90	27.24	99.92
11	3.42	22.84	26.89	99.88
12	3.42	22.85	26.89	99.94
13	3.85	22.80	26.56	99.92
14	3.85	22.77	26.55	100.06
15	4.39	22.56	26.00	100.00
16	4.39	22.52	25.96	99.83
17	1.16	23.20	30.91	100.03
18	1.16	23.22	30.94	100.14

LIST OF REFERENCES

1. Marto, P. J., "Heat Transfer and Two-Phase Flow During Shell-Side Condensation," *Heat Transfer Engineering*, vol. 5, Nos.1-2, 1984, pp. 31-61.
2. Wanniarachchi, A. S., Marto, P. J., and Rose, J. W., "Filmwise Condensation of Steam on Horizontal Finned Tubes: Effect of Fin Spacing, Thickness, and Height," *Multiphase Flow and Heat Transfer*, vol. 108, November 1986, pp. 960-966.
3. Yau, K. K., Cooper, J. R., and Rose, J.W., "Effects of Drainage Strips and Fin Spacing on Heat Transfer and Condensate Retention for Horizontal Finned and Plain Tubes," *Fundamentals of Phase Change: Boiling and Condensation*, HTD vol. 38, C. T. Avedisian and D. M. Rudy (eds.), pp. 151-156, December 1984.
4. Wanniarachchi, A. S., Marto, P. J., and Rose, J. W., "Filmwise Condensation of Steam on Externally-Finned Horizontal Tubes," *Fundamentals of Phase Change: Boiling and Condensation*, HTD vol. 38, C. T. Avedisian and D. M. Rudy (eds.), pp. 133-141, December 1984.
5. Marto, P. J., "An Evaluation of Film Condensation on Horizontal Integral-Fin Tubes," *Journal of Heat Transfer*, vol. 110, pp.1287-1305, November 1988.
6. Van Petten, T., *Filmwise Condensation on Low Integral-Fin Tubes of Different Diameters*, Master's Thesis, Naval Postgraduate School, Monterey, California, December 1988.
7. Wanniarachchi, A. S., Marto, P. J., and Rose, J. W., "Film Condensation of Steam on Horizontal Low Integral-Fin Tubes: Effect of Fin Spacing," *Journal of Heat Transfer*, vol. 108, pp. 960-966, November 1986.
8. Yau, K. K., Cooper, J. R., and Rose, J. W., "Effects of Fin Spacing on the Performance of Horizontal Integral-Fin Condenser Tubes," *Journal of Heat Transfer*, vol. 107, pp. 377-383, May 1985.
9. Katz, D. L., Hope, R. E., and Dasko, S. C., *Liquid Retention on Finned Tubes*, Dept. of Engr. Research, University of Michigan, Ann Arbor, Michigan, Project M 592, 1946.

10. Rudy, T. M., and Webb, R. L., "Condensate Retention of Horizontal Integral-Finned Tubing," *Advances in Enhanced Heat Transfer*, HTD, vol. 18, pp. 35-41, 20th National Heat Transfer Conference, Milwaukee, Wisconsin, August 1981.
11. Rudy, T. M., and Webb, R. L., "Theoretical Model for Condensation on Horizontal Integral-Fin Tubes," *AIChE Symposium Series*, vol. 79, no. 225, pp. 11-18, 1983.
12. Honda, H., Nozu, S., and Mitsumori, K., "Augmentation of Condensation on Horizontal Finned Tubes by Attaching Porous Drainage Plates," *Proceedings of the ASME-JSME Thermal Engineering Conference*, pp. 289-296, Honolulu, 1983.
13. Rudy, T. M., and Webb, R. L., "An Analytical Model to Predict Condensate Retention on Horizontal Integral-Finned Tubes," *Journal of Heat Transfer*, vol. 107, pp. 361-368, May 1985.
14. Masuda, H., and Rose, J. W., "Static Configuration of Liquid Film on Horizontal Tubes With Low Radial Fins: Implications for Condensation Heat Transfer," *Proceedings of the Royal Society of London*, vol. A410, pp. 125-139.
15. Marto, P. J., Mitrou, E., Wanniarachchi, A. S., and Fiatsuta, M., "Film Condensation of Steam on a Horizontal Wire Wrapped Tube," *Proceedings of the 2nd ASME-JSME Thermal Engineering Joint Conference*, P. J. Marto and I. Tanasawa (eds.), vol. 1, pp. 509-516, 1987.
16. Nusselt, W., "The Condensation of Steam on Cooled Surfaces," *Chemical Engineering Fundamentals*, vol 1, no. 2, pp. 6-19, May 1915.
17. Nobbs, D. W., *The Effect of Downward Vapour Velocity and Inundation of the Condensate Rates on Horizontal Tube Banks*, Ph.D. Thesis, University of Bristol, England, April 1975.
18. Hopkins, C. L., III, *Effect of Vapor Velocity During Condensation on Horizontal Finned Tubes* Master's Thesis, Naval Postgraduate School, Monterey, California, December 1988.
19. Shekriladze, I. G., and Gomelaury, V. E., "Theoretical Study of Laminar Film Condensation of Flowing Vapour," *International Journal of Mass and Heat Transfer*, vol. 9, pp. 581-591, 1966.

20. Fujii, T., Vehara, H., and Kurata, C., "Laminar Filmwise Condensation of Flowing Vapour on a Horizontal Cylinder," *International Journal of Mass Transfer*, vol. 15, pp. 235-246, 1972.
21. Fujii, T., Honda, H., and Oda, K., "Condensation of Steam on a Horizontal Tube--the Influence of Oncoming Velocity and Thermal Condition at the Tube Wall," *Condensation Heat Transfer*, The 18th National Heat Transfer Conference, San Diego, California, pp. 35-43, August 1979.
22. Beatty, K. T., Jr., and Katz, D. L., "Condensation of Vapors on Outside of Finned Tubes," *Chemical Engineering Progress*, vol. 44, no. 1, pp. 55-77, January 1948.
23. Owen, R. G., Sardesai, R. G., Smith, R. A., and Lee, W. C., "Gravity Controlled Condensation on Horizontal Low-Fin Tube," *Condensers: Theory and Practice*, Inst. Chem. Engrs. Symp. Ser. 75, pp.415-428, 1983.
24. Karkhu, V. A., and Borovkov, V. P., "Film Condensation of Vapor at Finely-Finned Horizontal Tubes," *Heat Transfer-Soviet Research*, vol. 3, no. 2, pp. 183-191.
25. Webb, R. L., Rudy, T. M., and Kedzierski, M. A., "Prediction of the Condensation of Steam on Horizontal Integral-Fin Tubes," *ASME Journal of Heat Transfer*, vol. 107, pp. 369-376, November 1985.
26. Adamek, T., "Bestimmung der Kondensationsgrößen auf Feingewellten Oberflächen zur Auslegung Aptimaler Wandprofile," *Wärme und Stoffübertragung*, vol. 15, pp. 255-270, 1981.
27. Honda, H., and Nozu, S., "A Prediction Method for Heat Transfer During Film Condensation on Horizontal Low Integral-Fin Tubes," *ASME Journal of Heat Transfer*, vol. 109, pp.218-225, 1987.
28. Morrison, R. H., *A Test Condenser to Measure Condensate Inundation Effects in a Tube Bundle*, Master's Thesis, Naval Postgraduate School, Monterey, California, March 1981.
29. Brower, S. K., *The Effect of Condensate Inundation on Steam Condensation Heat Transfer in a Tube Bundle*, Master's Thesis, Naval Postgraduate School, Monterey, California, June 1985.
30. Jakob, M., *Heat Transfer*, vol. 1, J. Wiley and Sons, Inc. pp. 667-673, 1948.

31. Kern, D. Q., "Mathematical Development of Loading in Horizontal Condensers," *AICHE Journal*, vol. 4, pp. 157-160, 1958.
32. Eissenberg, D. M., *An Investigation of the Variables Affecting Steam Condensation on the Outside of a Horizontal Tube Bundle*, Ph.D. Thesis, University of Tennessee, Knoxville, Tennessee, December, 1972.
33. Honda, H., Nozu, S., and Takeda, Y., "Flow Characteristics of Condensate on a Vertical Column of Horizontal Low-Finned Tubes," *Proceedings 2nd ASME-JSME Thermal Engineering Joint Conference* P. J. Marto and I. Tanasawa (eds.), vol. 1, pp. 517-524.
34. Honda, H., Uchima, B., Nozu, S., Nakata, H., and Torigoe, E., "Film Condensation of Downward Flowing R-113 Vapor on In-Line Bundles of Horizontal Finned Tubes," *1989 National Heat Transfer Conference*, HTD vol. 108, pp. 117-125.
35. Georgiadis, I. V., *Filmwise Condensation of Steam On Low Integral-Finned Tubes*, Master's Thesis, Naval Postgraduate School, Monterey, California, September 1984.
36. Poole, W. M., *Filmwise Condensation of Steam on Externally Finned Horizontal Tubes*, Master's Thesis, Naval Postgraduate School, Monterey, California, December 1983.
37. Flook, F. V., *Filmwise Condensation of Steam on Low Integral-Finned Tubes*, Master's Thesis, Naval Postgraduate School, Monterey, California, March 1985.
38. Cakan, O., *Filmwise Condensation of Steam on Low-Integral-Finned Tubes*, Master's Thesis, Naval Postgraduate School, Monterey, California, December 1986.
39. Lester, D. J., *Indirect Measurements of Local Condensing Heat Transfer Around Horizontal Finned Tubes*, Master's Thesis, Naval Postgraduate School, Monterey, California, September 1987.
40. Masuda, H., and Rose, J. W., "Condensation of Ethylene Glycol on Horizontal Integral Fin Tubes," *Proceedings of the ASME-JSME Thermal Engineering Joint Conference*, vol. 1, pp. 525-528, March 1987.

41. Search, H. T., *A Feasibility Study of Heat Transfer Improvement in Marine Steam Condensers*, Master's Thesis, Naval Postgraduate School, Monterey, California, December 1977.
42. Michael, A. G., Marto, P. J., Wanniarachchi, A. S., and Rose, J. W., "Filmwise Condensation of R-113 on Horizontal Integral-Fin Tubes of Different Diameter," *9th International Heat Transfer Conference*, Jerusalem, Israel, August, 1990.
43. Yau, K. K., Cooper, J. R., and Rose, J. W., "Horizontal Plain and Low-Finned Condenser Tubes-Effect of Fin Spacing and Drainage Strips on Heat Transfer and Condensate Retention," *Journal of Heat Transfer*, vol. 108, pp.946-950, 1986.
44. Yung, D., Lorenz, J. J., and Ganic, E. N., "Vapor/Liquid Interaction and Entrainment in Falling Film Evaporators," *Journal of Heat Transfer*, vol. 102, pp. 20-25, 1980.
45. Kline, S. J., and McClintok, F. A., "Describing Uncertainties in Single-Sample Experiments," *Mechanical Engineering*, vol. 74, pp.3-8, January 1953.
46. Mitrou, E. S., *Film Condensation of Steam on Externally Enhanced Horizontal Tubes*, Master's Thesis, Naval Postgraduate School, Monterey, California, March 1986.

INITIAL DISTRIBUTION LIST

	<u>No. Copies</u>
1. Defense Technical Information Center Cameron Station Alexandria, VA 22304-6145	2
2. Library, Code 0142 Naval Postgraduate School Monterey, CA 93943-5004	2
3. Department Chairman, Code 69He Department of Mechanical Engineering Naval Postgraduate School Monterey, CA 93943-5004	1
4. Professor Paul J. Marto, Code 69Mx Department of Mechanical Engineering Naval Postgraduate School Monterey, CA 93943-5004	5
5. Professor John W. Rose Department of Mechanical Engineering Queen Mary College, University of London Mile End Road London E1 4NS, England	1
6. Dr. Charles A. Garris Program Director Thermal Systems Program Division of Chemical and Thermal Systems National Science Foundation Washington, DC 20550	1
7. Naval Engineering Curricular Officer, Code 34 Department of Mechanical Engineering Naval Postgraduate School Monterey, CA 93943-5000	1
8. LT. James M. Coumes, USN c/o George R. Coumes 47834 McKenzie Hwy. Vida, OR 97488	1